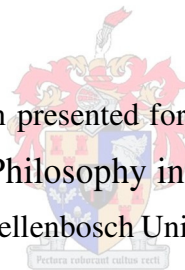


Tensile Creep of Cracked Macro Synthetic Fibre Reinforced Concrete

by

Adewumi John Babafemi

Dissertation presented for the degree of
Doctor of Philosophy in Engineering
at Stellenbosch University



Promoter: Prof., William Peter Boshoff
Faculty of Engineering

March 2015

Declaration

By submitting this dissertation electronically, I declare that the entirety of the work contained therein is my own, original work, that I am the sole author thereof (save to the extent explicitly otherwise stated), that reproduction and publication thereof by Stellenbosch University will not infringe any third party rights and that I have not previously in its entirety or in part submitted it for obtaining any qualification.

March 2015

Abstract

Macro synthetic fibres are known to significantly improve the toughness and energy absorption capacity of conventional concrete in the short term. However, since macro synthetic fibre are flexible and have relatively low modulus of elastic compared to steel fibres, it is uncertain if the improved toughness and energy absorption could be sustained over a long time, particularly under sustained tensile loadings.

The main goal of this study is to investigate the time-dependent crack mouth opening response of macro synthetic fibre reinforced concrete (FRC) under sustained uniaxial tensile loadings, and to simulate the flexural creep behaviour. For the purpose of simulating the in-service time-dependent condition, all specimens were pre-cracked.

Experimental investigations were carried out at three levels (macro, single fibre and structural) to investigate the time-dependent behaviour and the mechanisms causing it. At the macro level, compressive strength, uniaxial tensile strength and uniaxial tensile creep test at 30 % to 70 % stress levels of the average residual tensile strength were performed. To understand the mechanism causing the time-dependent response, fibre tensile test, single fibre pullout rate test, time-dependent fibre pullout test and fibre creep test were done. Flexural test and flexural creep test were done to simulate the structural level performance.

The results of this investigation have shown significant drop in stress and increase in crack width of uniaxial tensile specimens after the first crack. The post cracking response has shown significant toughness and energy absorption capacity. Under sustained load at different stress levels, significant crack opening has been recorded for a period of 8 month even at a low stress level of 30 %. Creep fracture of specimens occurred at 60 % and 70 % indicating that these stress levels are not sustainable for cracked macro synthetic FRC.

The single fibre level investigations have revealed two mechanisms responsible for the time-dependent crack widening of cracked macro synthetic FRC under sustained loading: time-dependent

fibre pullout and fibre creep. In all cases of investigation, fibre failure was by complete pullout without rupture.

Flexural creep results have shown that the crack opening increases over time. After 8 months of investigation, the total crack opening was 0.2 mm and 0.5 mm at 30 % and 50 % stress levels respectively.

Since the crack opening of tensile creep and flexural creep specimens cannot be compared due to differences in geometry, specimen size, load transfer mechanisms and stress distribution in the cracked plane, a finite element analysis (FEA) was conducted. Material model parameters obtained from the uniaxial tensile test and viscoelastic parameters from curve fitting to experimental uniaxial creep results have been implemented to successfully predict the time-dependent crack opening of specimens subjected to sustained flexural loading. Analyses results correspond well with experimental result at both 30 % and 50 % stress levels.

Opsomming

Makro sintetiese vesels is bekend daarvoor dat dit die taatheid en energie absorpsie van konvensionele beton beduidend verbeter in die kort termyn. Aangesien makro sintetiese vesels buigsaam is met 'n relatiewe lae styfheidsmodulus in vergelyke met staalvesels, is dit onseker of die verhoogde kapasiteit vir energie absorpsie en taatheid volgehou kan word oor die langer termyn, veral in gevalle waar dit aan volgehoue trekkragte blootgestel is.

Die hoofdoel van die studie is om die tydafhanklike-kraakvergrotingsgedrag van makro sintetiese veselversterkte beton (VVB) wat blootgestel is aan volgehoue trekkragte te ondersoek asook die simulering van die kruipgedrag in buig. Ten einde die werklike toestand te simuleer is al die proefstukke doelbewus gekraak in 'n beheerde manier voor die aanvang van die toetse.

Die eksperimentele ondersoek is uitgevoer op drie vlakke (makro, enkelvesel en strukturele) om die tydafhanklike gedrag sowel as die meganismes verantwoordelik vir hierdie gedrag te ondersoek. Op die makro-vlak is druktoetse gedoen saam met eenassige trek- en eenassige kruiptoetse met belastings tussen 30 % en 70 % van die gemiddelde residuele treksterkte. Om die meganisme wat die tydafhanklike gedrag veroorsaak te verstaan is veseltoetse, enkel vesel uittrektoetse, enkel vesel uittrek kruiptoetse asook kruiptoetse op vesels gedoen. Buigtoetse en buig kruiptoetse is ook gedoen om die gedrag op die strukturele vlak te ondersoek.

Die resultate van hierdie ondersoek wys dat daar 'n beduidende val in spanning is en dat daar gepaardgaande kraak opening in die eenassige trek proefstukke plaasgevind het na die vorming van 'n kraak. Die na-kraak gedrag wys beduidende taatheid en energie absorpsie kapasiteit. Gedurende die volgehoue trekbelasting by verskillende spanningsvlakke is beduidende kraakvergroting opgemerk, selfs by 30 % belasting na 8 maande. Kruipfaling het plaasgevind by proefstukke met belastings van 60 % en 70 % wat daarop wys dat hierdie spanningsvlakke nie geskik is vir gekraakte makro sintetiese VVB nie.

Op die enkel veselvlak is twee meganismes geïdentifiseer wat verantwoordelik is vir die kraakvergroting oor tyd vir gekraakte makro sintetiese VVB met volgehoue trekbelasting: tydafhanklike vesel uittrek en vesel-kruip. In alle gevalle in hierdie ondersoek was die falingsmeganisme vesels wat uittrek.

Buig kruiptoets resultate wys dat die kraake vergroot oor tyd. Na 8 maande van ondersoek was die kraakwydtes 0.2 mm en 0.5 mm by 30 % en 50 % spanningsvlakke onderskeidelik.

Aangesien die kraak opening van eenassige trek kruiptoetse en die buig kruiptoetse nie direk met mekaar vergelyk kan word nie weens die verskille in geometrie, proefstuk grootte en spanningsverdeling in die kraakvlak, is 'n eindige element analyses (EEA) gedoen. Materiaal eienskappe is bepaal deur gebruik te maak van die eenassige kruip trektoets se resultate en visko-elastiese parameters is bepaal deur middel van kurwepassing van die resultate. Dit was gebruik om suksesvol die buig kruip kraak opening gedrag te simuleer. Die analyses se resultate vergelyk goed met die eksperimentele data by beide 30 % en 50 % spanningsvlakke.

Acknowledgements

First and foremost, my profound gratitude goes to my supervisor, Prof. W.P. Boshoff for his immense and unquantifiable guidance throughout the course of this study. I am most grateful to you. I also like to thank my Head of Department, Prof G.P.A.G van Zijl for his encouraging words and friendliness throughout my study.

The support of the industry partners of the Structural Use of Macro Synthetic Fibre Reinforced Concrete project as well as the Technology and Human Resource for Industry Programme, an initiative by the Department of Trade and Industry, South Africa, Grant No. TP2011071300005 is well appreciated.

My sincere appreciation goes to the staff of the laboratory and workshop of the Civil Engineering Department, University of Stellenbosch, for their support during the laboratory work, the design and fabrication of the creep frame.

I cannot end the list without appreciating my employer, Department of Building, Obafemi Awolowo University, Ile-Ife, Nigeria, for giving me the opportunity to pursue my Doctorate degree at Stellenbosch University, South Africa. The financial support received from Tertiary Education Trust Fund (TET Fund), Nigeria, is appreciated.

I also like to acknowledge and give thanks to God for my Pastor, Dr. Funlola Olojede, for her support, prayers and encouragement throughout my study. Special thanks to the entire Brethren at my local church in Stellenbosch, The Desire of Nations of The Redeemed Christian Church of God for their prayers. God bless you all. My thanks also go to my Parent, Brothers, Mother-in-law, and Brother-in-law for their prayers and support. May God bless you all.

My special thanks also goes to my mother-in-law for standing by my family throughout my studies. She sacrificed everything to come and stay with my family for the whole period of this programme. I am grateful to you Ma. May the Lord bless you greatly.

Most importantly, I wish to thank the love of my life, my wife and best friend, Olayemi, for her support, prayers, encouragement and sacrifice during the pursuit of this programme. I can never forget the great sacrifice you made for this journey to be a success. May the Lord Almighty bless you beyond your wildest dreams. I thank all my beautiful daughters too: Esther, Victoria and Precious, for their prayers and encouragement.

Dedication

This dissertation is dedicated to the Almighty God and Father of our Lord Jesus Christ for grace and strength to begin and end this work. His name is praised forever (Amen).

Table of Contents

Declaration.....	ii
Abstract.....	iii
Opsomming.....	v
Acknowledgements.....	vii
Dedication.....	ix
Table of Contents.....	x
List of Tables.....	xx
List of Symbols.....	xxii
Chapter 1 Introduction.....	1
1.1 Statement of the Research Problem.....	2
1.2 Aim and Objectives of the Study.....	4
1.3 Research Plan Based on Objectives of the Study.....	4
1.4 Research Significance.....	5
1.5 Outline of the Thesis.....	5
Chapter 2 FRC: Mechanical and Time-Dependent Behaviour.....	8
2.1 Fibre Reinforced Concrete.....	8
2.1.1 Macro synthetic fibre.....	11
2.1.2 Single fibre pullout behaviour.....	15
2.2 Time Dependent Behaviour of Cement-Based Materials.....	22
2.2.1 Shrinkage of concrete.....	22

2.2.2	Creep.....	24
2.2.3	The mechanism causing creep in concrete.....	27
2.2.4	Creep behaviour of concrete under sustained load.....	28
2.3	Time-Dependent Behaviour of Cracked FRC.....	30
2.3.1	Uniaxial tensile response of cracked FRC.....	30
2.3.2	Flexural tensile response of cracked FRC.....	35
2.4	Summary.....	38
Chapter 3 Materials and Experimental Method.....		39
3.1	Materials.....	40
3.1.1	Concrete mix materials.....	40
3.1.2	Macro synthetic polypropylene fibre.....	40
3.1.3	Concrete mixture.....	42
3.2	Mould Preparation and Concrete Mixing.....	42
3.2.1	Assemblage of moulds for uniaxial tensile investigation.....	43
3.2.2	Mixing of the concrete.....	45
3.2.3	Workability of fresh concrete mix.....	46
3.2.4	Curing of test specimens.....	47
3.2.5	Preparation of samples for testing.....	47
3.3	Investigations on the Macro Level.....	47
3.3.1	Compressive strength test.....	47
3.3.2	Uniaxial tensile test.....	48
3.3.3	Uniaxial tensile creep test.....	50

3.3.4	Drying shrinkage test	55
3.4	Investigation on the Single Fibre Level	56
3.4.1	Time-dependent fibre pullout test.....	56
3.4.2	Single fibre creep.....	58
3.5	Other Experimental Investigations on the Single Fibre Level	59
3.5.1	Rate test on single fibre pullout	60
3.5.2	Tensile strength test of single fibres.....	61
3.6	Structural Level Investigations	63
3.6.1	Flexural tensile test	63
3.6.2	Flexural creep.....	66
3.7	Summary	70
Chapter 4	Macro Level Behaviour under Short and Long Term Loading.....	71
4.1	Compression Strength.....	71
4.1.1	Results.....	71
4.1.2	Discussion	72
4.2	Uniaxial Tensile Test	73
4.2.1	Results.....	74
4.2.2	Discussion	75
4.2.3	Experimental Observation during test.....	78
4.3	Uniaxial Tensile Creep.....	79
4.3.1	Results.....	80
4.3.2	Discussions	84

4.3.3	Effect of cracked plane fibre count on the variability of CMOD.....	87
4.4	Drying Shrinkage of Test Specimens.....	89
4.4.1	Results.....	89
4.4.2	Discussion	90
4.5	Summary.....	91
Chapter 5	Single Fibre Level Investigation.....	93
5.1	Uniaxial Tensile Strength of PP Fibres.....	94
5.1.1	Results.....	94
5.1.2	Discussion	96
5.2	Single Fibre Pullout Rate Test	97
5.2.1	Results.....	97
5.2.2	Discussion	103
5.3	Time-Dependent Behaviour.....	108
5.3.1	Single fibre pullout.....	109
5.3.2	Single fibre creep	111
5.3.3	Mechanisms causing time-dependent crack widening.....	113
5.4	Summary.....	113
Chapter 6	Structural Response of Macro Synthetic FRC	115
6.1	Flexural Tensile Behaviour.....	115
6.1.1	Results.....	116
6.1.2	Discussions	118
6.2	Flexural Tensile Creep.....	122

6.2.1	Result	123
6.2.2	Discussion	126
6.3	Summary	128
Chapter 7 Modelling the Time-Dependent Behaviour		130
7.1	Constitutive Model.....	131
7.2	Rheological Creep Model	132
7.2.1	Viscoelastic material model parameters.....	135
7.2.2	Results.....	135
7.3	Finite Element Modelling	137
7.3.1	Constitutive law of FRC: stress-crack width relationship.....	137
7.3.2	Tensile behaviour.....	138
7.3.3	Model description	140
7.4	Static Analyses.....	141
7.4.1	Non-linear analysis procedures	143
7.4.2	Prediction of four point flexural response.....	144
7.5	Prediction of Time-Dependent CMOD.....	147
7.5.1	Results and discussion	148
7.5.2	Relation between uniaxial tensile and flexural creep.....	150
7.6	Summary	152
Chapter 8 Conclusions and Recommendations		153
8.1	Macro Level.....	153
8.2	Single Fibre Level.....	154

8.3	Structural level.....	155
8.4	Time-dependent CMOD modelling.....	155
8.5	Recommendation.....	156
	References.....	157

List of Figures

Figure 1.1: Flow chart of experimental investigation	7
Figure 2.1: Classification of tensile response of cement-based composites	9
Figure 2.2: Structural synthetic fibres with different geometric deformations	14
Figure 2.3: Schematic representation of the interfacial transition zone (ITZ) of a FRC	18
Figure 2.4: Aggregate bridging mechanism in uniaxial tension and the resulting stress-crack opening relationship	18
Figure 2.5: Single fibre pullout behaviour of a straight fibre	19
Figure 2.6: Single fibre pullout test setup	20
Figure 2.7: Pullout specimen and test setup for single fibre pullout	21
Figure 2.8: Time-dependent deformation in concrete	25
Figure 2.9: Strain-time relationship of concrete under sustained loading.....	28
Figure 2.10: Component of creep strain.....	29
Figure 2.11: Schematic representation of creep fracture and creep limit	30
Figure 2.12: Effect of fibres on the fracture process in uniaxial tension	31
Figure 2.13: (a) Tensile creep setup, and (b) and (c), the tensile creep clamps	33
Figure 2.14: Uniaxial tensile creep frame	34
Figure 2.15: Tensile creep result of specimens	35
Figure 2.16: Flexural creep setup	37
Figure 3.1: Macro monofilament synthetic PP fibre with crimped geometry.....	41
Figure 3.2: Preparation of moulds with steel hooks protruding from the ends.....	44

Figure 3.3: Details of schematic representation of wooden block	45
Figure 3.4: Uniaxial tensile test setup	50
Figure 3.5: Schematic representation of uniaxial tensile creep frame with specimens in series	51
Figure 3.6: Calibration of creep frame	52
Figure 3.7: Upper section of creep frame showing stopper device	53
Figure 3.8: Creep frames showing specimens under sustained loads and LVDT position over a gauge length of 70 mm.	55
Figure 3.9: Shrinkage test specimens showing frame with LVDT extenders	56
Figure 3.10: Test setup of time dependent fibre pullout test	57
Figure 3.11: Fibre creep test setup	59
Figure 3.12: Single fibre pullout test specimens	60
Figure 3.13: Single fibre pullout rate test	61
Figure 3.14: Single fibre tensile strength test	62
Figure 3.15: Load- <i>CMOD</i> diagram and $F_j (j = 1, 2, 3, 4)$	64
Figure 3.16: Flexural tensile test under three point loading	65
Figure 3.17: Flexural tensile test under four point loading	65
Figure 3.18: Flexural creep frame	67
Figure 4.1: Response of macro synthetic FRC under uniaxial tensile load	74
Figure 4.2: Linear response up to ultimate strength at Point A	76
Figure 4.3: Fibre aligned in the direction of loading	78
Figure 4.4: Propagation of crack (a) out-of-plane bending (b) symmetrical propagation	79
Figure 4.5: Unloading and reloading response under uniaxial tensile test	80

Figure 4.6: CMOD of tensile creep tests.....	83
Figure 4.7: Creep coefficient of cracked FRC at different stress levels	87
Figure 4.8: Drying shrinkage of macro synthetic FRC	89
Figure 4.9: Time-dependent development of drying shrinkage	91
Figure 5.1: Single fibre tensile test result at different loading rate	95
Figure 5.2: Average maximum tensile strength of macro PP fibre.....	96
Figure 5.3: Fractured macro synthetic fibres	97
Figure 5.4: Rate dependence of single fibre pullout at embedment length, $E_L = 10$ mm.	98
Figure 5.5: Single fibre pullout tests results at embedment length, $E_L = 15$ mm.....	99
Figure 5.6: Single fibre pullout tests results at embedment length, $E_L = 25$ mm.....	100
Figure 5.7: Effect of loading rate and embedment length on the pullout load of single embedded fibres	101
Figure 5.8: Effect of loading rate and embedment length on τ_{max}	102
Figure 5.9: Macro PP fibre surface damage with varying fibre embedment length. a) SEM photo of unused fibre. b) $E_L = 10$ mm; c) $E_L = 15$ mm; d) $E_L = 25$ mm	102
Figure 5.10: Effect of pullout loading rate on macro PP fibre surface. a) SEM photo of unused fibre. b) Loading rate, LR = 1 mm/s; c) LR = 0.1 mm/s; d) LR = 0.01 mm/s; e) LR = 0.001 mm/s	103
Figure 5.11: Effect of pullout rate on the fibre tensile stress.....	105
Figure 5.12: Critical fibre length at different embedment length	105
Figure 5.13: Fibre pullout displacement against time.....	109
Figure 5.14: Tensile creep failure of specimen showing pulled out fibres	110
Figure 5.15: Time-dependent PP fibre creep	112

Figure 6.1: Flexural behaviour of beams under three point bending test.....	116
Figure 6.2: Extensive energy absorption capacity of cracked macro synthetic FRC.....	118
Figure 6.3: Graph showing linear response before ultimate strength	118
Figure 6.4: Simplified post cracking stress-crack opening diagrams (a) rigid plastic behaviour	121
Figure 6.5: Unloading response and the sustained flexural load levels	123
Figure 6.6: Flexural creep of cracked macro synthetic FRC	124
Figure 6.7: Idealised plot of pre-cracking and sustained creep load under flexure.....	125
Figure 7.1: Viscoelastic model for creep a) Kelvin element b) Kelvin chain.....	132
Figure 7.2: Example of Kelvin chain curve fitted to experimental creep result at 30 % stress level..	136
Figure 7.3: Predefined tension softening for Total Strain crack model (TNO Diana, 2009).....	139
Figure 7.4: The finite element mesh of the beam subjected to four point bending.....	141
Figure 7.5: Loading-unloading (TNO Diana, 2009).....	142
Figure 7.6: Modelled loading, unloading and applied creep load	142
Figure 7.7: The analysis of result compared to the experimental flexural results	145
Figure 7.8: Stress-strain graph showing true and adjusted tensile parameters.....	146
Figure 7.9: Parametric analysis of result compared to the experimental flexural results	147
Figure 7.10: Compressive and tensile stress distribution.....	148
Figure 7.11: The analysis result compared to experimental creep result at 30 % stress level	149
Figure 7.12: The analysis result compared to experimental creep results at 50 % stress level.....	149
Figure 7.13: Stress distribution over the height of a hinge during crack evolution	151

List of Tables

Table 2.1: Polymer fibre classification	11
Table 2.2: Types and properties of typical synthetic fibres	12
Table 2.3: Properties of different geometries of macro synthetic fibre	13
Table 2.4: Effect of geometry on bond strength of macro synthetic fibre	13
Table 3.1: Experimental tests conducted at macro and structural levels	40
Table 3.2: Properties of macro synthetic (polypropylene) fibres.....	41
Table 3.3: Concrete mixture design for PPFRC	42
Table 3.4: Direct tension test setups – notched prisms/cylinder specimens	49
Table 3.5: Test programme for the cracked uniaxial tensile creep specimens.....	54
Table 4.1: Mean 28-day compressive strength and density	72
Table 4.2: Load carrying capacity with increase in crack width.....	75
Table 4.3: Total average time-dependent CMOD after 8 months.....	84
Table 4.4: Uniaxial tensile creep parameters	86
Table 4.5: Average fibre count on cracked plane of specimens at different stress levels.....	88
Table 5.1: Average breaking load of PP fibre.....	95
Table 5.2: Percentage increase in average breaking load	96
Table 5.3: Increase in τ_{\max} at different loading rates and embedment lengths	106
Table 6.1: Residual flexural tensile strength parameters for 3-point test.....	117
Table 6.2: Classification of residual flexural strength ratio (Model code 2010)	120
Table 6.3: Parameters from experimental creep test.....	126

Table 7.1: Viscoelastic material model parameters at 30 % stress level.....	136
Table 7.2: Viscoelastic material model parameters at 50 % stress level.....	137
Table 7.3: Actual tensile parameters obtained from test.....	140
Table 7.4: Cases of adjusted tensile model parameters with the additional points highlighted.....	145

List of Symbols

A_c	Area of cube specimen
CMOD	Crack mouth opening displacement
CMOD _{creep}	Actual creep
CMOD _{inst}	Instantaneous CMOD
CMOD _{irr}	Irrecoverable CMOD
CMOD _{tot}	Total average time-dependent crack mouth opening displacement
CMOD _y	Measured CMOD at a distance y from the bottom surface of beam
COR(t_1-t_2)	Crack opening rate from time t_1 to t_2
d_1	Width of beam
d_2	Height of beam
d_f	Nominal diameter of fibre
d_e	Effective diameter of fibre
E	Young's modulus
E_{ci}	E-modulus of concrete at 28-day
e_f	fibre elongation
E_L	Embedment fibre length
F	Maximum load
F_a	Applied creep load
$f_{cf(3P)}$	Flexural strength in 3-point bending
$f_{cf(4P)}$	Flexural strength in 4-point bending

f_{cm}	Compressive strength
f_{ct}	Ultimate uniaxial tensile strength
f_{Fts}	Serviceability residual strength
f_{Ftu}	Ultimate residual strength
F_L	Load at limit of proportionality
f_L	Stress at the limit of proportionality
$f_{R,j}$	Residual strength at the corresponding CMOD
$F_{R,j}$	Load corresponding to CMOD
f_{R1k}	Characteristics residual strength significant for serviceability condition
f_{R3k}	Characteristics residual strength significant for ultimate condition
F_w	Load at w_p
$f_{\sigma,max}$	Average maximum flexural strength
h	Total depth of beam specimen
h_{ch}	Height of the mouth grip of hand drill chuck
h_{sp}	Distance between tip of notch and top of beam specimen
l	Span length of beam specimen
l_f/d_f	Aspect ratio of fibre
l_c	Critical fibre length
L_e	Original embedment fibre length
Δ	Pullout displacement
Δl	Elongation
Δ_n	Normalised displacement

l_f	fibre length
L_r	Reference fibre length
m	Number of element
n	time step
n_w	Notched width
$\varphi(t)$	Coefficient of creep
P	Applied/Crushing/Breaking force
P_{max}	Maximum load
S	Maximum grain spacing
t_o	Time at which drying begins
v_f	Volume ratio of fibre
w	Crack width/opening
w/b	Water-binder ratio
$w_{cd(t)}$	CMOD at the end of creep test
w_{ci}	CMOD at the beginning of the creep test
w_{irr}	Irrecoverable crack width
w_p	Maximum CMOD at the pre-cracking process
w_{pr}	Residual CMOD after unloading at the pre-cracking process
w_u	Maximum crack opening accepted in structural design
y	Distance of LVDT from bottom surface of beam
α_E	Factor dependent on aggregate type
δ_{sh}	Shrinkage displacement

δt	change in time
$\delta \varepsilon$	change in strain
$\delta \sigma$	change in stress
ε	Strain
ε_{inst}	Elastic deformation/recovery
$\varepsilon_s, \varepsilon_D$	Strain in the spring and dashpot
$\dot{\varepsilon}_s, \dot{\varepsilon}_D$	Strain rate in spring and dashpot
$\varepsilon_{t,m}$	Time-dependent strain
η	Viscosity of the material
σ	Stress
$\sigma_{f,max}$	Maximum pullout fibre tensile stress
σ_s, σ_D	Stress in the spring and dashpot
τ	Interfacial toughness
τ_{avg}	Mean interfacial shear resistance
τ_i	Relaxation time ($i = 1, 2, 3, 4$)
τ_{max}	Average interfacial shear stress
$\tau_{straight}$	Interfacial toughness for straight fibre
$\varphi(j)$	Creep coefficient
$\varphi_o(j)$	Creep coefficient referred to the origin

Abbreviations

ARS	Average residual strength
-----	---------------------------

CH	Calcium Hydrate
C-S-H	Calcium Silicate Hydrate
CMOD	Crack mouth opening displacement
CoV	Coefficient of variation
CTOD	Crack tip opening displacement
FEA	Finite element analysis
FEM	Finite element method
FM	Fineness modulus
FRC	Fibre reinforced concrete
HPFRC	High performance fibre reinforced concrete
ITZ	Interfacial transition zone
LOP	Limit of proportionality
LVDT	Linear variable displacement transducer
MOR	Modulus of rupture
PP	Polypropylene
PPFRC	Polypropylene fibre reinforced concrete
PVA	Polyvinyl alcohol
PVC	Polyvinyl chloride
RILEM	International Union of Laboratories and Experts in Construction Materials
SEM	Scanning electron microscopy
SFP	Single fibre pullout
SHCC	Strain hardening cementitious composites

SLS	Serviceability limit state
UHPFRC	Ultra high performance fibre reinforced concrete
ULS	Ultimate limit state
σ - w	Stress-crack opening

Chapter 1

Introduction

Concrete, the world's most used construction material has its usage dating back to ancient times (Sun et al., 2001). Brandt (2008) attributes the increasing consumption of concrete globally to a number of factors which includes the availability of its components and its application over large variety of building and civil infrastructure works. With the passage of time, the shortcomings of concrete became evident and there developed a need to find solutions to these problems. The limitations as well known and reported in literature, relate to the brittle failure of concrete under load (poor ductility) and a low tensile strength when compared to its compressive strength. Hence, concrete has a poor resistance to cracking and the propagation of the cracks. This necessitated the use of steel reinforcement in concrete. Steel is known to be stronger in tension than concrete. Clarke et al. (2007) reported that steel reinforcement is utilised to carry the tensile forces and prevent any cracking or by pre-stressing the concrete so that it remains largely in compression under load. Steel reinforcement has been successfully used in concrete over the years and it is still in use. However, cracking still occurs under load and this creates a pathway for various deleterious species such as chlorides, sulphates, moisture, CO₂, etc. This leads to the corrosion of the reinforcement thereby affecting the durability of the concrete structures. Other alternatives aside from steel reinforcement are also available for the reinforcing of concrete to control cracking. One of such alternatives currently being used is fibres.

Suji et al. (2007) concurred that the use of fibres in concrete may be of current interest, but it is not a new idea or concept. The use of fibres in reinforcing a brittle material can be traced back to the Egyptian times when straws or horse hair were used to strengthen mud bricks. Today, fibre reinforced concrete (FRC) using steel or synthetic fibres are becoming widely used in construction projects because of its favourable mechanical properties. It is now common knowledge that the use of fibres in concrete serve to improve its toughness, tensile strength, crack opening, crack propagation and

deformation characteristics amongst others. Though much information from scholarly articles is now available on the short term mechanical behaviour of structural elements reinforced with fibres, there exist a dearth of knowledge on its long term behaviour under sustained loading. Structural elements deform throughout their lifespan (creep), which could lead to serviceability issues such a cracking, deflection, etc. While FRC has shown significant ductility and energy absorption capacity in the short term, the sustainability of such properties in the long term is still uncertain.

1.1 Statement of the Research Problem

As mentioned earlier, the use of fibres is gaining more prominence in the construction industry. They are said to be substituting and/or replacing conventional types of reinforcements in a variety of structures (MacKay & Trottier, 2004). For example, wire mesh used in slabs on grade can now be completely replaced by fibres. Steel fibres have extensively been used since the 1950s and more recently, the use of structural fibres otherwise referred to as macro synthetic fibres such as polypropylene (PP) is being advanced. These fibres have been noted to have appealing characteristics, hence a gradual shift towards its use as a reinforcement material for concrete. Mu et al. (2002) and Richardson (2005) have reported that it has better economy when compared to other fibres such as glass fibre. It has also been found that the fibres do not deteriorate with age (Hannant, 1998; Richardson, 2004) and shows resistance to aggressive chemicals such as alkali (Wang et al., 1987). The merits of this fibre have led to the investigation of the mechanical behaviour of concrete reinforced with such fibres, particularly in the post-crack region. Some scholarly works have been published in this regards (Buratti et al., 2011; Cifuentes et al., 2013; Hsie et al., 2008). Though many scholarly works have been published regarding the significant improvement in the short term mechanical response of fibre concrete in general, information is still lacking on long term deformation of FRC (Bernard, 2010; Kurtz & Balaguru, 2000; MacKay & Trottier, 2004).

Some earlier studies have revealed concern over the creep behaviour of synthetic FRC. One such study revealed that sustainable flexural stress was significantly lower than the post crack strength

(Kurtz & Balaguru, 2000). It should be noted that a fibre volume of 0.1% was used in the investigation and fibre type was micro polypropylene and nylon. This is a critical aspect of the post crack behaviour of synthetic FRC that needs further investigation. MacKay & Trottier (2004) also characterised and compared the creep (time-dependent deformation) behaviour of cracked steel and synthetic FRC beams under sustained flexural loading. After investigation for a year, they reported that synthetic FRC showed more flexural creep compared to steel FRC at sustained load of 20 % and 60 % of the average residual flexural strength. The dosage of the self-fibrillating mono-filament synthetic fibre used in this work was also at a low volume (0.5 %). Perhaps, at higher fibre volume, higher sustainable stress could be achieved. Other works on the flexural creep of FRC are those reported by Granju et al., (2000), Tan & Saha (2005), Zerbino & Barragan (2012), García-Taengua et al. (2014), etc. These works were all done using steel fibres and were investigated under flexural loading.

One of the first published articles on the uniaxial tensile creep of cracked macro synthetic FRC is that reported by this author (Babafemi & Boshoff, 2015). Though Boshoff et al. (2009a) and Boshoff & Adendorff (2013) investigated the tensile creep of cracked strain hardening cement-based composite (SHCC) using micro polyvinyl alcohol (PVA) fibres, the behaviour is however quite different when compared to macro FRC which is strain softening. Mouton & Boshoff (2012) and Zhao et al. (2012) also did investigate the uniaxial tensile creep of FRC under sustained loading. However, the reinforcing material was steel fibres. Evidently, much remains to be known about the time-dependent deformation of macro synthetic FRC. Since fibres are engaged for controlling crack opening only after the initiation of cracks, it is worthwhile for such investigation to be conducted in the cracked state for the simulation of in-service condition.

It is common knowledge that most structural elements are subjected to flexural stresses. The need for an accurate simulation of the structural behaviour of elements under load cannot be overemphasised. This could be done through computational modelling. The modelling of the flexural creep could be achieved by implementing material tensile parameters obtained from a uniaxial tensile

test and viscoelastic parameters from a rheological model in a finite element analysis (FEA) software. This has recently become a subject of interest (Mouton & Boshoff, 2012). One of such FEA software that can be used to simulate the time-dependent response of cracked macro synthetic FRC under sustained flexural loadings is DIANA. In this dissertation, the prediction of the time-dependent crack mouth opening displacement (CMOD) under sustained flexural loading was implemented and the results validated using experimental results.

1.2 Aim and Objectives of the Study

The major aim of this study therefore, is to investigate the tensile creep behaviour of cracked macro synthetic FRC with a view to quantifying its time-dependent crack mouth opening displacement.

The specific objectives of this research project are:

- To examine the tensile creep mechanism of cracked macro synthetic FRC; and
- Quantifying and modelling of the behaviour under sustained loading.

1.3 Research Plan Based on Objectives of the Study

The aforementioned objectives were broken down into a number of stepwise procedures. Details of these work plans are discussed in Chapter 3. The summary is enumerated below:

- Determination of the mechanical properties of macro synthetic FRC. Compressive, uniaxial tensile and flexural strengths were investigated. Particular attention is focussed on the post cracking behaviour;
- Quantification of the time-dependent CMOD of cracked specimens under sustained loading at different stress levels of the average residual strength (ARS);
- Investigation of the time-dependent single fibre pullout behaviour of polypropylene (PP) fibre from cementitious matrix under sustained loading and the fibre creep to understand the

mechanism causing the creep of cracked macro synthetic FRC. Other tests conducted at the single fibre level include single fibre pullout rate dependence tests at different embedment lengths. Tensile rate tests were also performed on single fibres.

- Modelling of the time-dependent crack opening of cracked specimens subjected to sustained flexural loading using FEA.
- Validation of the results of the analysis with experimental results.

1.4 Research Significance

With the growing concern over the creep behaviour of structural systems constructed using composites with fibre under service loads, it is imperative that a study of the response of cracked macro synthetic FRC under sustained loading at different stress levels be carried out. A research of this nature will therefore provide information on the creep (time-dependent CMOD) of macro synthetic FRC tested in the cracked state under a variation of stress levels which is lacking in literature. Also, the sustainability of the improved ductility and energy absorption capability in a short term test will be revealed in the long term investigation thus providing more information for users of this technology.

1.5 Outline of the Thesis

This dissertation on the tensile creep of cracked macro synthetic FRC is presented in eight chapters. The investigations conducted have been grouped into three: macro, single fibre and structural level investigations. It starts with an introduction of the subject and the goals set to be achieved.

In Chapter 2, a literature background of fibre reinforced concrete, macro synthetic fibres, the mechanical properties of FRC and the time-dependent behaviour under sustained loading are presented.

Chapter 3 provides a detailed description of the methods employed in investigating the mechanical and long term behaviour of macro synthetic FRC. Test methods described include compressive, uniaxial tensile, flexural strength tests. Others are uniaxial creep, flexural creep, drying shrinkage, time-dependent fibre pullout, fibre creep, rate dependence single fibre pullout and fibre tensile rate tests.

In Chapter 4, results and discussions at the macro level investigation (compressive strength, uniaxial tensile test, uniaxial tensile creep test and drying shrinkage) are presented.

In Chapter 5, attention is focussed on all tests at the single fibre level. This begins with the investigation of the tensile strength of fibre used and the effect of loading rate, rate dependence of single fibre pullout at different embedment length and single fibre tensile creep test.

Results and discussion on the structural level of investigation is presented in Chapter 6. The short term flexural response and time-dependent flexural creep of cracked specimens were evaluated.

Chapter 7 reports on the constitutive modelling of the time-dependent behaviour of cracked macro synthetic FRC under sustained loading using FEA. Tensile parameters from the uniaxial tensile test as well as viscoelastic material model parameters of cracked macro synthetic FRC at different stress level was obtained using the Kelvin chain model by curve fitting to experimental creep results. These were implemented using the Total Strain crack model to simulate the time-dependent crack opening in cracked specimens subjected to sustained flexural loading.

In Chapter 8, the significant findings of this study are presented and recommendations for further studies are enumerated.

A detailed flow chart of the outline of all experimental investigations carried out in this work is shown in Figure 1.1.

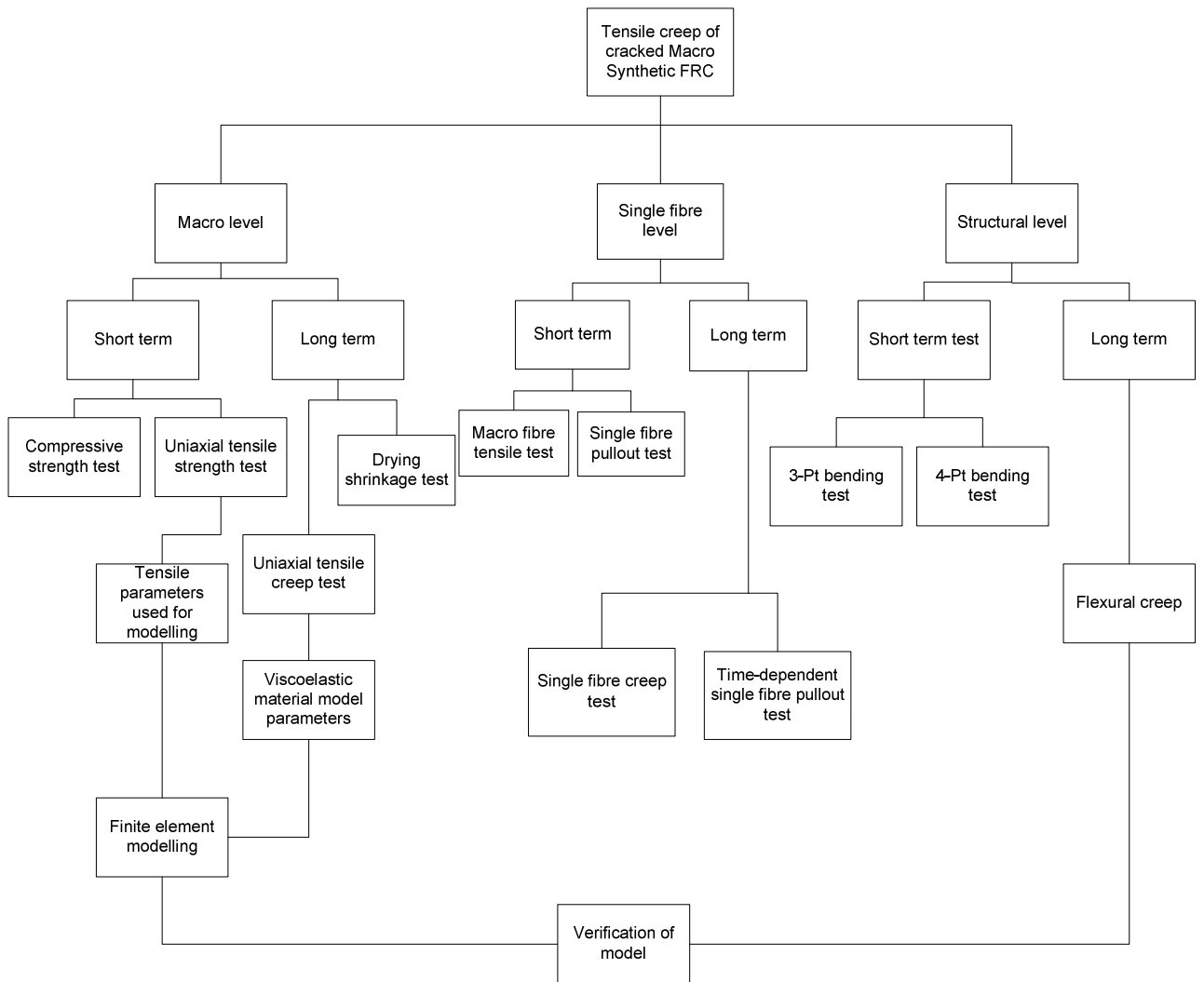


Figure 1.1: Flow chart of experimental investigation

Chapter 2

FRC: Mechanical and Time-Dependent Behaviour

This chapter begins with a brief review of the main characteristics of fibre reinforced concrete (FRC), macro synthetic fibre, and the dynamics of fibres in concrete at the micro level. Thereafter, an overview of the time-dependent response of cement based materials and the mechanism responsible for the delayed deformation in concrete is presented. Lastly, attention is directed towards the review of existing knowledge on the time-dependent deformation of FRC with emphasis on pre-cracked test specimens. Some methodologies for testing certain parameters relating to FRC are also reviewed.

2.1 Fibre Reinforced Concrete

Due to the brittle nature of concrete, cracks occur under stress which eventually affects the strength and durability of concrete. FRC is concrete consisting of binder, aggregates (fine and coarse), water with the inclusion of short, discrete and usually randomly distributed fibres, thus improving its properties in all directions. It should also be mentioned that a number of cement extenders could be added and superplasticisers to modify the rheology of the mix. The purpose of fibres in concrete is to improve the energy absorption capacity, tensile strength, cracking and deformation characteristics of concrete thereby controlling the fracture process by bridging the cracked plane (Zile & Zile, 2013). This leads to reduction in the crack width and deflection in members subjected to flexure. Since the fibres only become effectively active after the crack formation, the inclusion of fibres in concrete alters the post cracking behaviour of normal concrete. Depending on the type of fibre, fibre volume, geometrical properties, the post cracking behaviour can be classified as either strain-hardening or strain-softening (Naaman & Reinhardt, 2006; Wille et al., 2014), Figure 2.1.

The post cracking behaviour is said to be strain hardening if the post crack strength increases beyond the first cracking strength (σ_c) of the composite. Materials exhibiting these characteristics are usually described as high performance material composites and the post cracking region is

characterised by multiple cracking. At stress σ_w , crack localisation then begins and the crack width (w) increases with decreasing stress. Examples are strain hardening cementitious composites (SHCC), high performance fibre reinforced concrete (HPFRC) and more recently, ultra-high performance fibre reinforced concrete (UHPFRC) (Barnett et al., 2010; Ferrier et al., 2015; Li & Maalej, 1996; Maalej & Li, 1995; Naaman & Reinhardt, 2006; Yang et al., 2009).

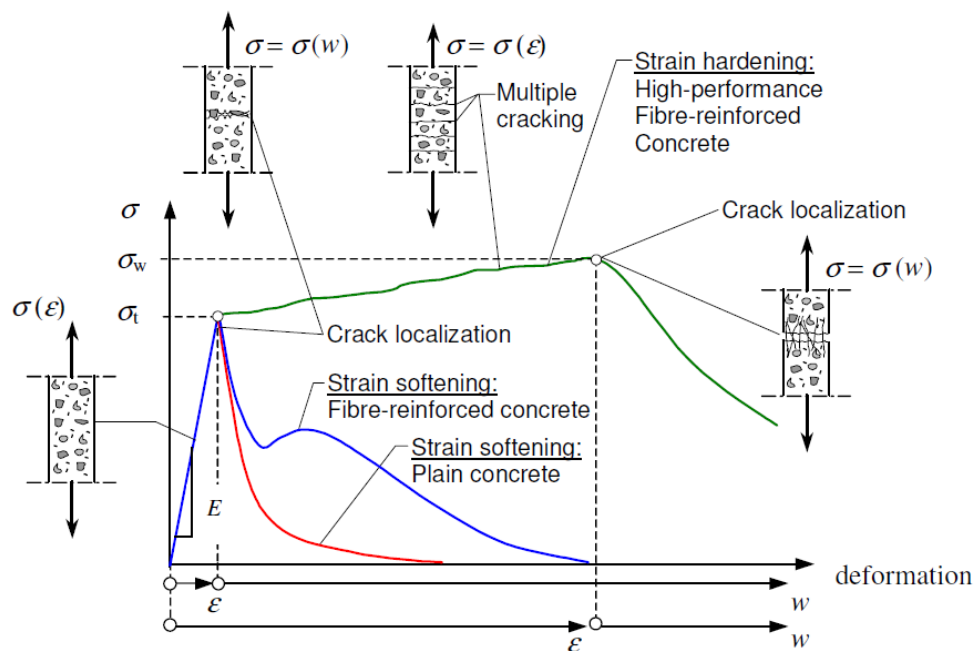


Figure 2.1: Classification of tensile response of cement-based composites (Löfgren, 2005)

On the other hand, composites showing strain softening behaviour have their post cracking strength lower than the first cracking strength (σ_t) and the crack is usually localised. Typical FRC generally falls into this category. The macro synthetic FRC used in this research exhibits a strain softening post cracking behaviour. Figure 2.1 shows the typical response of fibre reinforced cementitious composite beyond the first crack strength. Plain concrete shows no resistance whatsoever after the first crack while the conventional FRC shows an initial drop in stress but soon reflects increased energy absorption due to fibres bridging the cracked planes. Strain hardening composites such as SHCC are still basically being used as protective coatings in structures such as large dams, tunnels or irrigation canals (Wittmann et al. 2010).

The post cracking responses of fibre reinforced cementitious composites do have much to do with the type of fibres used in its production. Some fibres are known to have relatively high tensile capacity and when used in concrete translates to improved tensile capacity of the concrete. The most important aspect of this enhanced tensile capacity is based on the interaction between the fibre and matrix under the action of load. This is further discussed in Section 2.1.2.

When stress is applied to a FRC element, the stress is initially almost completely borne by the concrete matrix until cracking sets in and the stresses are then transferred from the matrix to the fibres. It should be noted that unlike strain hardening cement-based composite (SHCC), the crack bridging capacity of fibres in typical FRC is less than the cracking strength of the concrete. When the pullout stress exceeds the bond stress between the matrix and the fibre, debonding begins to take place and the process controlling stress transfer at this stage becomes more of a frictional slip (Marotzke & Qiao, 1997). It should be known that the major role played by the fibres is only significant after a crack has formed in the matrix. Since the fibres are often randomly distributed in the matrix, stress is redistributed across all sections of the concrete member thereby enhancing the energy absorption capacity of FRC. The high deformation energy of fibre reinforced composites is now of great advantage (significant ductility and crack control) in many applications such as pavements, offshore structures, shotcrete, seismic structures, repairs, precast structures, hydraulic structures, etc. (Marara et al., 2011).

Despite all the significant research and developments in the field of FRC, structural applications using FRC are still limited. One of the factors inhibiting its use is the lack of appropriate standards and suitable certification (Laranjeira de Oliveira, 2010). Also, available guidelines for the use of fibre reinforced concrete e.g. fib Model Code 2010 (fib, 2010), do not take into account the creep deformation of this type of concrete (Zerbino & Barragan, 2012). A study of the time-dependent behaviour of macro synthetic FRC under sustained loading will be a major contribution to the future development of a harmonised design guidelines for the short and long term use and behaviour of structural synthetic fibres in concrete.

2.1.1 Macro synthetic fibre

Typical fibres that have been used over the past decades are steel, glass, xylon, asbestos, polyester, polyethylene, polyvinyl alcohol, rayon, wool and polypropylene. Those commonly used in concrete applications are steel, carbon and synthetic fibres (Yao et al., 2003). These fibres are available in different shapes and sizes and have a wide area of applications. Some areas of applications that have been noted include slabs on grade (industrial floors and pavements), shotcrete tunnel lining, prestressed concrete bridge beams, airport runways, and many non-structural elements (Brandt, 2008; Soutsos et al., 2012; Wang et al., 1987). In general, based on their sizes, they are divided into two categories; micro and macro fibres, see Table 2.1. Micro fibres are usually used at low volumes (up to 0.2 %) while macro fibres are used at high volumes (up to 2.0 % or more). The fibre used in this research project falls into Class 2. At higher dosages, workability problem is caused due to their relatively high surface areas necessitating the use of water reducers such as superplasticisers (MacKay, 2002).

Table 2.1: Polymer fibre classification (BS EN 14889-2, 2006)

Class 1a	Micro fibres, < 0.3 mm in diameter, mono-filament
Class 1b	Micro fibres, > 0.3 mm in diameter, fibrillated
Class 2	Macro fibres, > 0.3 mm diameter

Macro fibres or what is known as ‘structural fibres’ (steel or synthetic) are larger than the micro fibres and their diameters could range from 0.3 mm to 1.0 mm while their length could be between 15 to 60 mm. They are said to be structural because they exhibit structurally effective properties: increased toughness and/or load carrying capacity after cracking (Hwan Oh et al., 2005).

Macro synthetic fibres are gaining significant level of usage in a number of applications particularly in pavements and shotcrete. The use of these structural synthetic fibres has been reported to provide a significant level of post crack control in the same way as that achieved by steel fabric and steel fibres (Clements, 2002; Hwan Oh et al., 2005; Oh et al., 2007). According to Zheng & Feldman (1995), synthetic fibres, relatively also serve as cost effective replacement for the more expensive

fibres such as glass, asbestos and steel. Table 2.2 presents some types of synthetic fibres and their properties.

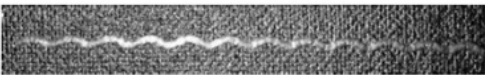
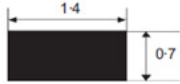
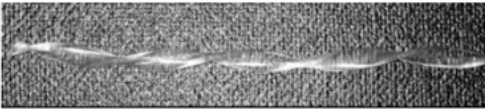
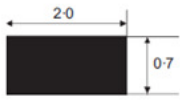
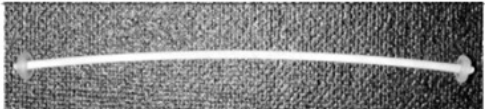
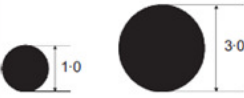
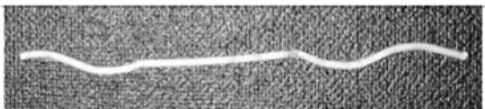

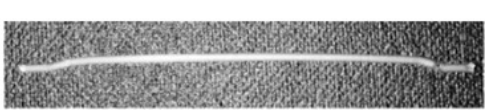

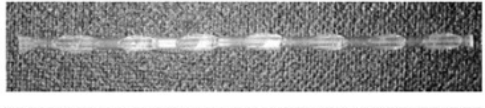
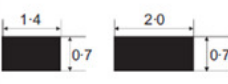


An important characteristic of fibres that generally determines the performance of the composite behaviour is the geometry of the fibre. The geometry of the fibre has an effect on the bond strength between the fibre and the matrix. A number of scholarly works has been published on the optimum geometry of macro synthetic fibres.

Table 2.2: Types and properties of typical synthetic fibres (Bentur & Mindess, 2006)

Fibre type	Diameter (mm)	Tensile strength (MPa)	Elastic modulus (MPa)	Ultimate Elongation (%)
Acrylic	0,020-0,350	200-1000	14000-19000	10-50
Carbon	0,008-0,019	500-4000	30000-480000	0,5-2,4
Kevlar	0,010-0,012 2	300-3500	63000-120000	2,0-4,5
Nylon	0,023-0,400	750-1000	4100-5200	16-20
Polyester	0,010-0,200	230-1,200	10,000-18,000	10-50
Polyethylene	0,025-1,000	80-600	5000	3,0-100
Polyolefin	0,150-0,640	275-2700	15	
Polypropylene				
-Monofilament	0,100-0,200	450-500	3500-5000	15-25
-Fibrillated	0,300-1,000	550-760	3500-9000	8,0
PVA	0,014-0,650	800-1500	29000-36000	5,7
Steel	0,100-1,000	500-2600	210,000	0,5-3,5
Concrete	3,0-7,0	10000-45000	0,02	

Won et al. (2006) investigated a number of macro synthetic fibres to determine the optimum geometry on the basis of the peak load produced between the fibre and the matrix and the interfacial toughness (see Table 2.3).

Table 2.3: Properties of different geometries of macro synthetic fibre (Won et al., 2006)

Photo of fibre	Fibre	Fibre geometry	Length: mm	Cross section: mm
	F1	Crimped type	50	
	F2	Twist type	50	
	F3	Enlarged ends type	50	
	F4	Sinusoidal ends type	50	
	F5	Hooked type	50	
	F6	Double duoform type	50	
	F7	Straight type	50	

The result of their work showed that crimped macro synthetic fibre gave better interface toughness (τ_b) in relation to the interface toughness of straight fibres, $\tau_{b, \text{straight}}$ (see Table 2.4).

Table 2.4: Effect of geometry on bond strength of macro synthetic fibre (Won et al., 2006)

Nature of fibre geometry	τ_b (MPa)	$\tau_b/\tau_{b, \text{straight}}$
Straight	0.28	1.00
Crimped	1.82	6.50
Twisted	0.56	2.00
Enlarged ends	0.71	2.54
Sinusoidal ends	0.72	2.57
End-hooks	0.40	1.43
Double Duoform	1.10	3.93

Similar studies were also carried out by Richardson (2005), Oh et al. (2007) and Choi et al. (2012). Some typical structural synthetic fibres with different geometric deformation investigated by

Oh et al. (2007) are shown in Figure 2.2. These authors have also reported optimum fibre geometry similar to the findings of Won et al. (2006). The macro synthetic fibre employed in this investigation has a crimped shape with a star cross-section similar to one of the fibre investigated by Choi et al. (2012). It is envisaged that with the double advantage of geometry and cross-section, the structural performance of macro synthetic FRC will be enhanced.

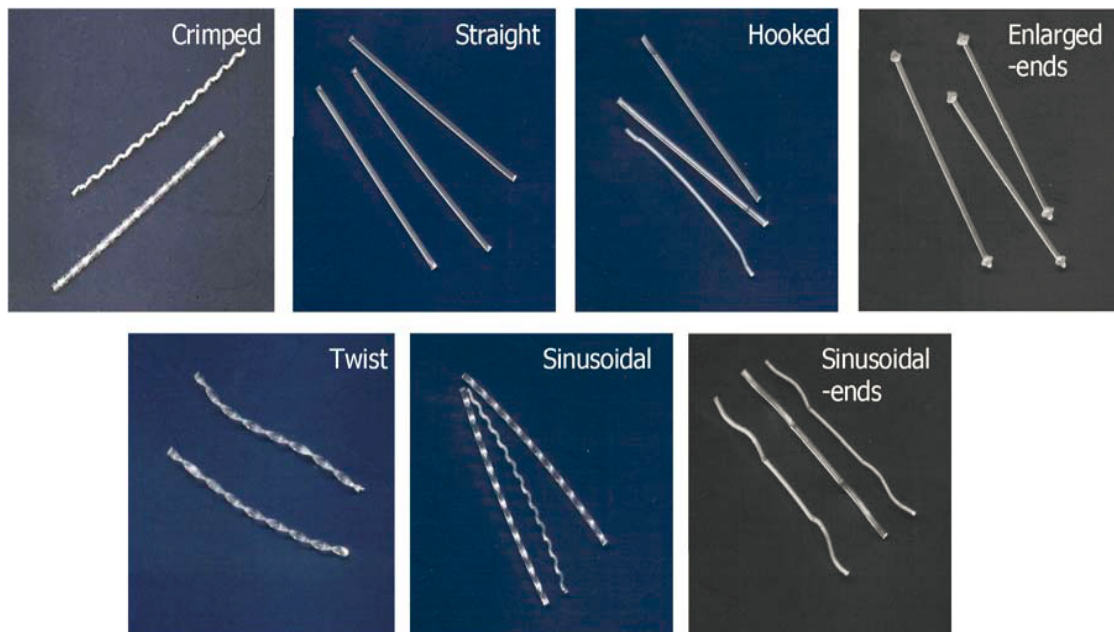


Figure 2.2: Structural synthetic fibres with different geometric deformations (Oh et al., 2007)

However, macro synthetic fibres are known to have a low elastic modulus varying between 5 and 10 GPa. Hence, they exhibit a poor deformation response under load (Hollaway, 1990). A number of factors can influence its mechanical response under load; stress, duration of application of load, loading rate, temperature, void content, fibre loading and dimensions (Banik et al., 2008; Hollaway, 1990). When these fibres are used in concrete, the mechanical behaviour of the composite in the cracked state is in turn influenced by the nature of the fibre/matrix interface and the response of the fibre.

Under long term loading, the fibres exhibit viscoelastic properties. Viscoelastic materials combine the dual properties of elastic solids and viscous fluids (MacKay & Trottier, 2004). If they are subjected to short time loading, they behave like elastic solids. If the load is removed, they recover all

the elastic strain created during the application of the load. On the other hand, if the load is maintained for a longer duration, then their behaviour becomes like that of a viscous fluid. Under this behaviour, if the load is eventually removed, they do not recover the viscous portion resulting in a permanent deformation.

In order to be able to understand the influence of fibre elongation on the time-dependent behaviour of macro synthetic FRC as done in this work at the macro level, a tensile creep test at the single fibre level was conducted. This helps to understand the elongation-time response of PP fibre under sustained load. Banik et al. (2008) acknowledged that the time-dependent behaviour of polymeric materials under a quasi-static state is usually studied by creep. Boshoff et al. (2009a) investigated the effect of the creep of a micro-fibre, Polyvinyl Alcohol (PVA) on the time-dependent behaviour of SHCC. The result of their experimental work showed that insignificant time-dependent deformation of PVA fibre was measured indicating that the fibre creep does not contribute to the widening phenomenon of cracks under sustained load. However, it is known that the creep of polymers occur because of a combination of the viscous flow components of viscoelastic deformation (Houshyar, et al., 2005). It is expected that the creep behaviour of PP fibre will have significant influence on the time-dependent behaviour of macro synthetic FRC.

2.1.2 Single fibre pullout behaviour

The mechanism responsible for the enhancement in performance of macro synthetic FRC at both macro and structural levels is rooted in the understanding of the micro level phenomenon. The micro-mechanical observation of FRC has to do with the response at the single fibre level and its pullout performance from a cementitious matrix. An understanding of the pullout mechanism of single fibres is paramount to designing structural elements for their desired mechanical performance.

Though this study does not intend to model the fibre pullout behaviour, an understanding of the pullout behaviour of macro synthetic PP fibre from the matrix will nevertheless give further insight into the mechanism responsible for the time-dependent crack widening of cracked fibre concrete.

Some factors influencing the pullout behaviour of fibres from the matrix are discussed in the following sections.

Fibre/matrix interface

In FRC, the region of bond between fibre and matrix has been noted to play a significant role if the fibres are to effectively control cracking, transfer load and enhance the energy absorption (Currie & Gardiner, 1989; Singh et al., 2004). This region known as the interfacial transition zone (ITZ). Wille & Naaman (2012) and Won et al. (2006) reported that the major parameter influencing the toughness and tensile response of FRC is the bond between the fibre and the cementitious matrix in this zone. The ITZ is made up of two layers; coarse aggregate surface (aggregate contact layer) and the porous transition zone otherwise called matrix contact layer (Bentur, 1990). The nature of this region has been reported to be different in the vicinity of the aggregate particles because the spatial arrangement of anhydrous grains becomes looser in this region (Ollivier et al, 1995; Prokopski & Halbiniak, 2000; Yue et al., 1995). While the former layer (aggregate contact) is composed of the CH crystals and C-S-H gel, the latter (matrix contact) has the formation of more CH compared to the former, some C-S-H gel and little ettringite (Liao et al., 2004). These two layers are weak in nature due to wall effect and hence, the nature of the zone influences the durability of the concrete. When dealing with FRC, the mechanical bond property of this zone is related to the geometric deformation of the fibre and the transversal stress resistance of the matrix (Bentur & Mindess, 2006; Wille & Naaman, 2012).

However, with increase in curing age of concrete, hydration products of C-S-H is said to increase rapidly in this region and filling the porous structures of this zone (Liao et al., 2004). The modification of this zone in normal concrete to improve strength of aggregate-paste interface has been adjudged to a number of factors, namely coating of aggregates with water-glass and CaCl₂ mixture, increasing grain roughness among others (Xueqan, et al., 1988). When fibres are introduced into concrete, fibre-matrix interface becomes an integral part. Usually, the fibres tend to introduce more

voids into the matrix if not well compacted and could lead to loss of strength. If the nature of the ITZ is to enhance the pullout behaviour of the fibre from the matrix, considerations have to be made. These relate to the aspect ratio (l_f/d_f) of the fibre, coarse aggregate size, strength of the matrix, fibre elastic modulus and the surface geometry of the fibre (Balaguru & Shah, 1992; Bentur & Mindess, 2006; Nanni et al., 1995). Fibres of different surface configurations, ranging from straight and smooth to deformed fibres have been used over the years to improve the bonding between the fibre and the matrix. It has been reported that when macro fibres are used in cementitious composites, adequate reinforcing efficiency can be achieved by inducing deformation in the fibres (Bentur & Mindess, 2006; Singh et al., 2004). They reported that this is particularly true for steel and polymeric fibres. In the investigation of the bond behaviour of macro synthetic fibre with different surface deformation, it has been reported that though the fibre is known to have a poor bond with the matrix because of its hydrophobic nature, crimped synthetic fibres have shown better interface toughness (Richardson, 2005; Richardson, 2004; Won et al., 2002; Won et al., 2006). The synthetic fibre used in this research work is a macro polypropylene fibre with a crimped surface geometry and an 'X' cross-sectional profile to enhance mechanical bonding. Details of the properties are presented in Chapter 3.

Cement fillers have also been reported to greatly improve the strength of the ITZ (Bentur & Mindess, 2006; Scrivener et al., 2004). A schematic description of the nature of the ITZ of a FRC is presented in Figure 2.3.

With the type of PP fibre used in this research as described, the bond between the matrix and the fibre is expected to be greatly increased compared to similar types with a smooth surface and a considerable pullout load is expected (Choi et al., 2012).

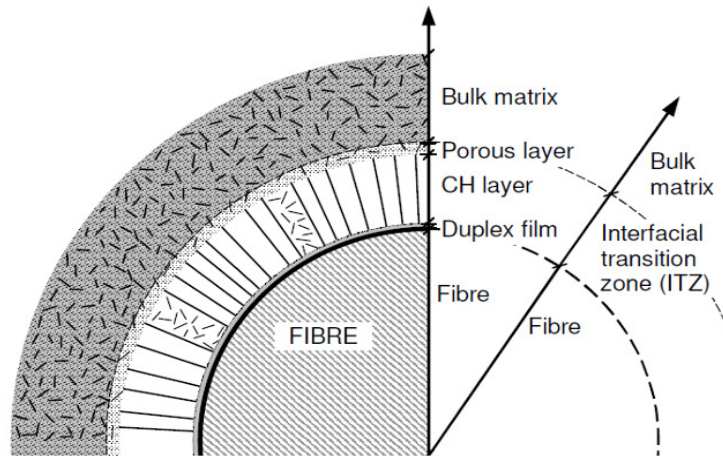


Figure 2.3: Schematic representation of the interfacial transition zone (ITZ) of a FRC (Bentur, 1991)

Crack bridging mechanism

When a crack occurs in normal concrete, coarse aggregates tend to bridge the crack. However, the crack propagates through the interface between the matrix and the aggregate. When the crack is a micro crack, coarse aggregate bridges the crack initiated. The bridging mechanism of coarse aggregate is fully described by Löfgren (2005) and schematically represented in Figure 2.4. At point (A), internal micro cracks are said to grow at the ITZ between cement paste and the coarse aggregate which eventually get into the mortar (B). At the peak stress (C), localization of crack begins and further propagates and the mechanism is that aggregate bridging and branching.

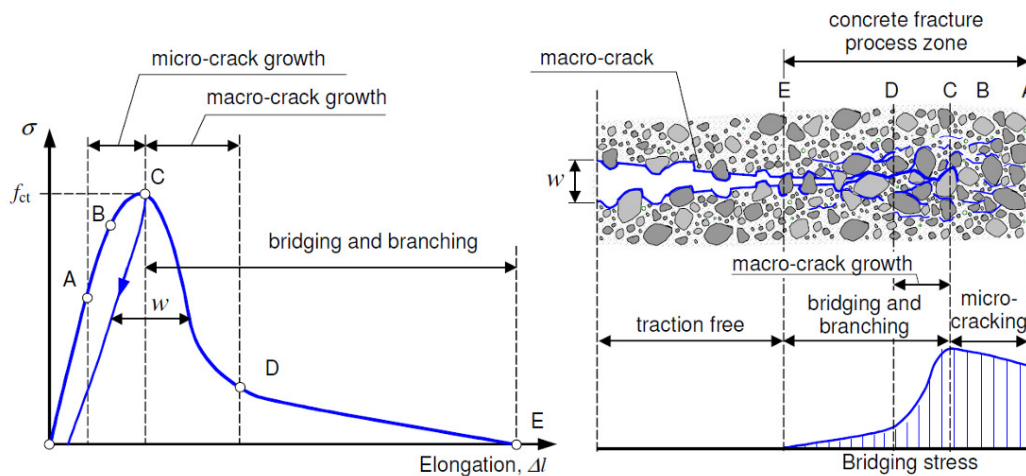


Figure 2.4: Aggregate bridging mechanism in uniaxial tension and the resulting stress-crack opening relationship (Löfgren, 2005)

In FRC, there are two possibilities depending on the crack width, namely combined bridging effect of aggregates and fibres, and fibre bridging mechanism. In the cracked state, stresses are transferred to the fibres. The fibres bridge the crack and reduce the opening rate thereby reducing the stress intensity factor at the crack tip (Singh et al., 2004). The crack width increases with time, but the composite shows high energy absorption during the crack propagation as a result of the fibre bridging mechanism. The fibre-matrix bond of the cement-based composite is of great importance as the crack propagates if the bridging mechanism of the fibres will stabilise the crack propagation. As earlier pointed out, the fibre bridging mechanism is itself influenced by a number of factors: the nature of the fibre/matrix interface, fibre aspect ratio (l_f/d_f), geometry of the fibre, matrix composition, orientation of the fibres and fibre volume.

Fibre bridging mechanism may be a complex phenomenon, but the response of a single fibre under a pullout load does help to understand the mechanism. The single fibre pullout test has come to be generally accepted for investigating fibre bridging mechanism in fibre reinforced composites (Bentur & Mindess, 2006; Zile & Zile, 2013). When load (P) is applied to a single fibre, three stages of stress transfer have been used to describe the bridging mechanism: debonding of the interface surrounding the fibre, frictional slip and finally, pullout of the fibre from the matrix (Li et al., 1993; Li & Stang, 1997). The load-pullout displacement (P - δ) curve can vary significantly from a straight to deformed fibre. Typical pullout behaviour of a straight fibre at an embedment length, L_e showing the stages of pullout is shown in Figure 2.5.

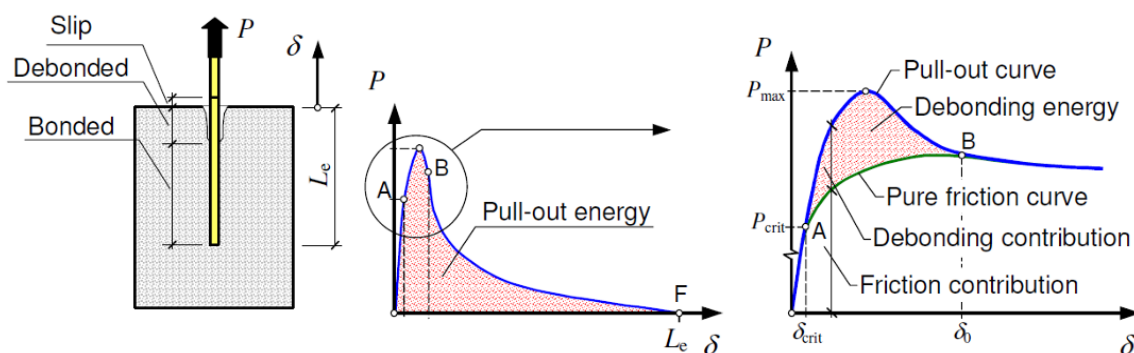


Figure 2.5: Single fibre pullout behaviour of a straight fibre (Löfgren, 2005)

In reality, fibres are randomly distributed and the inclination of the fibres at different angle is a factor for consideration in understanding the totality of the pullout behaviour. At a cracked plane, several fibres are acting to bridge the crack which makes it quite different from the single fibre pullout test. Increased fibre pullout force with an increase in angle of inclination has been reported (Fu & Luke, 1996; Li et al., 1990). It is acknowledged that there exist numerous research articles on the modelling of the pullout behaviour of steel and polymeric fibres taking orientation into consideration. However, in this research, fibre pullout was only investigated perpendicular to the crack plane in order to gain insight into the mechanism causing the time-dependent deformation of cracked FRC under sustained loading.

Test setup for single fibre pullout

Whereas it has become generally accepted to use the single fibre pullout test to investigate the fibre bridging mechanism in FRC, there is yet to be a generally accepted standard test setup for such investigation. Some of the test setups reported in literature for the single fibre pullout test are complex but a host of others are quite simple to develop and produces accurate results. Oh et al. (2005), Won et al. (2006) and Oh et al. (2007) used the same kind of setup to investigate the fibre pullout behaviour of macro synthetic fibres from cementitious matrix (see Figure 2.6).

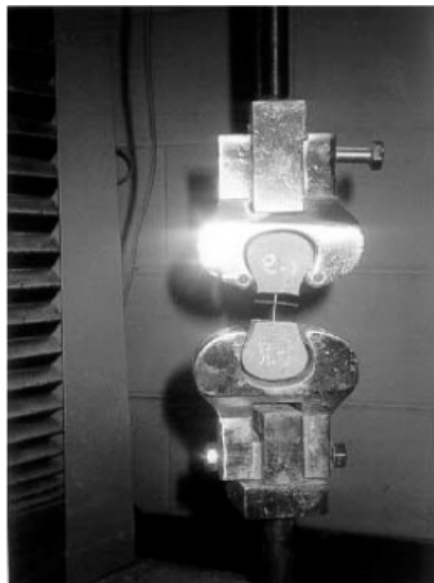


Figure 2.6: Single fibre pullout test setup (Hwan Oh et al., 2005; Oh et al., 2007; Won et al., 2006)

This setup has proven to produce accurate results from the report of the authors. However, the setup requires the fabrication of a special grooved component attached to the testing machine to hold the specimen in position (Figure 2.6). A different test setup was used by Kim et al. (2008) and Kay & Naaman (2012) as shown in Figure 2.7. It should be remarked that the fibre used in their investigation was steel fibres. The gripping system used for the fibre cannot be used for plastic fibres due to the possibility of damage to the fibre. Hence, a better gripping system that would not cause any damage to the plastic fibre is needful. In this work, two test specimens were produced from a concrete cube of 100 mm. Each mould was halved by a wooden block before casting of concrete was done. Demoulded specimens were then tested in a Zwick Z250 machine after the curing period of the specimens. The specimens were held in position by the hydraulic clamp of the test machine. The specimens are simple to produce and no further fabrication of grooved component is required as done by Hwan Oh et al. (2005); Oh et al. (2007) and Won et al. (2006). The details of the test specimens, clamping device and test procedures are fully discussed in Chapter 3.

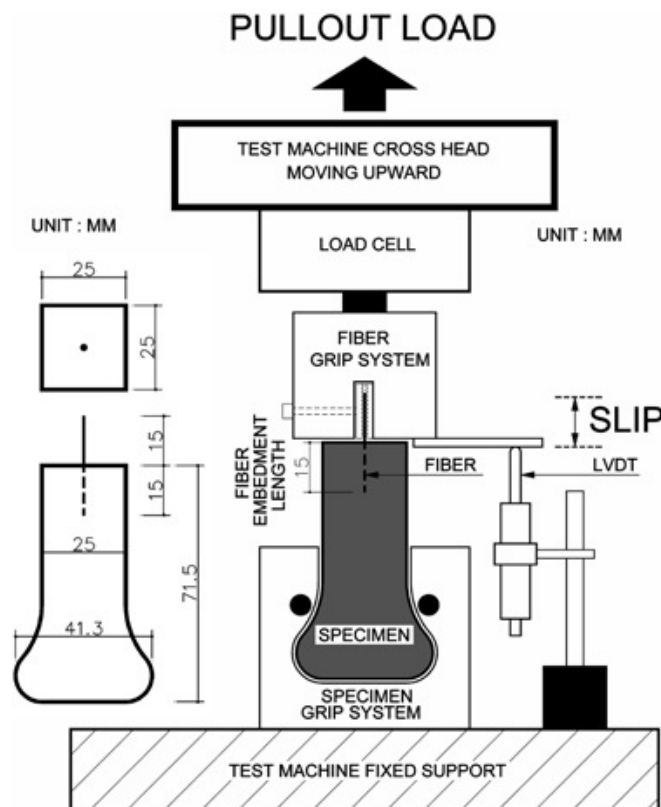


Figure 2.7: Pullout specimen and test setup for single fibre pullout (Kim et al. 2008; Kay & Naaman, 2012)

2.2 Time Dependent Behaviour of Cement-Based Materials

It has been acknowledged that the gradual increase of deformation of concrete with time is caused by shrinkage and creep under constant temperature and stress. Kovler (1995) noted that when serviceability, durability and long-term reliability of concrete structures are discussed, creep and shrinkage are important factors. While shrinkage is independent of stress, creep is a function of sustained stress. The description of these phenomena has been approached by scholars in different ways. As reported by Boshoff (2007), authors have approached it on the macro (phenomenological) and micro levels. He affirmed that the examination of these mechanisms at the micro level pose a difficulty due to the complexity and variability of the micro-structure of cement-based materials. However, to adequately and efficiently predict the effects of creep and shrinkage in a structure, there must be the availability of reliable data of the creep and shrinkage characteristics of the particular concrete.

2.2.1 Shrinkage of concrete

Shrinkage of concrete is a time-dependent volume change that occurs due to a number of mechanisms. Several mechanisms can be attributed to shrinkage at the micro and macro levels. Primarily, shrinkage has been reported to occur due to the movement of water in both fresh and hardened states (Neville, 2012). Since the focus of this research is to investigate the creep mechanism of cracked macro synthetic FRC, the mechanism of shrinkage on the macro level shall be focussed on. At this level, Boshoff (2007) reported that four phenomena have been identified, viz. drying shrinkage, hardening shrinkage also known as chemical shrinkage, autogenous shrinkage and carbonation shrinkage. Of these, the shrinkage that results in volume change after setting (post-setting shrinkage) of the cement-based composites is what is significant to unsealed specimens tested under creep loading.

Autogenous shrinkage results from water moving from capillary pores in the cement paste to unhydrated cement particles thereby causing macroscopic volume or length change (self-desiccation).

Practically, autogenous shrinkage is said to occur in the interior of the concrete mass and high values have been reported especially when the water-binder ratio (w/b) is very low, say 0.17 Neville (2012). This is usually the case when high strength/performance concrete (over 60 MPa) is involved. Since little water is available for hydration, the withdrawal of water from capillary pores for the hydration of unhydrated cement occurs. This process is known as self-desiccation. Neville (2012) also reported that it is usually measured alongside with drying shrinkage because it is expressed as a linear strain even though it is three-dimensional. It should however be noted that the strain caused by autogenous shrinkage is relatively small.

Drying shrinkage is the additional reduction in volume caused principally as a result of loss of water to unsaturated environment during the drying process of the cement-based material. Concrete undergoes autogenous shrinkage before drying shrinkage. As the concrete specimen begins to undergo drying at time t_0 , drying shrinkage occurs. Then when loaded, both basic and drying creep occurs in the drying specimen. Though it is known that shrinkage of concrete will almost continue throughout its existence, however Neville (2006) posited that for normal concrete, it does majorly occur within the first 90 days of placement. In dealing with the subject of shrinkage in concrete, as earlier mentioned, the aspect most concerned with structural performance of the concrete is that which deals with the exchange of moisture between the concrete and its environment.

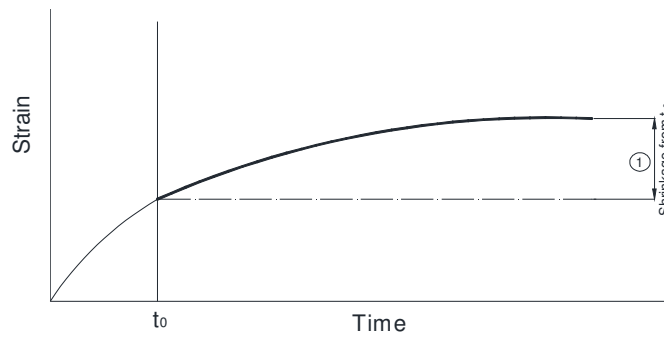
Shrinkage of concrete can occur both in the plastic and hardened state. In the plastic stage, fine synthetic fibres at a low volume have been successfully used to mitigate shrinkage cracking (Aly et al., 2008; Banthia & Gupta, 2006; Naaman et al., 2005; Qi et al., 2003). In the hardened state, few works have been reported on the effect of macro fibres on the drying shrinkage of FRC. Slight reduction in the free shrinkage of FRC has been reported using macro PVA fibre (Passuello et al., 2009; Sun et al., 2001). Whereas Passuello et al. (2009) attributed the small reduction in shrinkage to the modification of the water movement in the matrix due to the fibres, Sun et al. (2001) have suggested that the elastic modulus of the fibre, the fibre dosage and the aspect ratio have shown effects on the shrinkage. Indeed, the reduction or increase in drying shrinkage could

be fundamentally related to the mix properties, fibre properties and distribution within the matrix. Micro fibres are less spaced one from the other in the matrix and maybe responsible for the lesser shrinkage (Swamy & Stavrides, 1979) when used compared to macro fibres with more spacing (Sun et al., 2001). Some deviations have however been reported where micro PVA fibre was said to have resulted in an increase in the drying shrinkage due to increased voids created by the fibre addition (Amin et al., 2014). However, the shrinkage test conducted in this study does not seek to investigate the effect of macro fibres on shrinkage rather to distinguish it from the actual creep taking place on specimens subjected to tensile creep loads.

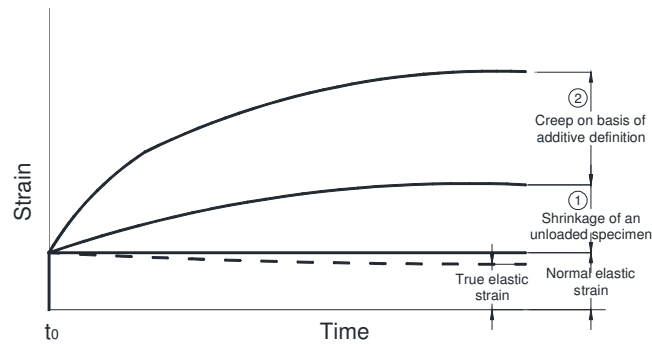
2.2.2 Creep

Creep is the tendency of materials to deform gradually with time under a sustained load. To structural engineers, time-dependent issues like shrinkage and creep of concrete under sustained load are a concern. It is known that creep can sometimes be beneficial in some structures as it lead to the re-distribution of stresses whereas in some cases, it leads to adverse effects (Bernard, 2004; Fanourakis & Ballim, 2003). Some of the adverse effects of creep can be seen in excessive deflection, elongation or shortening of concrete structures. These consequences of creep are known to render structures unserviceable with time and result in great economic losses. The other form of creep is experienced when strain is held constant with time in a stressed concrete specimen. This is termed as relaxation (Neville, 2012). The total deformation of cement-based composites under sustained load is due to the combined effect of shrinkage and creep. The additive nature is presented in Figure 2.8 a-d).

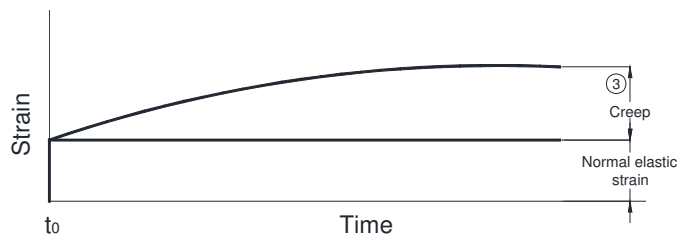
Figure 2.8 clearly shows that for a drying specimen under load, creep of the specimen is purely the addition of both basic and drying creep (Fanourakis & Ballim, 2003). As it has been earlier mentioned, four phenomena are used to explain the time-dependent behaviour of concrete: autogenous shrinkage, drying shrinkage, basic and drying creep. Since shrinkage has been discussed, the phenomena of basic and drying creep are discussed in the next section.



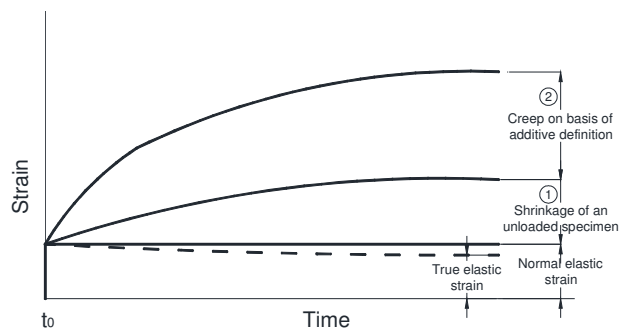
(a) Shrinkage of an unloaded specimen



(b) Changes in strain of loaded and drying specimen



(c) Creep of a loaded specimen in hygral equilibrium with the ambient medium



(d) Changes in strain of a loaded and drying specimen

Figure 2.8: Time-dependent deformation in concrete (Neville, 2012)

The net effect of creep for a drying specimen is therefore the total time-dependent deformation excluding the initial elastic strain and drying shrinkage.

Basic creep of concrete

The basic creep is the time-dependent deformation that occurs when the concrete specimen is loaded in a sealed condition so as to prevent the exchange of moisture with the environment. Research works such as those reported by Østergaard et al. (2001) and Westman (1995) examined the early age basic creep of concrete under compression and tensile response. Altoubat & Lange (2001) similarly investigated the basic tensile creep of concrete (normal weight and fibre reinforced). The purpose of their study was to distinguish autogenous shrinkage from the basic creep of early age concrete since drying of specimen is known to still occur even if there was no moisture loss to the environment. They investigated the difference by the moist cover test condition. The result of their experimental study at early age (first two days after casting) using steel fibres was able to distinguish autogenous shrinkage from basic creep. It is however significant to know that their results reported the influence of fibres on the basic creep. They reported high rate of basic tensile creep of the FRC within the first 10 to 20 hours of loading the concrete specimens as acknowledged by Østergaard et al. (2001). Hence, age at loading is a significant factor when creep is discussed. Westman (1995) also opined in his investigation that the basic compression creep was age dependent. Some other researchers have reported attempts to distinction between autogenous shrinkage and basic creep by experimental measurements. This is however not a part of this study since it had been earlier mentioned that the total shrinkage (addition of autogenous and drying shrinkage), referred to as drying shrinkage, measured on an unloaded drying specimen is what is of interest for this study. This is because the specimens were tested unsealed, hence drying occurred at the same time.

Drying creep of concrete

Drying creep is said to be the time-dependent deformation that occurs in a specimen under constant stress in a drying or unsealed condition. While basic creep is a material property only, drying creep and shrinkage depend on the environment and size of the specimen. Altoubat & Lange (2003) reported that surface micro-cracking and stress-induced shrinkage are the phenomena responsible for

drying shrinkage. The total creep occurring in reality will be the combination of the basic and drying creep phenomena, sometimes, one being the dominating factor. The Pickett-effect describes the effect that no creep is experienced if concrete has been previously dried before loading but that when it is prevented from exchange of moisture with the environment (basic creep), the more the evaporable water it contains, the more the creep experienced during loading condition. The creep is even said to be more pronounced than the first two cases when the concrete is drying out during loading. The discrepancy earlier mentioned is reported to be caused by a mechanism named drying creep and was said to be first reported by Pickett (1942).

2.2.3 The mechanism causing creep in concrete

It has been observed that unlike other construction materials like steel, concrete is known to considerably undergo deformation under a constant application of stress and service conditions (MacKay & Trottier, 2004). Even though a number of scholarly works have been produced on the time-dependent changes in the mechanical properties of concrete, Alizadeh et al. (2010) observed that creep of cement-based systems is yet to be fully understood. Since creep is the increase in the strain of a material or structure under a constant load over a period of time, most authors have agreed that it occurs primarily in the hydrated cement paste (Alizadeh et al., 2010; Hope & Brown, 1975; Neville, 2012). Since it has been observed that when concrete is subjected to loading, the normal weight aggregate does not actually creep, the mechanism of creep rests with the paste (Neville, 2012). In this light, Bernard (2004) posited that concrete under sustained load, will cause the movement of moisture within the calcium silicate hydrated (C-S-H) phase of cement paste. This statement was also corroborated by MacKay (2002).

Though a number of factors have been adjudged to be responsible for or contributing to creep in concrete, however, solidification theory for short-term aging and microstress of creep sites in cement gel microstructure, causing the Pickett effect and long-term aging have been reported (Bažant, 2001) to be sufficient to explain most if not all the basic experimental evidence. Bažant in

Alizadeh et al. (2010) explained the microprestress-solidification theory to mean that the overstressed unstable atomic-scale bonds are locally broken and reformed in the ‘hindered’ adsorbed water molecule sites (including that in the C-S-H interlayer). This eventually leads to the quasi-dislocation of surrounding particles which contributes to the long-term creep.

2.2.4 Creep behaviour of concrete under sustained load

The well-known behaviour of concrete under the action of sustained stress is depicted in Figure 2.9. It is common knowledge that concrete will creep for a long time if not indefinitely under load as reported by Troxell et al. (1958). When concrete is under a constant load, it first experiences an instantaneous (elastic) deformation after which the primary creep starts. The rate of this deformation soon decreases with the passage of time. If the sustained load is however removed, the concrete experiences full recovery of the elastic strain (elastic recovery).

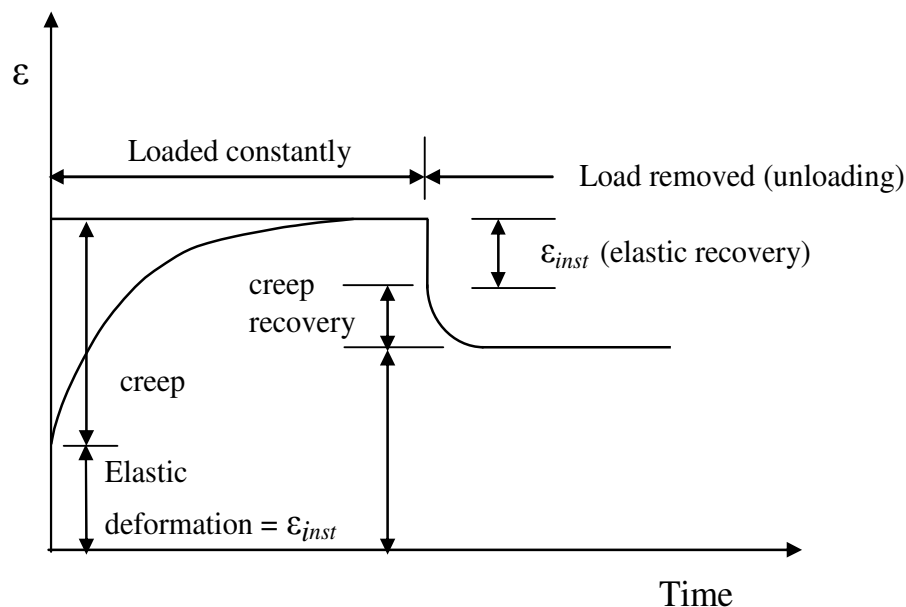


Figure 2.9: Strain-time relationship of concrete under sustained loading

It has been acknowledged by several scholars that this recovery is usually smaller than the initial elastic strain, as the modulus of elasticity increases with time. Thereafter, a delayed recovery of creep is experienced. MacKay & Trottier (2004) reported a similarity between the shapes of creep recovery curve as somewhat the inverse of the creep curve but however observed that creep recovery occurs

more rapidly than creep due to loading. After concrete has undergone creep deformation and creep recovery, a residual deformation is often the end product. One study has shown that after several years, creep strain typically reaches 2 to 6 times larger than the initial elastic strain. This behaviour of concrete demonstrates its viscoelastic response under time-dependent investigation.

Creep deformation of concrete occurs in three stages (Illston, 1965). The essence of the distinction was to show the difference between recoverable and residual deformation. When concrete is loaded, the initial increase in deformation is referred to as primary creep and the secondary creep is relatively a steady deformation region which is dominant in the medium to long term. This is depicted schematically in Figure 2.10

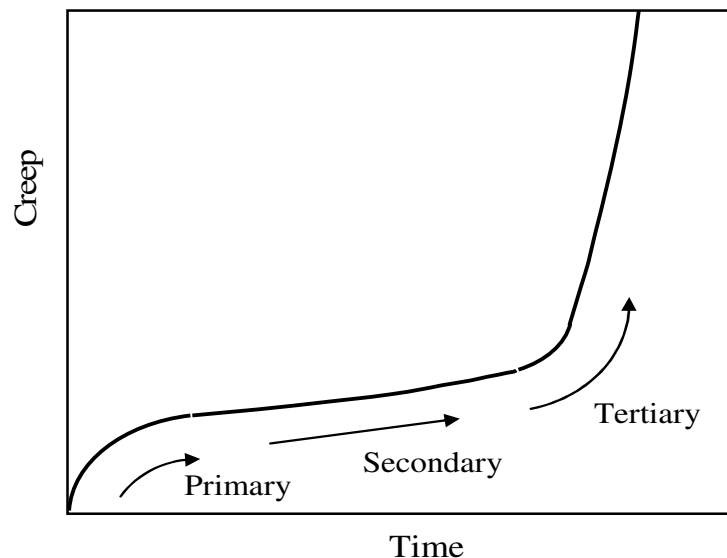


Figure 2.10: Component of creep strain

The tertiary creep region is said to lead to creep failure when the creep limit is exceeded as shown in Figure 2.11.

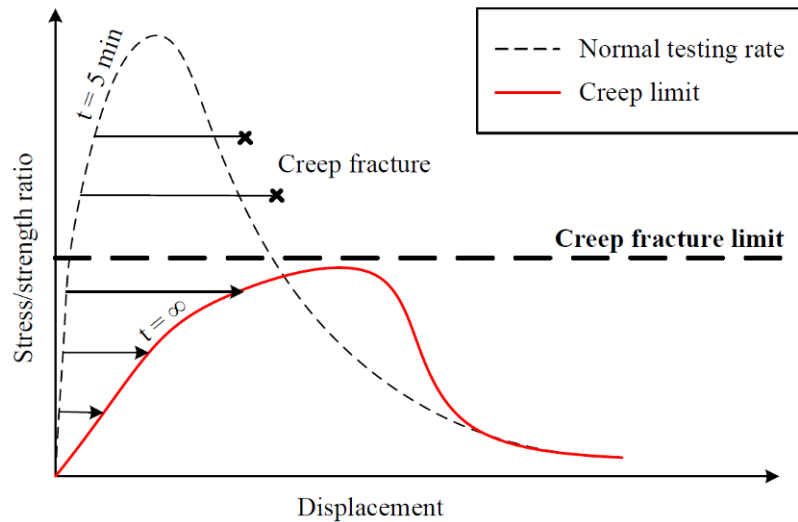


Figure 2.11: Schematic representation of creep fracture and creep limit (Boshoff, 2007)

2.3 Time-Dependent Behaviour of Cracked FRC

The time-dependent behaviour of concrete has been discussed in the preceding section. Creep of concrete has been extensively discussed and quantified in literature. With FRC however, much still remains unknown. Since fibres only become engaged after the initiation of the first crack, the time-dependent behaviour of FRC should be investigated and discussed in its cracked state. More interestingly, since there seems to be no available design code that takes into account the creep of FRC in the cracked state, a study of this nature will provide useful information, particularly with respect to the time-dependent behaviour of macro synthetic FRC which is the focus of this research project.

2.3.1 Uniaxial tensile response of cracked FRC

Due to the weakness of concrete in tension, cracks propagate easily and damage emanating from tensile stresses can lead to serious serviceability and durability problems. However, with the inclusion of fibres in concrete, as earlier discussed, these problems have been greatly curtailed. Though several test methods (modulus of rupture test, direct tension test, wedge splitting test, split cylinder) are being used to investigate the behaviour of concrete under tension, it has been acknowledged that the uniaxial tension test provides a more accurate and reliable test results (Mallat & Alliche, 2011; Stang

& Li, 2004; Swaddiwudhipong et al., 2003). The response of a specimen tested under uniaxial tensile test for steel FRC is shown in Figure 2.12. The behaviour shown for the steel FRC is also similar to the behaviour of strain softening macro synthetic FRC.

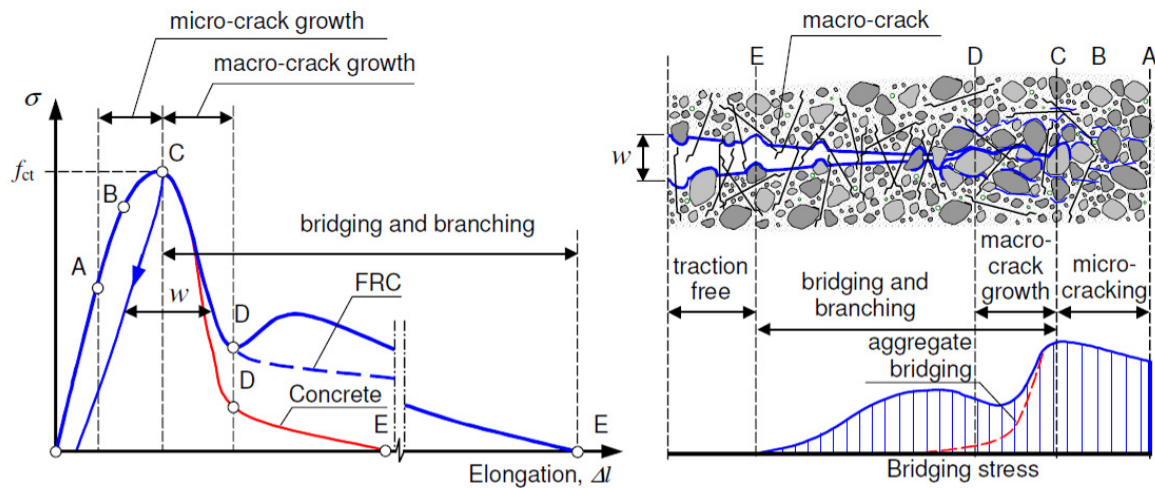


Figure 2.12: Effect of fibres on the fracture process in uniaxial tension (Löfgren, 2005)

A linear elastic behaviour characteristic of the concrete matrix is first observed (up to Point A). Synthetic fibres have no contribution at this stage until the first crack is initiated (Point B). As a result of the low elastic modulus of the fibre compared the concrete, there is a sudden drop in ultimate uniaxial strength, f_{ct} (Point C to D) before the synthetic fibres are fully engaged for crack bridging. This phenomenon of significant loss in stress before fibre activation is much lower when steel fibres are used because of its higher elastic modulus. Thereafter, a non-linear phase is entered which is characterised by crack bridging with controlled crack opening (w). At this stage, fibre pullout, elongation, Δl and finally fracture are some of the possibilities that can be experienced.

Most studies on creep of concrete have been on compressive creep. Though some researchers have multiplied the creep coefficient of compressive stress by a factor between 1 to 3 to describe the equivalent coefficient describing tensile creep (Bazant & Oh, 1984), it has been suggested that it appears the mechanism of creep in tension differs from that in compression (Gilbert & Ranzi, 2010). Østergaard et al. (2001) affirmed that the rate of change of tensile creep with time does not decrease in the same manner as for compressive creep.

The limited number of works on uniaxial tension test/creep has to do with the technicalities of the experimental setup: load transmitting mechanism (stress concentration) and boundary condition (moment transmission) (Kanakubo, 2006). One study has acknowledged the fact that it is a difficult type of test to execute (Altoubat & Lange, 2001). Some works have been published on tensile creep but majority of these researches are still limited to a short-term study (Bissonnette et al., 2007; Gutsch & Rostásy, 1995; Kamen et al., 2009; Kanakubo, 2006; Østergaard et al., 2001; Swaddiwudhipong et al., 2003). Some scholars have reported results of the long term uniaxial tensile creep of uncracked fibre reinforced composites as mentioned in Chapter 1. Not many works can be found on the time-dependent uniaxial tensile deformation of (pre-) cracked FRC.

The few published articles on the uniaxial tensile creep of cracked FRC were reported by Boshoff et al. (2009a), Mouton & Boshoff (2012), Zhao et al. (2012), Boshoff & Adendorff (2013) and Zhao et al. (2014). Apart from the work reported by Boshoff et al. (2009a) and Boshoff & Adendorff (2013), which used a micro synthetic fibre (PVA), all others investigated steel FRC.

Mouton & Boshoff (2012) cracked notched uniaxial tensile specimens made from self-compacting concrete to crack width of 0.5 mm under a uniaxial tensile test and then transferred the specimens to a uniaxial tensile creep frame where they were subjected them to permanent loads equivalent to 50% of the residual axial tensile strength. Though a significant scatter in results were reported for the three prismatic specimens tested, total crack opening range from 0.07-1.23 mm (almost double the instantaneous cracking opening for each specimen) after a period of three months. This study adopted the same approach used by Mouton & Boshoff (2012) to investigate the time-dependent crack widening of cracked macro synthetic FRC subjected to different stress levels. Details of the specimen design and uniaxial tensile creep frame used is discussed in Chapter 3.

Boshoff et al. (2009a) and Boshoff & Andendorff (2013) examined the tensile creep of SHCC using dumb-bell shape specimens. Test setup used to investigate the tensile creep at different stress levels and the time-dependent crack widening is shown in Figure 2.13. Significant tensile strain of

SHCC under uniaxial tensile loading was reported which is directly influenced by the load level. The mechanisms responsible for the time-dependent creep of cracked SHCC were reported to be crack widening and fibre pullout. It was remarked in their investigation that the creep of PVA fibre did not contribute to the overall creep of tested specimens. For macro synthetic fibres, significant creep of the fibre is expected to contribute to the time-dependent crack widening as reported in Section 2.1.1.

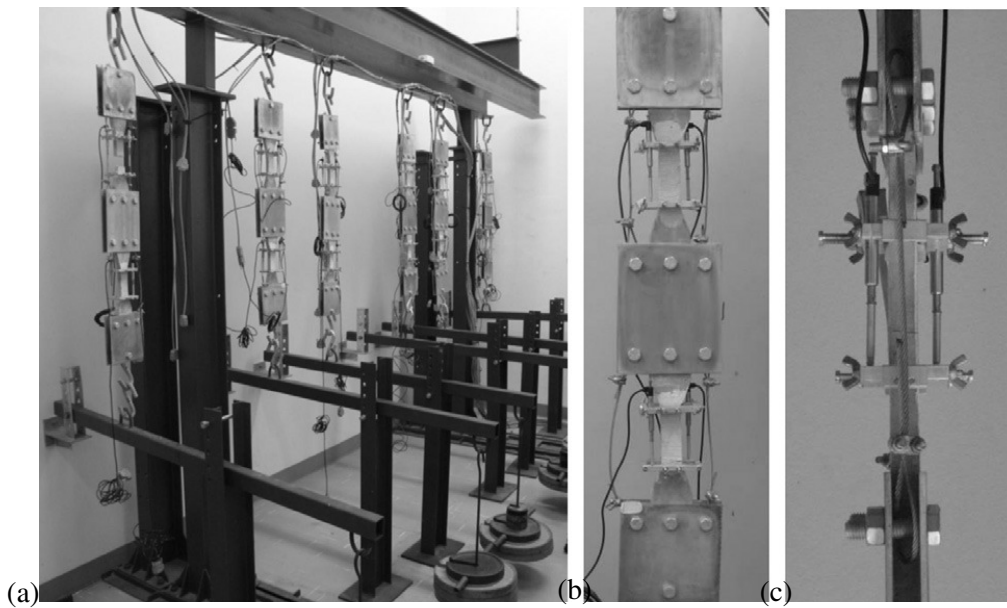


Figure 2.13: (a) Tensile creep setup, and (b) and (c), the tensile creep clamps (Boshoff & Anderdoff, 2013)

Recently, Zhao et al. (2014) reported the tensile creep of cracked steel FRC. The variables considered were precracked width and load level. Cylindrical specimens cored from prisms were initially cracked in a uniaxial tensile test to a crack width of 0.05 mm and 0.2 mm before being subjected to creep load at 30 % and later increased to 60 % of the average residual strength of each specimen. A schematic representation of the tensile creep frame developed to investigate the response of cracked steel FRC under sustained loading is shown in Figure 2.14.

After 6 months of subjecting specimens to sustained uniaxial tensile loading, the result of their investigation is presented in Figure 2.15.

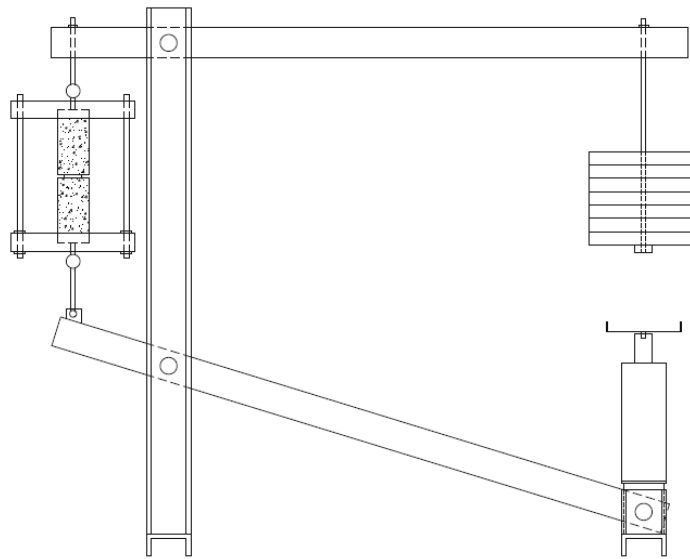


Figure 2.14: Uniaxial tensile creep frame (Zhao et al., 2014)

Zhao et al. (2014) reported that the deferred crack opening after an initial 3 months period is almost the same as the instantaneous deformation which proved it to be an elastic deformation. It should be noted that steel fibres do not creep under sustained load. As previously discussed, with macro synthetic FRC, this phenomenon might not be expected because macro synthetic fibres behave as viscous material under sustained loading. The results in Figure 2.15 a-c) indicate that at 30 % of the maximum pre-cracking load P_{max} , the deferred crack opening did not exceed 0.25 mm. Specimens labelled s6.1, s3.1, and s12.2 were unloaded after 180 days of sustained loading and reloaded to the same stress level whereas Specimens s4.1 and s4.2 were unloaded after 160 days before they were reloaded to a higher load level of 60 % P_{max} . The irrecoverable crack width of each specimen after pre-cracking, w_{irr} , is shown in Figure 2.15.

For specimens whose load where latter increased to 60 %, the creep increased as well. Hence, load level is a major consideration when investigating the time-dependent crack opening of crack FRC.

The tensile creep of cracked macro synthetic FRC could result in significant crack width increase more than cracked steel FRC, increase in deflection for structural elements and even creep fracture, hence, raising a serious concern.

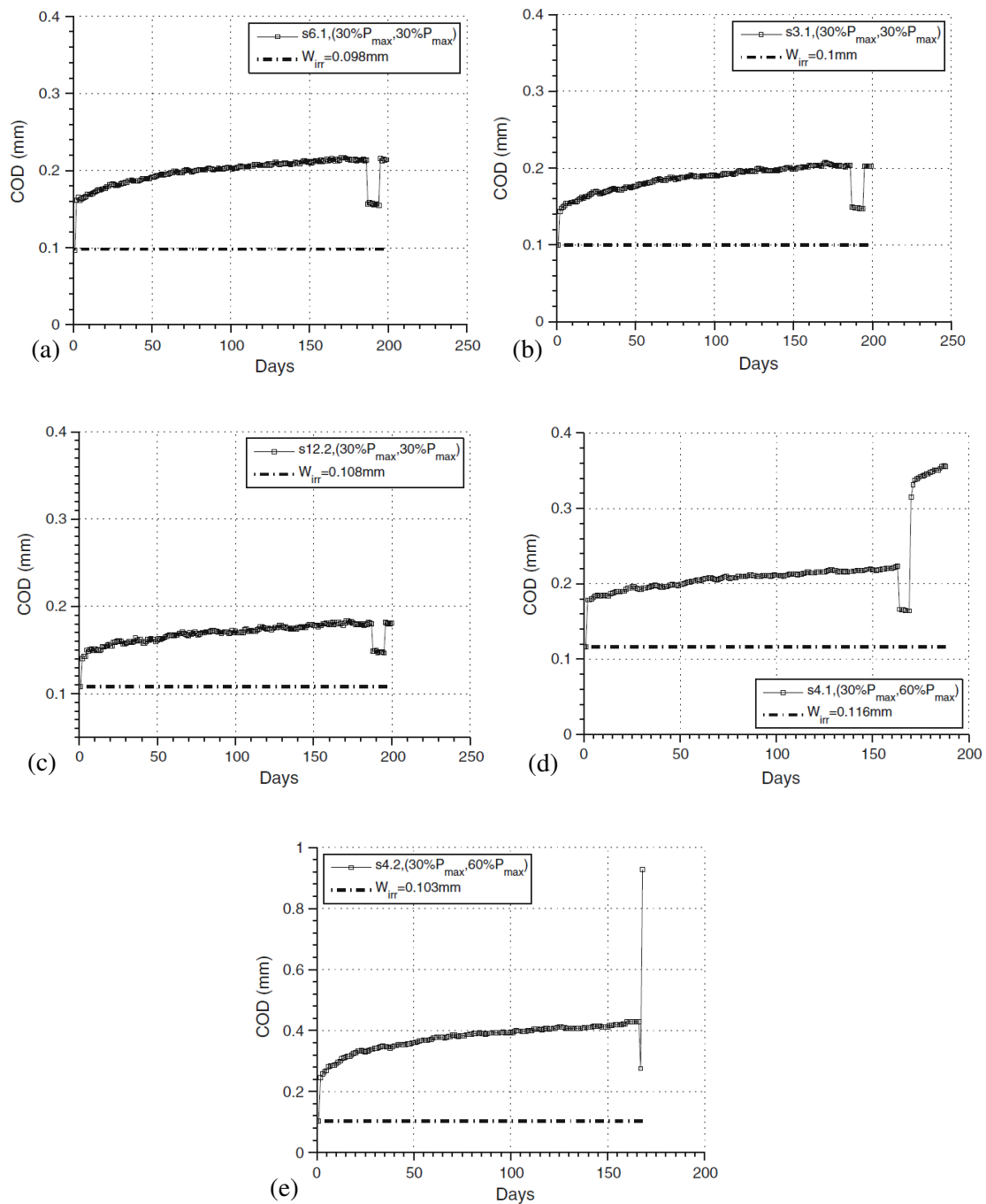


Figure 2.15: Tensile creep result of specimens (Zhao et al., 2014)

2.3.2 Flexural tensile response of cracked FRC

RILEM TC 162-TDF (Vandewalle, 2000) committee's proposal for the bending test of steel FRC has made significant advances regarding toughness and residual strength characterization under bending (Barragán et al., 2008). Even though the possibility of cracking in service was considered, the long-term behaviour under cracked condition was not considered. Since most structural elements are

usually under flexural stresses, design rules ignoring the long term behaviour of cracked FRC under sustained loading would be inadequate.

Lately, scholarly articles are now giving attention to the investigation of the time-dependent behaviour of cracked FRC under sustained flexural loading. However, majority of the works have been focussed on steel FRC (Arango et al., 2012; Barragán et al., 2008; Barragán & Zerbino, 2008; Chanvillard & Roque, 1999; García-Taengua et al., 2014; Kanstad & Zirgulis, 2012; Nakov & Markovski, 2012; Zerbino & Barragan, 2012).

Granju et al. (2000) investigated the creep behaviour of cracked steel FRC under sustained stress of 60 % of the residual flexural strength for one year and reported the stability of the creep strain after a period of six months. Though Granju et al. (2000) observed that the effect of creep was lesser than that of fatigue in specimens tested, their detrimental effect on a structure should be a concern.

In a similar research project using steel fibres, data from Arango et al. (2012) showed crack width in the range of 0.8 to 1.4 mm after sustained load for 365 days. Zerbino & Barragan (2012) reported the flexural creep response of self-consolidating steel FRC ($V_f = 0.5\%$) at varying load levels tested for about 21 months. The results of the specimens which showed strain-hardening behaviour indicate low crack opening rate for 1.5 years for pre-cracked width of 0.2 mm and 0.5 mm even when the stress level applied was 100 % of the residual flexural strength. In fact, at 50 % stress level, crack-opening rate was said to be very minimal.

Others have compared the creep of steel FRC to synthetic FRC (MacKay, 2002; MacKay & Trottier, 2004). MacKay & Trottier (2004) reported sustainable creep behaviour of steel FRC and synthetic FRC at 60 % residual flexural strength for 1 year. Kurtz & Balaguru (2000) compared the flexural creep behaviour of two polymeric FRC: PP fibre (fibrillating) and nylon 6 (single filament) at $V_f = 0.1\%$. Their results indicated that PP fibre could only sustain a stress of 24.9% of the average residual strength at such low volume.

Since most of this research was on steel FRC, the flexural creep behaviour of cracked macro synthetic FRC still needs further investigation. The study above only used PP fibre at 4.55 kg/m^3 (0.5 % by volume). This study uses macro synthetic fibres at a higher content, 9.1 kg/m^3 (1.0% by volume).

Arango et al. (2012) acknowledged the need to develop a flexural test setup that is simple, and guarantees enough stiffness throughout test duration. Building from previous flexural creep frames, a new and reliable concept was developed (see Figure 2.16). More recent works have employed the same setup for the investigation of flexural creep of cracked steel FRC (Zerbino & Barragan, 2012; García-Taengua et al. 2014). The investigation of the time-dependent crack widening of cracked macro synthetic FRC under sustained loading has also adopted this setup with minor modifications. Details of the flexural creep setup are presented in Chapter 3.

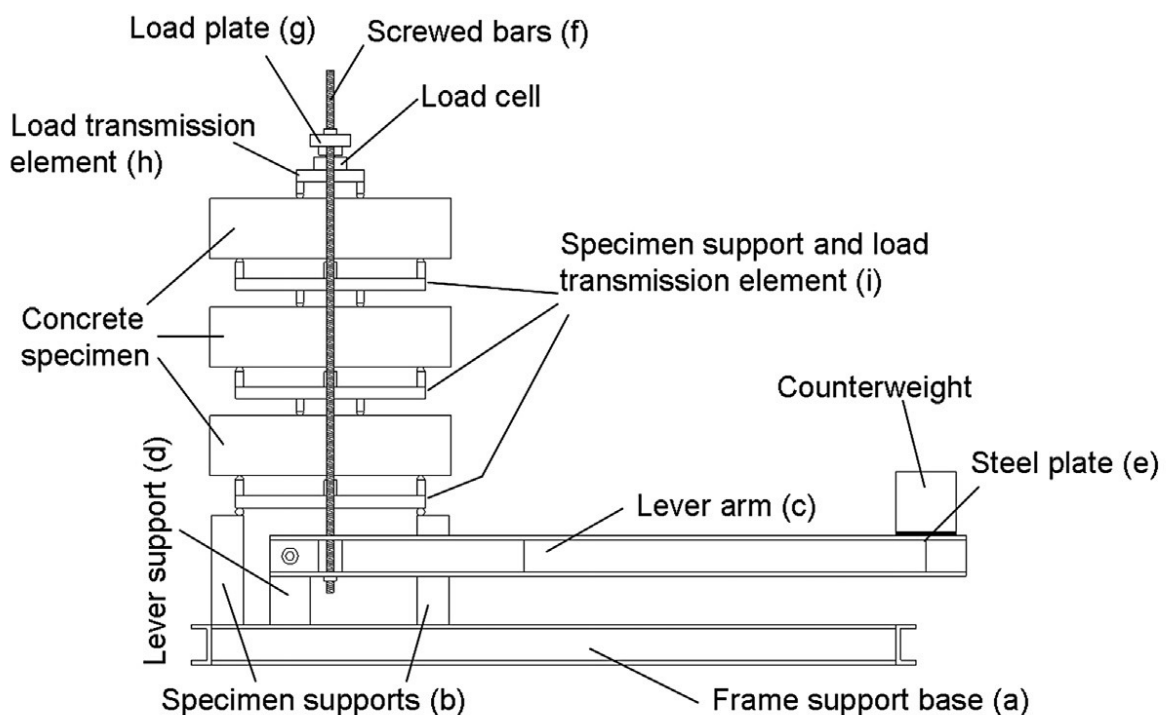


Figure 2.16: Flexural creep setup (Arango et al., 2012; García-Taengua et al. 2014)

2.4 Summary

The use of macro synthetic fibres in concrete has been said to date back to the mid-1980s (The Concrete Society, 2003). While several articles have been published dealing with the technical merits of using fibre reinforced concrete, the time-dependent behaviour of such material under sustained loading is a matter still little investigated. Under sustained load, materials deform with time which could lead to serious serviceability issues and ultimately collapse. Since fibres in concrete become engaged only after the formation of cracks, it is important to investigate such phenomenon of FRC in a cracked state to simulate the in-service condition. A review of the existing body of knowledge has been presented beginning with an understanding of the peculiar behaviour of FRC under quasi-static loads. It has been shown that the synthetic fibres also play major role in the overall behaviour of elements reinforced with such fibres. An understanding of the time-dependent behaviour of FRC under sustained loading in uniaxial tension and flexure has also been discussed. It is evident that much is still not understood about the creep (time-dependent crack widening) of cracked macro synthetic FRC and the mechanism causing it. This is due to the fact that there is no published work on the uniaxial tensile creep of cracked macro synthetic FRC. To understand the time-dependent behaviour, this study has been grouped into three sections: macro, single fibre and structural level investigations. The single fibre level is done to understand the mechanisms causing creep.

Chapter 3

Materials and Experimental Method

To understand the behaviour of macro synthetic FRC under short term and particularly, the time-dependent deformation of this type of concrete and the mechanism responsible for the deformation, experimental tests were performed at three levels of investigations. These are the macro, single fibre and structural levels. At the macro level, the compressive strength of concrete reinforced with and without macro synthetic fibres, uniaxial tensile strength test and uniaxial tensile creep of cracked macro synthetic FRC were investigated. The single fibre level of the experiments entails the study of the mechanism causing the time-dependent crack widening of the cracked macro synthetic FRC. This was pursued through the time-dependent single fibre pullout test and the response of a single fibre to creep under sustained loading. Other tests at the single fibre level also performed were the responses of single fibres embedded in the concrete matrix at different embedment lengths to loading rates, and the behaviour of single fibres to loading rates under tensile loadings. At the structural level, beams were subjected to three and four point flexural loadings to study their post cracking behaviour. Time-dependent flexural tests were also performed on the structural level to investigate the crack widening behaviour of the cracked macro synthetic FRC and the results were used to validate the finite element analysis carried out.

The materials used for the investigations were: cement, sand, stone, fibre and superplasticiser, the concrete mixture, preparation of moulds, casting of specimens and demoulding, curing, specimen preparation for testing, experimental test instrumentations, and the test procedures employed to achieve the set objectives of this research project. A presentation of the step by step methodology followed in performing the aforementioned investigations is then presented. The summary of the type of tests performed at the macro and structural levels indicating the condition of the specimens at testing, numbers of specimen per test, and specimen sizes are presented in Table 3.1. Details of the

tests performed at the single fibre level are presented in subsequent sections. All tests were conducted in a climate controlled room with a temperature of 23 ± 1 °C and a relative humidity of $65\pm 5\%$.

Table 3.1: Experimental tests conducted at macro and structural levels

Test conducted	Specimen condition	No. of specimen	% loading	Specimen size (mm ³)
Macro level investigations				
Compressive strength	-	10	-	100 × 100 × 100
Uniaxial tensile strength	Notched	3	-	500 × 100 × 100
Uniaxial tensile Creep	Notched	16	30/40/50/60/70	
Drying shrinkage	Un-notched & unloaded	4	-	
Structural level investigations				
Flexural strength (3- and 4-point)	Notched	5	-	700 × 150 × 150
Flexural creep	Notched	6	30 and 50	

3.1 Materials

3.1.1 Concrete mix materials

The materials used for the concrete mix throughout the investigations conducted in this research work are: CEM I 52.5N Portland cement, natural sand (with fineness modulus, FM = 2.34), 6 mm greywacke crushed stone and polypropylene (PP) fibres added at a fibre volume of 1 %. At least 90 % of the coarse aggregate used passes through the 6 mm sieve size and retained on a 4.75 mm sieve. A superplasticiser based on acrylic polymer, classified according to BS EN 934-2 (2009) was added to adjust the workability of the concrete mix at a dosage of 0.2 % by weight of the binder.

3.1.2 Macro synthetic polypropylene fibre

The fibre used in this investigation as mentioned was macro PP. They were supplied by Fibsol (Fibre Reinforcing Solutions), South Africa, with a trade name Macrosol CX 50/40 SS. The fibres were supplied in a collated form with an “X” profile. The intent of the fibre profile is to enhance the bond between the fibre and the matrix. To the author’s knowledge, no study on this type of fibre has been reported in literature yet. According to the manufacturers, the fibre is designed to enhance proper

bonding between the fibre and the matrix by giving it a star cross-section and crimped geometry. Figure 3.1 shows the monofilament fibre with its crimped configuration while Table 3.2 gives the properties of the fibre as obtained from the suppliers.

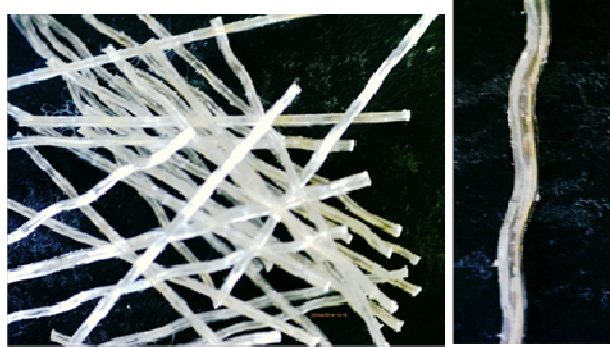


Figure 3.1: Macro monofilament synthetic PP fibre with crimped geometry

Macrosol fibres are said to be manufactured from 100 % virgin polypropylene with a continuous deformed profile along the entire length of the fibre resulting in optimum performance within the concrete matrix.

Table 3.2: Properties of macro synthetic (polypropylene) fibres

Specific gravity	0.88-092
Modulus of elasticity	4.3 GPa
Colour	Translucent
Elongation at yield	15 and 25 %
Tensile strength	400 MPa
Melting point	150-170 °C
Length (l_f)	40 mm
Diameter (d_f)	0.8 mm
Aspect ratio (l_f/d_f)	50

It should be mentioned that, since the fibre does not have a circular cross-sectional area, the effective fibre diameter was computed and used in the analysis of all results. The effective fibre diameter was computed by weighing ten fibres to obtain the mass (in grammes) and divided by the density of the fibre to obtain its volume. Since the length of the fibre is known, the effective diameter was obtained from the area.

3.1.3 Concrete mixture

In this research project, all samples cast and tested were performed from only one mix. In designing a concrete mixture for FRC, adequate care should be taken in the choice of constituent material and the size of the coarse aggregate. The fibre aspect ratio and fibre volume are also factors for consideration. These factors have been reported to have some influence on the ultimate behaviour of the fibre concrete (Susetyo et al., 2010). The choice of appropriate fibre aspect ratio and volume will ensure the correct distribution of fibres in the mixture and improve the fibre/matrix structure; hence, the relationship between maximum grain size and fibre volume in per cent given by Kobayashi & Cho (1976) and represented the following equation:

$$S = 5 \sqrt{\frac{\pi}{0.002 l_f / d_f + 0.4} \frac{d_f}{\sqrt{v_f}} - d_f} \quad 3.1$$

where S = maximum grain size in [mm]; l_f = fibre length in [mm]; d_f = diameter of fibre in [mm]; V_f = volume ratio of fibre.

A normal strength concrete of Strength class C45 (cube compressive strength) based on the Model Code 2010 was set out to be achieved. Several trial mixes were carried out without neglecting the consideration for workability. The concrete mix design used in this research is presented in Table 3.3.

Table 3.3: Concrete mixture design for PPFRC

Materials Type	kg/m ³
Cement (CEM I 52.5N)	395
Stone (Greywacke, max. 6 mm)	800
Sand	990
Water	190
Macro Synthetic Fibre (Polypropylene)	9.1
Superplasticiser (0.2 % by weight of binder)	0.79

3.2 Mould Preparation and Concrete Mixing

In preparation to cast samples for the investigation of the behaviour of macro synthetic FRC in this research, specific moulds had to be prepared for the various tests. Table 3.1 already shows the tests

carried out at the macro and structural levels: compressive strength, uniaxial tensile, uniaxial creep, drying shrinkage, flexural strength and flexural creep tests. Compressive strength was tested using 100 mm polyvinyl chlorides (PVC) cube moulds. Steel moulds were used to cast specimens for the uniaxial tensile and flexural tests. It should be remarked that while the moulds for the flexural investigation had no need for any adjustment to meet its intended purpose, the moulds used for the uniaxial tensile investigation were modified to fit the purpose of the test. The design of the moulds for the uniaxial tensile response is discussed in the next section. The inner surface of all moulds was properly oiled with mould oil to allow for easy demoulding of the specimens.

3.2.1 Assemblage of moulds for uniaxial tensile investigation

The moulds used to produce specimens for the uniaxial tensile strength and uniaxial tensile creep tests had to be modified. The modification to the moulds and the test setup employed are based on a previous work performed by Mouton (2012). The details of the modifications to the moulds and the development of steel hook for anchoring test specimens to the testing machine can be found in Mouton (2012). It should be stated that the work of Mouton (2012) was focused on self-compacting concrete using steel fibres whereas this research work is focused on FRC using macro synthetic fibres.

Specially designed steel hooks with eye-like end loops were used as anchors for the application of uniaxial tensile load in the test machine and were positioned at the centroid of the steel moulds before the casting of the fresh concrete (Figure 3.2a). The hooks protruded at both the ends of the moulds which were held into position with the aid of a wooden block measuring $100 \times 100 \times 200$ mm having a central hole of 18 mm in diameter. The wooden blocks were divided into two equal halves to allow for the placement of the hooks before the top half was placed and fastened together with the screws of the moulds (Figure 3.2a). The detail of the block dimension is shown in (Figure 3.3). To ensure proper alignment of the hooks placed at both ends of the mould so as to avoid internal moment as much as possible during testing, similar wooden blocks of 18 mm thick were placed under the central stud of

the hooks and a spirit level was used to further ensure side and top alignment of both central studs (Figure 3.2c).

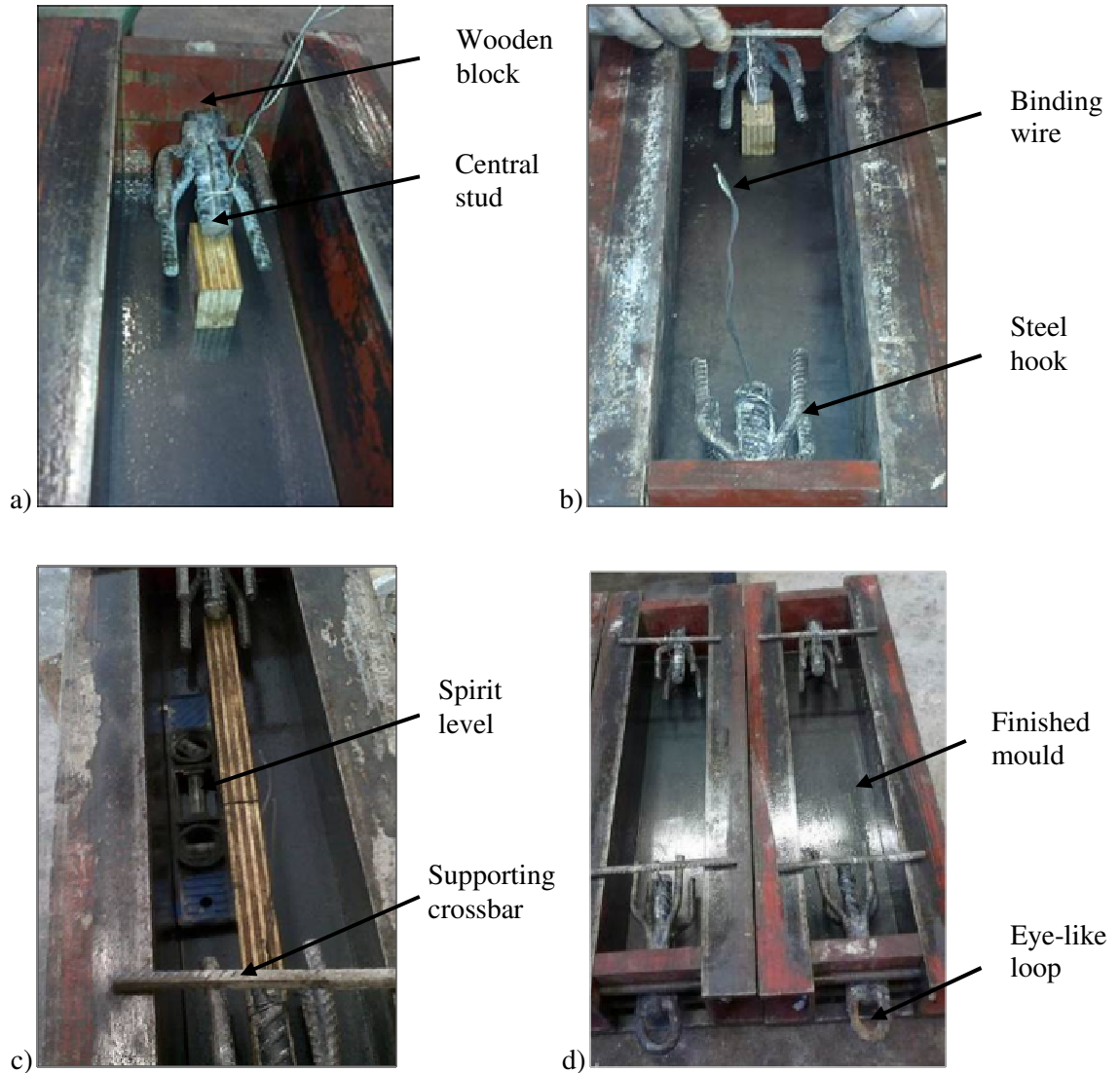


Figure 3.2: Preparation of moulds with steel hooks protruding from the ends

Thereafter, the central studs, which had been wound round with a binding wire were kept in place by winding the binding wire around an 8 mm supporting steel rod which rested across the mould (Figure 3.2c). This was done at both ends of the moulds and the whole setup was made firm through the screws attached to the moulds at both ends to prevent misalignment of the studs during vibration of the fresh concrete.

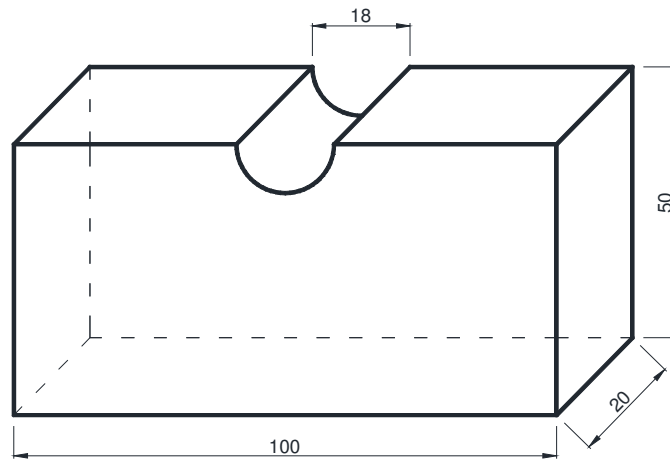


Figure 3.3: Details of schematic representation of wooden block

3.2.2 Mixing of the concrete

As soon as the moulds were prepared and ready for use, mixing of the FRC proceeded. Materials based on the mix design already established were batched by weight. Mixing was done in a 50 litres Gustav Eirich Concrete Mixer. It was ensured that the number of specimens needed for each investigation was cast from the same batch of mixture. For example, since four specimens were mostly tested for each loading level in the uniaxial tensile strength and uniaxial tensile creep tests, eight specimens were cast from each batch of concrete mixture. Three specimens each were cast for the flexural strength and flexural creep tests from the same batch of mixture. Other samples meant for test at the single fibre, which is discussed later, were also cast from the same batch of concrete to maintain consistency. The mixing procedure for the FRC is enumerated below:

- The mixing drum was properly rinsed with water and dried with industrial tissue paper.
- The dry aggregates and the cement were added to the mixing drum in the order of sand, cement, and stone and were allowed to mix for about 3 minutes.
- The water, which already had the measured superplasticiser mixed to it was then added to the mix and allowed to mix for another 5 minutes until a uniform mix was visible.

- Slump test was then carried out to verify the workability value of the mix without fibres immediately after the mixing. This was done in all batches of the mixes to monitor the consistency of each mix.
- For mixes without fibres, the mixing procedure stopped at this point. However, for mixes with fibres, the fibres were then carefully sprinkled into the mix to prevent balling. This stage was allowed to go on for another 5 minutes until a good visible dispersion of fibres was observed.
- Finally, a slump test of the FRC mixture was conducted to study the effect of the fibres on the workability of the concrete.

Thereafter, the fresh concrete was cast into the moulds which were already lying on the vibrating table. Casting was done in two layers for the uniaxial tensile test specimens. Since the hooks were on both ends of the mould, the concrete was placed in the middle portion and allowed to gently flow under vibration to fill up the hooks. In this way, the hooks were undisturbed by the placement of the concrete.

The procedure for filling the moulds of specimens for flexural tests was carried out in accordance with the requirement of EN 14651 (2005). After casting, all samples cast were covered with plastic sheets at room temperature for 21 ± 1 hours. After this duration, the samples were carefully demoulded and transferred to the curing tank.

3.2.3 Workability of fresh concrete mix

Adding fibres to concrete can pose serious workability issues if the concrete mix is not properly designed to accommodate the fibres. The normal concrete mixture for this study was designed to allow for the inclusion of a fibre volume of $V_f = 1\%$. The procedure for the slump test was carried out in accordance with the requirement of BS EN12350-2 (2000). A slump test value of 160 mm was obtained for the normal concrete before the introduction of the fibres. This procedure was done for each batch of concrete mixture as earlier mentioned to ensure consistency. In cases where slight

variations were observed in the slump values, additional amount of superplasticiser was used. After the fibres were added, slump test was also conducted to observe the effect of fibres. The slump of the fibre concrete taken showed a value of 100 mm. This indicates a 37.5% reduction in the slump value of the normal concrete when 1% macro synthetic polypropylene fibre was added to the mix.

3.2.4 Curing of test specimens

All test samples were carefully demoulded after 21 ± 1 hours in the mould and transferred to the curing tank where they were cured for a further 27 days before testing at an age of 28 days. All specimens tested in this research were cured by complete immersion in water at a temperature of 21 °C and were prevented from shock or vibration. Shortly after the removal of samples from the curing tanks, they were prepared for testing.

3.2.5 Preparation of samples for testing

All samples tested at the macro and structural levels were notched (wet sawing) appropriately before they were tested as required except for samples meant for compression and drying shrinkage tests. Specimens for the uniaxial tensile test were notched at the centre with a diamond blade of 3 mm on all four sides to a depth of 10 mm resulting in an effective area of 6400 mm².

For specimens tested in bending, they were rotated over 90° around their longitudinal axes and notched through the width at midspan to a depth of 25 mm before they were tested.

3.3 Investigations on the Macro Level

3.3.1 Compressive strength test

The concrete mixture was designed for a compressive strength of 45 MPa. The provision for specimen size and procedure of test was done according to the requirement of BS EN 12390-3 (2002) using cube sizes of 100 mm. Ten cube samples were tested for compressive strength at a loading rate of 0.3 MPa/s using a Contest Material Testing Machine which had a maximum capacity of 2000 kN.

Five samples were used as control (without fibres) whereas the other five samples had fibres. Cubes were tested for the 28-day strength. The cubes were rotated over 90° before they were tested. This investigation is of importance in assessing the influence of macro synthetic fibres on the compressive strength of concrete. Test samples were all tested for 28-day cube strength.

3.3.2 Uniaxial tensile test

There exist a number of scholarly articles on the test setup for performing a direct tensile test. Due to the intricate challenges with the setup of this test as previously mentioned, there is no harmonised standard test method yet for performing this test. Wille et al. (2014) presented a comprehensive review of diverse methods reported in literature for conducting the uniaxial tensile test. A review of specimen shape (dogbone, prism, and cylinder), test condition (notched and unnotched), material type, etc., were reported. Table 3.4 presents details of their compilation of test setups of notched specimens tested in direct tension.


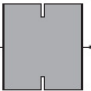
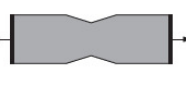

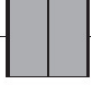
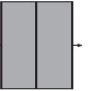
They also reported that these wide variations in the setups further show the lack of standardisation of the test. However, RILEM TC 162-TDF (Vandewalle, 2000) gave a proposed recommendation for testing steel FRC in uniaxial tension. Despite the difficulties in carrying out the uniaxial tensile test, this is still favoured to provide the direct tensile material properties of concrete (Boshoff, 2007; van Mier & van Vliet, 2002; Wille et al., 2014).

The methodology for performing the uniaxial tensile test by Mouton (2012) has been adopted for the design simplicity and practicality.

Experimental test instrumentation

The uniaxial tensile tests were performed in a Zwick Z250 Universal Testing Machine which had a capacity of 250 kN (Figure 3.4). In Section 3.2.1, a description of an eye-like steel loop welded to the central stud was described.

Table 3.4: Direct tension test setups – notched prisms/cylinder specimens (Wille et al., 2014)

Shape notched prism/cylinder	Material (-)	Performance level (-)	Length, width and depth of constant area (total specimen) in (mm)			Diff. area	Grip/attachment	DOF ^a top-bottom
			L	W	D			
	FRC	<3	2	51	51	44%	Top glued	0-0
	FRC	<3	(152) 3	(76) 42	(76) 50	70%	Top glued	0-0
	FRC	2	(55) 1	(60) 51	(50) 13	67%	Top glued	0-0
	UHP-FRC	3-4	(254) ~5	(76) 160	(13) 50	80%	Side glued + anchored (greased)	0-0
	FRC/UHP-FRC	2/3	(500) 2-5	(200) 135 ^a	(50) -	81%	Top glued	0-0
	UHP-FRC	3-4	(150) 2	(150) ^b 44 ^b	-	35%	Top glued	0-0
			(60)	(74) ^b				

^a DOF – degree of freedom.

^b Diameter of the cylinder.

The purpose of the eye-like steel loop welded to the central steel stud is to allow for connections to the Zwick Z250 Machine and the cables of the creep frame as further explained in Section 3.6.

Figure 3.4 shows the details of the specimen in the Zwick Z250 machine. At the support of the specimen, two galvanised threaded bolts (20 mm diameter) were passed through two 10 mm thick plates on both sides of the eye-like steel hook anchors (lower and upper ends) through a central supporting plate (10 mm thick). The supporting plates at both ends were clamped by the machine to hold the specimen in place for load transfer. This connection, which is flexible, does not produce fully rigid boundary condition. This connection type allowed rotation around the two horizontal axes, therefore preventing internal moments.

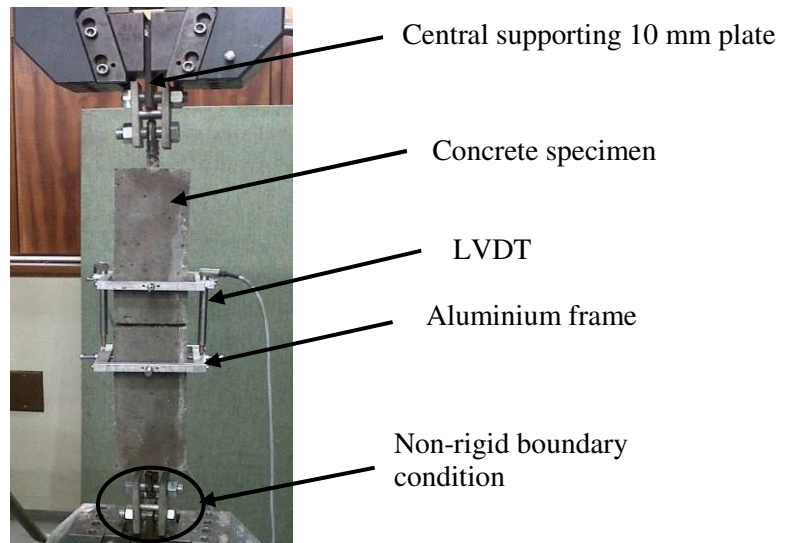


Figure 3.4: Uniaxial tensile test setup

Experimental test programme

Before the test specimens were positioned in the Zwick Z250 machine, aluminium frames with a gauge length of 120 mm were attached to the specimens as shown in Figure 3.4. These frames were used to measure the opening of the notch during testing. Two linear variable displacement transducers (LVDT) which controlled the loading rate of the test (displacement-controlled) were attached to the aluminium frames. It should be noted that the frames were secured tightly to the concrete specimens with the aid of screws to prevent any movement which could lead to errors in the displacement reading. The displacement readings from the LVDT's were electronically acquired through a data acquisition unit of the testing system. The tests were performed at a loading rate of 0.01 mm/s. Specimens were pre-loaded to 500 N before the test started and the test was stopped when a crack mouth opening displacement of 3 mm was reached.

3.3.3 Uniaxial tensile creep test

The creep frame

The uniaxial tensile test was carried to study the post crack behaviour of macro synthetic FRC and to determine its residual tensile strength. This was necessary because the uniaxial creep loads were based on the residual tensile strength obtained from the uniaxial tensile strength test. The

experimental setup for this test was also based on the work of Mouton (2012). A schematic representation of the creep frame is shown in Figure 3.5.

The setup of the uniaxial creep test was designed to accommodate two test specimens in series and uses a lever arm system for load application (Figure 3.5). Test specimens for the creep test have the same configuration with those described in the uniaxial tensile strength test. The specimens meant for the creep test were initially cracked in the Zwick Z250 testing machine and then unloaded to an average irrecoverable crack width of 0.5 mm before they were taken to the creep frame where the creep loads were applied at different stress levels (see Table 3.1) of the average residual uniaxial tensile strength.

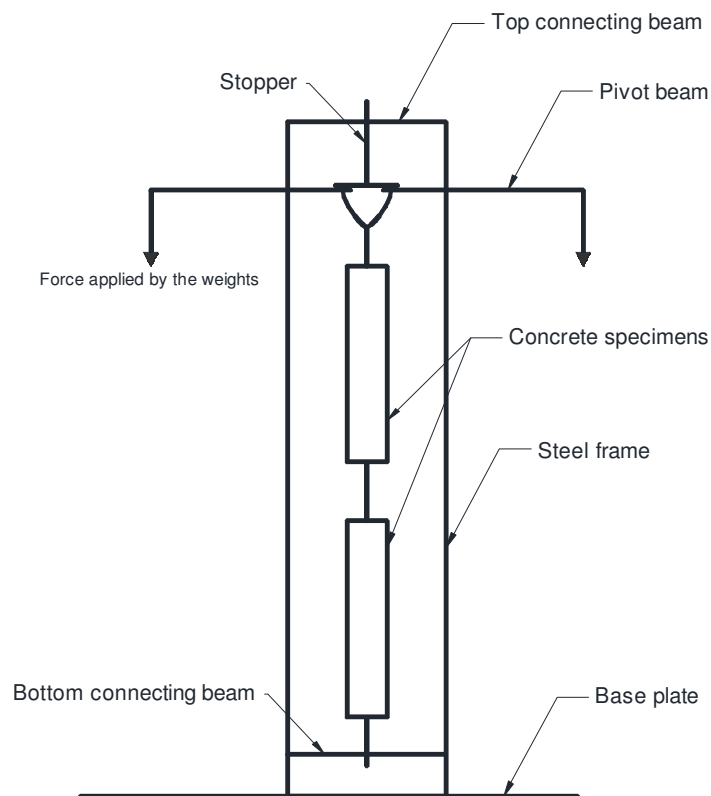


Figure 3.5: Schematic representation of uniaxial tensile creep frame with specimens in series

Prior to the setting up of test specimens, the frames were calibrated by using a HBM 50 kN tensile load cell which was placed in the position that were occupied by the specimens (Figure 3.6).

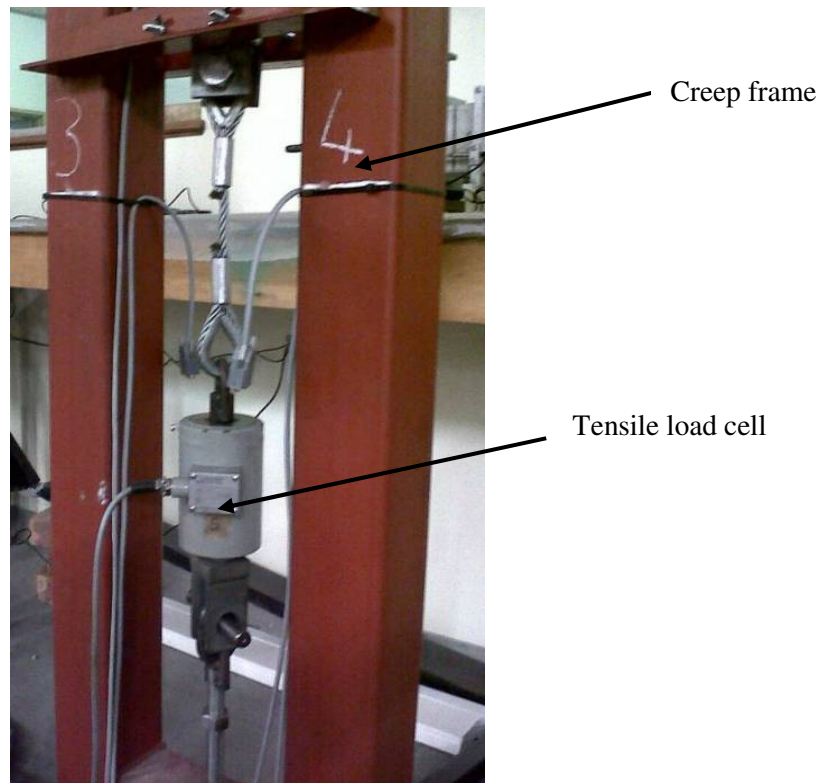


Figure 3.6: Calibration of creep frame

The load cell was connected to a Spider8 data logger which in turn was connected to a computer. The weights of both pivot beams of the frame, the cables connected to the beams and free hanging weights were used to determine the creep load for each frame. The free hanging weights were conventional steel weights of 5 kg and 10 kg. Starting with the 10 kg weight, one weight at a time was placed on the free hanging cables connected to the pivot beams on either sides of the frame until the desired load output was achieved. Smaller weights were also used to be able to obtain that exact load at each stress level. This calibration was done for all the frames according to the various creep load classifications. The frame has a stopper device (see Figure 3.7) which serves a dual purpose. It allows for the pivot beams to be positioned in such a way that no load is applied on test specimens while in the test frame and can also be released for load application through the operation of the bolts indicated in Figure 3.7. Secondly, it also functions as a safety mechanism to stop the sudden drop of the pivot beams if one or both specimens failed under sustained load.

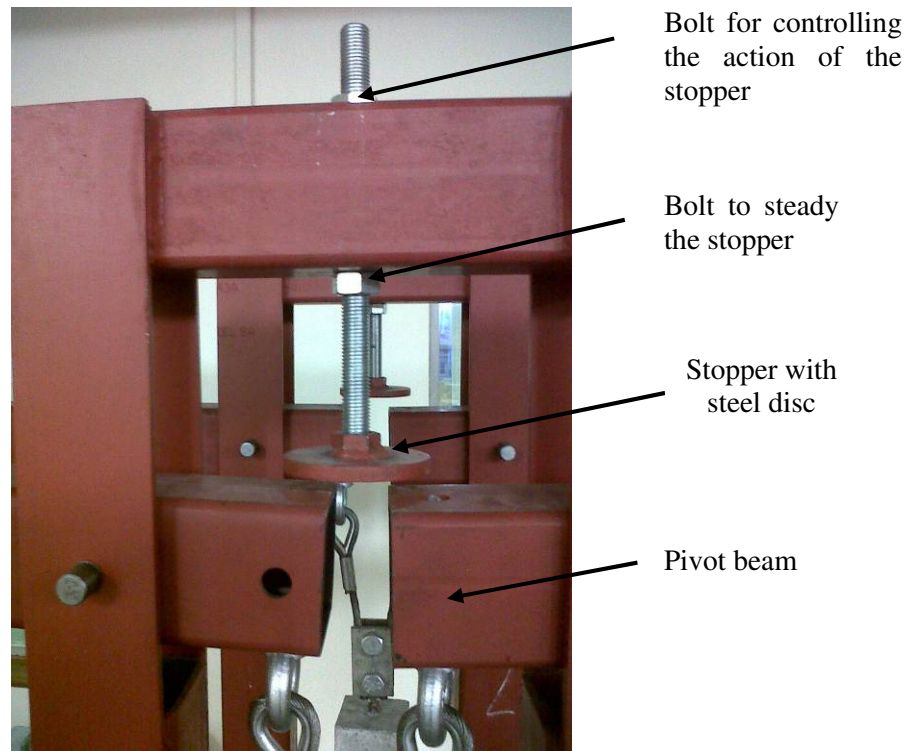


Figure 3.7: Upper section of creep frame showing stopper device

Experimental test programme

After the calibration of all the frames, the actual specimens were prepared for testing. Aluminium frames similar to those used in the uniaxial tensile strength test were also fitted to each cracked specimen. Unlike specimens tested in uniaxial tensile strength test which had a gauge length of 120 mm, the aluminium frames fitted to specimens for the uniaxial tensile creep test were set to a gauge length of 70 mm. The difference in the gauge length was as a result of the smaller LVDTs used for the displacement reading in the creep test. The test specimens were connected to the creep frame using cables fixed to the eyes that were welded on the anchors of the specimens. It should be remarked that to prevent bending moment being induced in the specimens, the eyes were positioned on the centre line of the specimens in a similar fashion as shown in Figure 3.4.

After positioning the test specimens in the uniaxial tensile creep frames according to their respective load levels (Table 3.5), LVDTs were then attached to the aluminium frames across the

notch to measure the CMOD Figure 3.9 shows the creep frame with actual specimens in position and an enlarged view.

Table 3.5: Test programme for the cracked uniaxial tensile creep specimens

Load levels as % of the post-crack strength	30%	40%	50%	60%	70%
Actual applied stress (MPa)	0.234	0.312	0.39	0.468	0.546
Equivalent creep load (N)	1498	1997	2496	2995	3494
Number of specimens	4	4	4	2	2

After the whole setup with the specimens was ready for the commencement of the test, the data acquisition was started before the loads were applied on the set of the specimens. The load was applied within thirty seconds by releasing the stopper using a spanner to loosen the top bolt of the frame as described above while ensuring that no dynamic loading occurred.

The deformation over the notched area was measured using two 10 mm LVDTs. The displacement readings were acquired using the HBM Spider8 Electronic Measuring System. Data were saved at regular intervals for the full duration of the tests. The displacement reading obtained from the creep test will include material creep and drying shrinkage. The specimens were tested unsealed, therefore basic creep, drying creep, crack widening and drying shrinkage occurred at the same time. The drying shrinkage could be subtracted as it was measured separately while the material creep is insignificant.

Five load levels were investigated using four specimens for each test except for the 60% and 70% stress levels where two specimens were used due to the limitation of the creep frames (Table 3.5). Since all the specimens were tested unsealed, drying shrinkage was measured on two load-free specimens and subtracted from the total creep deformation measured from the creep specimens to obtain the actual creep deformation.



Figure 3.8: Creep frames showing specimens under sustained loads and LVDT position over a gauge length of 70 mm.

3.3.4 Drying shrinkage test

Shrinkage deformation of the macro synthetic FRC was studied to distinguish it from the measured deformation behaviour under sustained loading. The test specimens for the uniaxial tensile creep were tested unsealed, hence drying shrinkage occurred during the test duration. The time-dependent drying shrinkage was measured using two load free samples. The specimens were tested in an unrestrained condition by placing them on PVC rollers to minimise the restraint against shrinkage. The readings were measured electronically using a HBM Spider8 Electronic Measuring System. The shrinkage was measured over a gauge length of 285 mm (100 mm × 100 mm × 500 mm samples) which were achieved using an LVDT extender fixed to the specimens using two aluminium frames as shown in Figure 3.9. Shrinkage strain was multiplied by the gauge length of the creep specimens to determine the displacements caused by shrinkage in the creep specimens over a gauge length of 70 mm. A deduction of these strains from the measured CMOD gave the actual creep of the specimens under sustained loading.



Figure 3.9: Shrinkage test specimens showing frame with LVDT extenders

3.4 Investigation on the Single Fibre Level

3.4.1 Time-dependent fibre pullout test

To understand the mechanisms causing creep in cracked macro synthetic FRC, time-dependent pullout tests on single fibres embedded in concrete matrix were performed. The matrix for these tests contained no fibres except for the single fibres embedded. A simple experimental setup similar to that reported by Richardson et al. (2010) was developed using free hanging weights.

Experimental test setup

This test setup used concrete cube specimens measuring 100 mm. The cubes were produced from the same mix used throughout this study. Single fibres were carefully inserted by hand into the matrix to a depth of 25 mm. To prevent the embedment depth from going beyond 25 mm, the fibres were pre-marked with black ink before they were inserted. Thereafter the moulds were gently vibrated to ensure closure of the void created around the fibre after insertion. Adequate care was taken to ensure the fibres remained vertical. Specimens were then moved to a safe place in the laboratory where samples were undisturbed until demoulding. After 23 ± 1 hours, the specimens were demoulded and transferred to the curing tank where they were cured in water for additional 27 days. Curing was done at 21 °C by complete immersion. At an age of 28 days, a hole of 12 mm diameter was drilled on the opposite side to where the fibre was embedded to a depth of about 30 mm and threaded bars with 10 mm diameter to support the specimens were fixed in the holes with epoxy glue and left in the climate

controlled room to set for 24 hours before testing commenced. Prior to the positioning of the test specimens, a steel frame built from channel sections had been erected as shown in Figure 3.10. The top part of the frame had holes drilled into it at specific intervals to allow for the specimens with the threaded bars glued to them to be hanged on the frame.

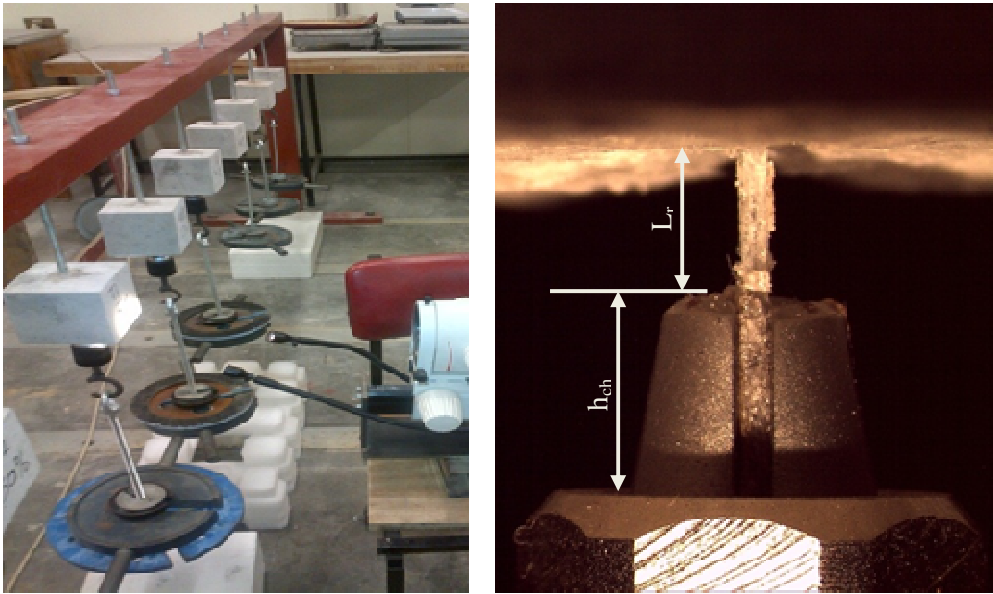


Figure 3.10: Test setup of time dependent fibre pullout test

The free ends of the fibres were gripped with a hand drill chuck having an aperture of 0.5 mm such that the fibres could not be damaged (which could lead to fracture) at that point and there would not be any slippage of the chucks from the fibres. Trial tests were conducted to be certain that the chucks could grip the fibres properly without slippage or damage to the fibres. Though the diameter of the fibres was 0.8 mm and the aperture of the chucks was 0.5 mm, trial test showed slippage of the chucks from the fibres as the sustained weights dropped down without fibres completely pulling out. To solve this problem, “Q bond glue” comprising of an ultra strong adhesive and filling powder was applied to the free ends of fibres before they were gripped with the chucks. This was carefully applied to the free end to prevent any contact with the end of the embedded fibre which could result in higher pull-out force. The stability was confirmed with more trial tests before the actual tests proceeded. The process of applying the glue to the free ends of the fibres and gripping with the chucks was carefully done to avoid the application of force that could lead to debonding or pull-out.

Experimental test programme

The time-dependent fibre pullout displacement was measured optically with the aid of a microscope with a 3.1 Mega-pixel Leica EC3 camera. Before the application of the weights, a photo of the setup was taken to serve as the reference photo. The height of the mouth grip of the hand drill chuck, h_{ch} , 5 mm, was used as a scale reference (Figure 3.10). With this scale, the reference fibre length (from reference photo) before pull-out, L_r , was determined. Subsequently, photos were taken at regular intervals of the fibre pull-out from the matrix and the new pull-out length was then subtracted from L_r to obtain the time-dependent fibre pull-out displacement.

Sustained loads between 50% and 80% of the average interfacial shear resistance of specimens tested at 25 mm embedment length were applied to the fibres individually to study the time-dependent pull-out behaviour. The force reading from the pullout rate test was expressed as the average interfacial shear stress by dividing it by the surface area of the embedded fibre that is in contact with the matrix as:

$$\tau = \frac{P}{L_e \pi d_e} \quad 3.2$$

Where P is the applied force, d_e is the effective fibre diameter and L_e is the original embedment length.

3.4.2 Single fibre creep test

An important characteristic of polymeric materials such as polypropylene is creep. This could eventually have an effect on the creep of the specimens under investigation as already discussed in Chapter 2. Therefore a creep test on a single fibre was carried out to study its effect on the time-dependent behaviour of macro synthetic FRC. One fibre was tested for creep using a similar test setup to the time-dependent fibre pullout test.

To investigate the creep of the single fibre, a means was sought to grip the fibres at both ends without damage. Hand drill chucks, as presented in the previous section, were used at both free ends

of the fibre after the glue had been applied to both ends following the same procedure in the time-dependent pull-out test. The fibre was firmly gripped by hand drill chucks at both ends to prevent slippage and then hung on the supporting frame used for the time-dependent pull-out test before the load was applied (Figure 3.11).

The same procedure for measuring the time-dependent pullout test was also used to determine the time-dependent elongation of the fibre under sustained load of 143 MPa. This represents 30% of the average tensile strength of the fibres tested in tension at a rate of 0.5 mm/s.

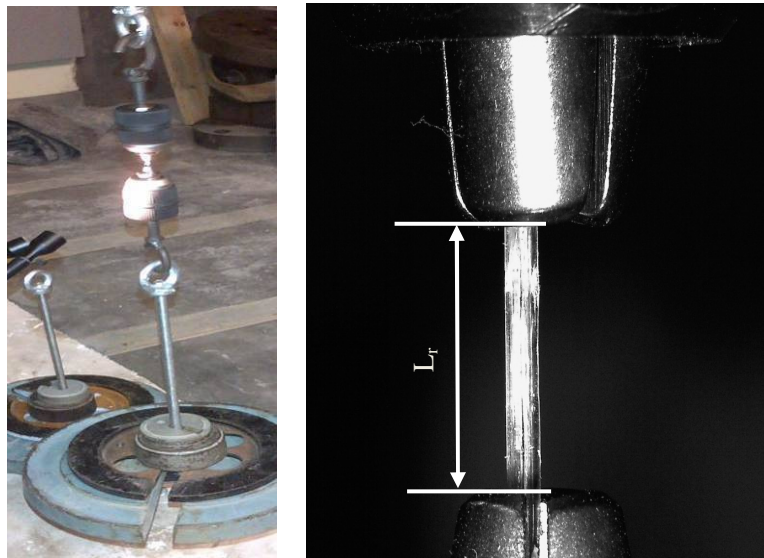


Figure 3.11: Fibre creep test setup

3.5 Other Experimental Investigations on the Single Fibre Level

Up to now, discussions have been focused on the experimental procedures for investigating the time-dependent behaviour of macro synthetic FRC and the mechanisms that could be responsible for such behaviours. It should also be borne in mind that among other factors that may be responsible for the time-dependent pullout behaviour of macro synthetic FRC, the interaction between the synthetic fibre and the matrix is of great importance. Won et al. (2006) reported that due to the hydrophobic nature of macro synthetic fibres, they exhibit poor bond with cement matrix. Though Won et al. (2006) investigated different geometry of macro-monofilament synthetic fibres, none of the fibres investigated have the same 'X' profile cross section of the fibre used in this study.

The experimental methodology to investigate the effect of pullout rate on the mechanical response of the interface between the fibre and the matrix is presented. The experimental method to investigate the effect of loading rate on the tensile response of synthetic fibres is also reported.

3.5.1 Rate test on single fibre pullout

The test specimens were prepared from 100 mm cube moulds. The moulds were divided into two halves with a wooden block measuring $100 \times 100 \times 40$ mm giving two specimens from each mould. As done with the time-dependent single fibre pullout test, the mix was cast into the mould and single fibres were carefully inserted. Pullout behaviour was investigated at three embedment lengths: 10 mm, 15 mm and 25 mm. After casting the specimens, the moulds were then gently vibrated to ensure closure of the void created. Adequate care was taken to ensure that the fibres remained vertical (see Figure 3.12). Samples were cured by complete immersion in water at 21 °C before been tested at an age of 28 days about three hours after removal from the curing tank.



Figure 3.12: Single fibre pullout test specimens

The specimens were tested in the Zwick Z250 Universal Testing Machine (Figure 3.13) over four displacement loading rates; 0.001 mm/s, 0.01 mm/s, 0.1 mm/s and 1 mm/s in the displacement control mode. The samples were clamped in the lower hydraulic clamp of the testing machine. It was ensured that for all specimens tested, the clamped portion of the specimens were well below the depth of the fibres. At the upper clamp of the machine, a steel platen to which a 2 kN tensile load cell was mounted was clamped, see Figure 3.13.

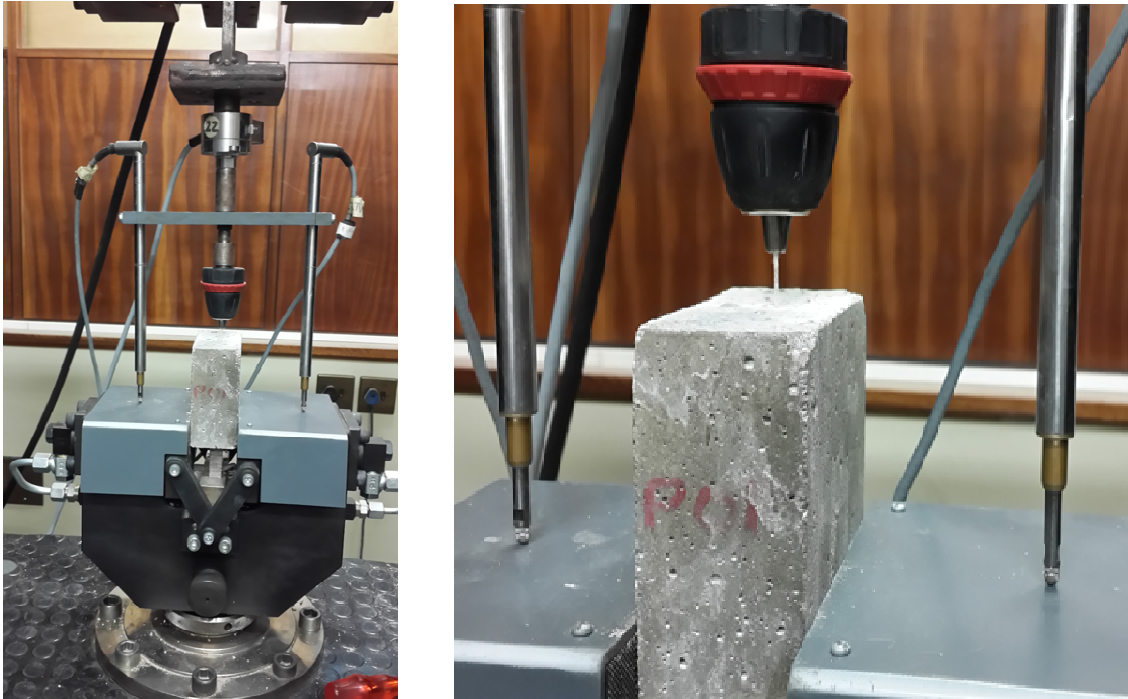


Figure 3.13: Single fibre pullout rate test

A polyvinyl chloride (PVC) strip that supported two 50 mm LVDTs for measuring the fibre pullout displacement was placed in-between the load cell and the hand drill chuck which gripped the fibre. Adequate care was taken to ensure that no force was applied to the fibre that could have led to debonding or pull-out prior to the commencement of the test. In cases where this was suspected, specimens were discarded. All force readings obtained from the tests were converted to interfacial shear resistance according to Eqn. 3.2 while the pullout displacements (Δ) were normalised for the purpose of comparison using:

$$\Delta_n = \frac{\Delta}{L_e} \quad 3.3$$

with Δ_n the normalized displacement, and L_e the embedment length. SEM photos were taken of some of the pulled out fibres to examine the effect of rate on the damage to the fibres during pullout.

3.5.2 Tensile strength test of single fibres

In a bid to investigate the tensile strength property of the synthetic fibres and the influence of loading rate, the uniaxial tensile strength test of the fibre was performed following the same procedure

for the single fibre pullout test. A simple and practical setup was developed for this investigation as shown in Figure 3.14. The setup was developed from a combination of hand drill chucks, rods supporting the chucks, two 50 mm LVDT's and PVC strip to support the LVDT's for measuring the elongation during testing. The arrangement at the upper part of the setup is the same with that discussed in Section 3.5.1. Since only single fibres were tested, similar hand drill chuck was utilised at the lower part of the setup.

A single fibre was inserted into the apertures of the chucks and the chucks were screwed firmly to the fibre without any damage. This was first done for the upper chuck followed by the lower chuck. Having positioned the upper part of the setup as described previously, the rod supporting the lower chuck, which could move freely, was then clamped by the hydraulic clamp of the testing machine. It was ensured that prior to clamping, the rod bearing the lower chuck was positioned to align vertically with the top chuck before being clamped. As soon as the whole setup was ready, testing could commence. Four loading rates were also investigated and the results presented as force-elongation graphs.



Figure 3.14: Single fibre tensile strength test

3.6 Structural Level Investigations

3.6.1 Flexural tensile test

In conventional concrete, the flexural tensile strength, often called the modulus of rupture (MOR), is usually investigated using either the three or four point bending tests. The requirement for these tests is covered in the European Standard, EN 12390-5 (2000). When dealing FRC, the post-peak behaviour is usually of interest. In this regards, two documents, EN 14651 (2005) and RILEM TC 162-TDF (2002) have given similar recommendations for the characterisation of the residual flexural tensile strength and toughness characteristics of FRC. In characterising the behaviour of FRC subjected to bending, the beam specimens are usually notched at midspan to a depth of 25 mm for prisms having a cross sectional area of 150 mm × 150 mm as previously discussed. Though none of the aforementioned recommendations covered the characterisation of the four point bending test of FRC, it will be worthwhile to compare the performance of test samples under both conditions of loading.

In this research work, the requirement of EN 14651 (2005) in characterising the residual flexural tensile strength of FRC beam specimens under three point loading was adopted. Specimens were tested to study the load-CMOD response. The residual flexural tensile strength at different CMOD as shown in Figure 3.15 was evaluated and discussed.

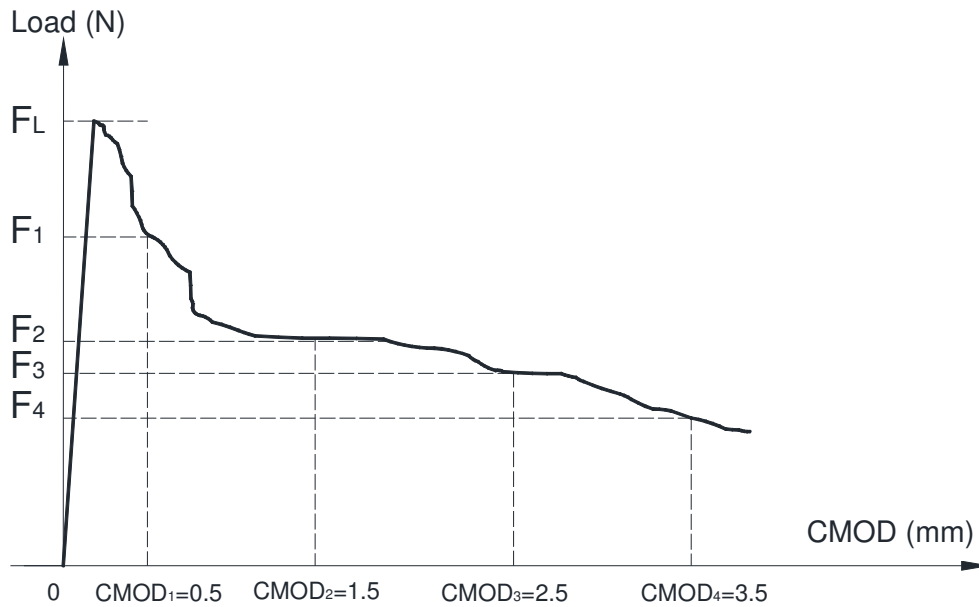


Figure 3.15: Load-CMOD diagram and F_j ($j = 1, 2, 3, 4$)

Experimental test instrumentation

The size of the specimens tested under three point bending has been described in Table 3.1. Three test samples were investigated under three point bending and two others under four point bending tests. Beams for the three and four points bending tests were all notched to a width, $n_w = 3$ mm and the distance between the tip of the notch and the top of the specimen in the mid-span section, $h_{sp} = 125$ mm. Specimens were wiped clean of excess moisture, then marked to ensure correct placement of the beams on three and four points loading, as the case may be. All specimens were tested in the Zwick Z250 machine as done in the uniaxial tensile test. For the samples tested under three point, one LVDT was attached to the beam at mid-width across the mouth of the notch on the bottom surface to measure the CMOD as shown in Figure 3.16. Consideration for the distance between the LVDT and the bottom face of the beam was made while calculating the actual CMOD. This is further discussed in Chapter 6.



Figure 3.16: Flexural tensile test under three point loading

In both test cases, the deflection was not of importance, hence, not measured. It should be reiterated that the purpose of this test is to study the CMOD in the short term and when subjected to creep under sustained loadings. Cracks propagated from the notch in all test cases.

However, for specimens tested under four point bending, two LVDTs were used; they were placed at the tip of the notch on opposite sides as shown in Figure 3.17. The displacement reading in this case was taken as the crack tip opening displacement (CTOD).



Figure 3.17: Flexural tensile test under four point loading

Experimental test programme

After the samples were placed appropriately, testing commenced. The machine was then controlled in sequence using one LVDT at a constant displacement rate of 0.05 mm/min up to a CMOD = 0.1 mm. When CMOD = 0.1 mm, the machine was operated at a constant rate of 0.2 mm/min until the test was stopped according to the recommendation of EN 14651 (2005). It should however be noted that the interpretation of the results were based on the average of the two LVDT's. Since readings from both LVDT's were similar (four point test), the effect of using only one of the LVDT's to control the loading rate was negligible. This has also been reported by Soutsos et al. (2012). The single LVDT in the three point bending test was used to control the crack opening rate.

It should be noted that the same procedure was also used to pre-crack specimens for the flexural creep test before they were taken to the flexural creep frame where they were subjected to sustained loadings (see Section 3.6.2).

3.6.2 Flexural creep

For a constitutive model to be verified, the analysis of flexural test using parameter obtained from uniaxial tensile test should accurately simulate the experimental results. Hence, the essence of the flexural creep is to study the time-dependent behaviour of cracked macro synthetic FRC under bending stresses as well as for the verification of the finite element analysis (FEA) of the time-dependent behaviour of macro synthetic FRC using material model parameters obtained from the uniaxial tensile creep tests.

Experimental test setup

The test setup for the flexural creep followed the design concept reported in Arango et al. (2012) and Zerbino & Barragan (2012) with some minor modifications to the components of the creep frame

and the measuring device. The flexural creep frame developed and used in this research consisted of the following arrangement (see Figure 3.18):

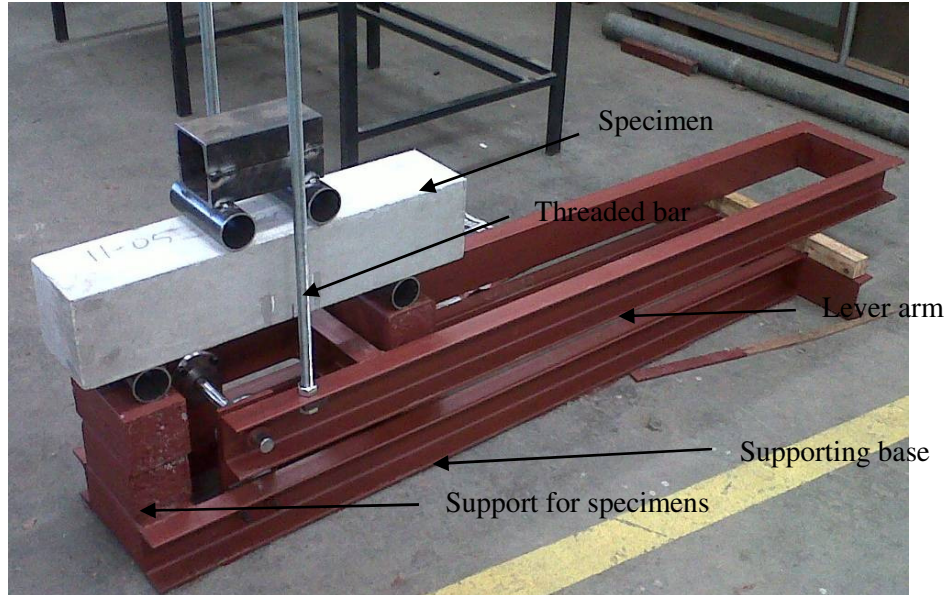


Figure 3.18: Flexural creep frame

- A support base made of two longitudinal 100 mm × 50 mm channel sections with transverse steel channel sections welded to it at defined interval to ensure a stiff base. The longitudinal sections are 1.6 mm long and spaced 200 mm apart.
- Vertical supports for the column of specimens made of square hollow steel sections (100 mm × 100 mm × 6 mm) which were filled with concrete were welded to be base. The supports were located such that a test specimen span of 450 mm could be achieved.
- The load was applied through a lever arm mechanism. The lever arm was also made of 100 mm × 50 mm channel sections similar to the base with two transverse channel sections placed only at the free end for supporting the counterweight. Two vertical flat plates (10 mm thick) bolted to the internal surface of the supporting base and the lever arms on either side were used to support the lever arm at one end. The point of connection between the plates and lever arm has a hole drilled to a diameter of 27 mm to allow for the placement of

roller bearings. A Bright mild steel round bar (diameter = 25 mm) was then passed through both roller bearings on both sides to act as the fulcrum for the lever arm.

- Holes were drilled on the flanges of the lever arm on either side at the points where the threaded bars will lie exactly at mid-point of the column of specimens. A couple of M20 threaded bars were then connected vertically to the lever arm between the support points for the application of load. M20 galvanised hex nuts and washers were used to fasten the threaded bars to the level arm.
- Each test specimens was supported on a circular hollow steel section; one of the circular sections was prevented from rotating by using wedges while the other was not wedged. Specimens were stacked in column of three specimens referred to in this dissertation as top, middle and bottom specimens. After the positioning of the bottom and middle specimens, the top specimen then had a load transmission element (made of square hollow section with two hollow circular sections attached) placed on it.
- A 20 mm thick flat load plate connecting both threaded bars as a couple was finally placed on the load transmission element. It was ensured in the design of the frame that the setup was stiff enough for the level of load applied such that no additional deformation from the threaded bars, lever arm, specimen supports and load transmission element was expected.

The specimens were positioned in a four point bending test setup with a span of 450 mm and specimen supports at 150 mm. Due to the shortage of LVDT's, dial gauges with a resolution of 0.01 mm were used to measure the crack tip opening displacement (CTOD) of specimens for a period of eight months. The dial gauges measuring the CTOD of specimens were borne by angle plates glued to the specimens across the notched area. They were only placed on one surface of each specimen as shown in Figure 3.19c. Though the measurements reported were not average values, it will nevertheless give an indication of the deferred deformation of Macro synthetic FRC under sustained flexural loadings. Measurements were taken at regular intervals throughout the test period.

Experimental test programme

The flexural creep test was commenced after the specimens had been cracked in the Zwick Z250 Universal Testing Machine to a crack width of 0.2 mm and then unloaded under a 3-point bending test following the same procedure already discussed in Section 3.3.3. Specimens were tested under three stress levels as presented in Table 3.1. The equivalent sustained loads for each stress level was obtained as a percentage of the average residual strength at $CMOD = 0.2$ mm.

Prior to loading the cracked specimens on the creep frame, the frames were calibrated with a 50 kN HBM load cell placed on the setup (Figure 3.19a).



Figure 3.18: Flexural creep setup (a) Calibration of frame showing load cell (b) Constant load and Enerpac cylinder (c) Stacked beams already loaded

I-steel section was put in the position where the actual test specimens occupied and the transverse load plate connecting both threaded bars together was in turn placed on top of the load cell. It was ensured that the nuts did not exert any force on the specimens before the gravity loads were applied. It should be remarked that the load cell was not left in the frame during the actual tests as the constant gravity load needed to be sustained at the stress levels had been determined (Figure 3.19b). Three beams were stacked in each frame and the gravity loads already placed during the calibration were gradually applied by releasing an extended Enerpac hydraulic cylinder that was connected to a hand-operated hydraulic pump beneath the weights as shown in Figure 3.19c.

3.7 Summary

This chapter presented all the experimental test materials used, preparation of moulds for casting, concrete mixing, workability investigation, preparation of specimens for test, test procedures performed to investigate the short term and the time-dependent behaviour of macro synthetic FRC at the macro, single fibre and structural levels. A well defined experimental methodology is necessary for the successful achievement of all the stated objectives in this study.

At the macro level, the short and long term behaviour of macro synthetic FRC were investigated. These included the performance of specimens under compression, uniaxial tension, uniaxial tensile creep and drying shrinkage tests. Methodology for the investigation of the long term behaviour of cracked specimens subjected to sustained loadings was also presented in detail. These tests included the uniaxial tensile and flexural creep, time-dependent single fibre pull-out and fibre creep tests to study the mechanisms causing the time-dependent crack opening of cracked macro synthetic FRC.

Other tests conducted at the single fibre level were the single fibre pull-out rate test and tensile rate test of single fibres. Results of all tests and the discussion of findings are presented in the subsequent chapters.

Chapter 4

Macro Level Behaviour under Short and Long Term Loading

The results of the behaviour of macro synthetic FRC at the macro level are presented and discussed in this chapter. The presentation commences with the results of the short term mechanical responses of concrete reinforced with macro synthetic fibres. The compressive strength characteristics is presented and discussed followed by the behaviour under uniaxial tensile test. The uniaxial tensile test was used to gain better understanding of the stress-crack opening behaviour of the concrete reinforced with short discrete macro synthetic fibres. To understand the time-dependent behaviour of macro synthetic FRC in the cracked state, results of the uniaxial tensile creep tests over a period of 8 months are presented and also discussed. The drying shrinkage result which is required to distinguish between creep and drying shrinkage was subtracted from the creep test results, is briefly presented alongside.

4.1 Compression Strength

The compression strength test was carried out to investigate the influence of polypropylene (PP) fibres. This was done at a loading rate of 0.3 MPa/s. 100 mm cube specimens were used to study the compressive strength characteristics of the fibre concrete in comparison to the plain concrete using the same concrete mix.

4.1.1 Results

The result of the average compressive strength of plain concrete in comparison to macro synthetic FRC is shown in Table 4.1. The compressive strength is calculated using:

$$f_{cm} = \frac{P}{A_c} \quad (4.1)$$

where f_{cm} is the compressive strength in MPa, P is the crushing load in N and A_c is the cross-sectional area of the specimen in mm^2 .

Table 4.1: Mean 28-day compressive strength and density

Concrete type	Specimen size (mm^3)	Crushing strength (MPa)	Density (kg/m^3)	Coefficient of variation (CoV) (%)
Macro synthetic FRC	100 × 100 × 100	40.19	2218	3.42
Plain concrete		43.80	2420	4.21

The mean values represent the averages of five specimens for each set. This result shows that the addition of macro PP fibres to plain concrete at the dosage used lowers the compressive strength. A decrease of 8.24 % in the compressive strength of plain concrete is observed. In both cases, the CoV is far less than 10 % which is a good indication of repeatability and consistency (Boshoff, 2007; Richardson et al., 2010).

4.1.2 Discussion

Three conclusions are usually made by scholars with regard to the influence of PP fibres on compressive strength of FRC, namely it has no significant effect, it has a loss of strength or it increases the strength. The result of the experimental investigation in this research has shown that the addition of macro PP fibres reduced the compressive strength of plain concrete of the same mix. This is consistent with the results of Richardson (2006) who investigated the effect of synthetic fibres (macro and monofilament) on the compressive strength of plain concrete as a result of the conflicting reports in literature. Some of the macro synthetic fibres used by Richardson (2006) were much like those used in this investigation having a crimped geometry, length of 40 mm and a diameter more than 0.3 mm. It is acknowledged that the concrete mix is different and the fibre dosage used in his work is 6 kg/m^3 . In a recent study, Emdadi et al. (2013) also reported a decrease in the compressive strength of a micro fibrillating PP fibre reinforced cementitious material. The result obtained in this

research calls for the need to ascertain the compressive strength of concrete mix with macro synthetic fibres before use, particularly in applications where compressive strength is desirable.

Though this study did not investigate the micromechanics responsible for this observed phenomenon, a number of reasons may be attributed to the decrease in compressive strength. The inclusion of fibres into the concrete mix made it difficult for proper compaction and hence, likely to have created more air voids content when compared to the plain concrete mix. The air content measured during the preliminary test shows air void contents of 4 % and 2 % respectively for the fibre and plain concrete. This increase in air void content led to a decrease in the density of the fibre concrete and invariably, the compressive strength. Fibres are known to generally have the tendency of balling in a concrete mix thereby entraining air which results in lower density and consequently, lower compressive strength (Gold, 2000). This seemingly negative impact of fibres on the compressive strength due to the likelihood of fibres balling was also recently reported by Mehdipour et al. (2013). The mechanisms responsible for the reduction in the compression strength of concrete produced from macro fibres have been summed up to be those related to different concrete mix composition, fibre type (aspect ratio, geometry, fibre class – micro or macro), dosage of fibre used and the manufacturing conditions (Alhozaimy et al., 1996).

An important observation of the failure pattern of specimens tested under compression was that, whereas the plain concrete showed quasi brittle mode of failure attendant with spalling matrix, the macro synthetic FRC exhibited a ductile failure with fibres holding the split matrix together as they resist the propagation of cracks.

4.2 Uniaxial Tensile Test

The uniaxial tensile tests as previously reported were carried out to determine the average residual uniaxial tensile strength upon which the creep loads were based. However, the results also give an understanding of the stress-crack opening relationship of macro synthetic FRC under uniaxial tensile loading. All the specimens were tested on the 28-day after curing by complete immersion in water.

4.2.1 Results

The result of the stress-crack opening (σ - w) relationship performed on three specimens at a loading rate of 0.01 mm/s is presented in Figure 4.1.

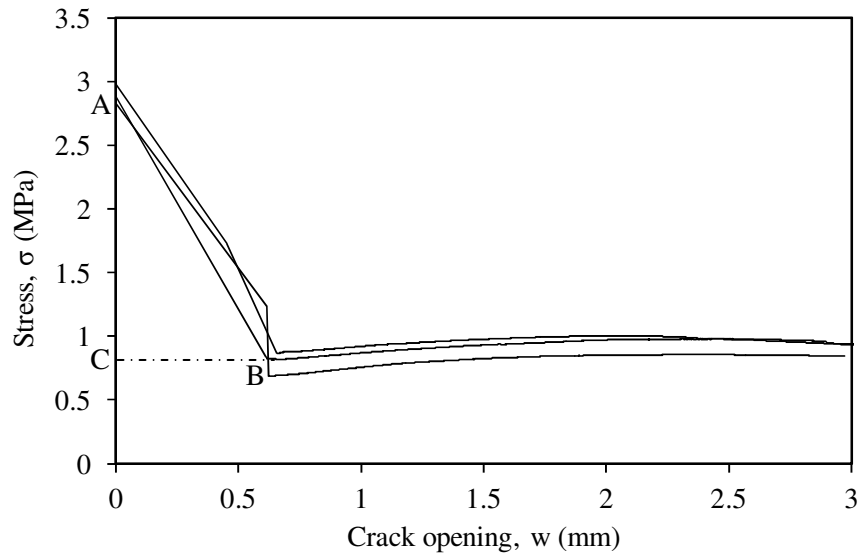


Figure 4.1: Response of macro synthetic FRC under uniaxial tensile load

The crack opening (w) is calculated from the average signal of the displacement transducers (LVDT) over a gauge length of 120 mm by subtracting the average displacement at peak stress, neglecting the elastic unloading. The stress (σ) was obtained by dividing the load by the net cross-sectional area of the notched specimens (6400 mm²). In this investigation, the region beyond the ultimate strength is of interest since the creep loads are based on percentages of the average post-peak strength hereafter called the average residual strength (ARS).

The result of the uniaxial tensile behaviour shows an average ultimate strength of 2.90 MPa. The ultimate strength is usually not influenced by the fibres at this stage except at high fibre content which is not the case for these tests (Richardson et al., 2010). It can however be observed that after the first crack (ultimate strength), significant crack opening results.

The ARS of the three specimens at the point where fibres are fully engaged, Point B is 0.78 MPa with an average CMOD of 0.60 mm. At the post crack region, the fibres are already fully engaged to control the crack opening of the specimens resulting in high energy absorption characteristics. Beyond

Point B, load carrying capacity of the specimens continues to increase (pseudo-hardening) as shown in Table 4.2.

Table 4.2: Load carrying capacity with increase in crack width

Crack width (w) in mm	Average residual stress (σ) in MPa
1	0.85
1.5	0.95
2.5	0.96
3	0.88

At a crack width of 3 mm, the load carrying capacity starts to decay and it is expected to continue until a complete fibre pullout occurs which is the characteristic failure mechanism. This shall be given further attention in the course of this dissertation. It is important to observe from Figure 4.1 that the scatter of the uniaxial tensile behaviour is low for the macro synthetic FRC investigated. Similar observation has been reported (Buratti & Mazzotti, 2012). The significant similarity in the post-peak behaviour could indicate a good fibre distribution in the cracked plane of all three specimens.

4.2.2 Discussion

At first glance, the result reveals a typical strain-softening behaviour of the macro synthetic FRC under uniaxial tensile loading. It should be noted that cracks propagated from the notched area for all specimens tested, which is the point of stress concentration. One clear observation from the result is that, as soon as the specimens cracked at the ultimate strength of the matrix, the failure was brittle leading to significantly drop in stress (Figure 4.1). This is known to be a material characteristic of concrete in general. Up to the ultimate strength of the matrix, a linear increase with deformation is observed (Figure 4.2). At ultimate load, high amount of energy is released from the matrix upon cracking resulting in an average crack opening of 0.013 mm at point A (before deduction of elastic response) and 0.6 mm at point B. This observed phenomenon could be attributed to the significant difference in the elastic moduli of concrete (about 30 GPa) to synthetic fibres (3-7 GPa) causing considerable fibre slip at the cracked plane (Hwan Oh et al., 2005).

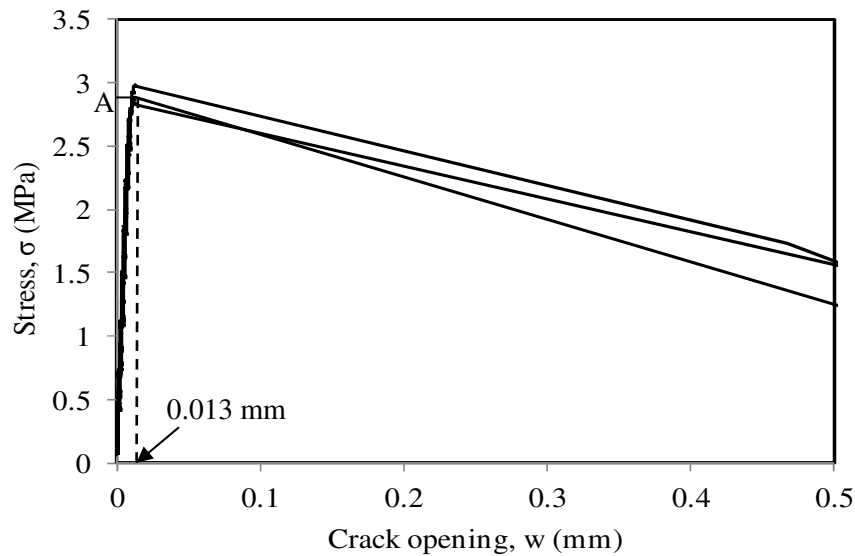


Figure 4.2: Linear response up to ultimate strength at Point A

The significant crack opening also leads to a significant reduction of the residual strength of the concrete before the fibres were fully engaged to control the crack opening. It is noted that there are no data points captured between the ultimate strength (point A) and the point where fibres are fully activated (point B) as presented in Figure 4.1. This gives an indication that there might not have been enough stiffness after cracking at ultimate strength to control the crack opening. The extensive drop in stress for strain softening composites under uniaxial tensile test has also been reported by Barragán et al. (2003) and Mouton & Boshoff (2012).

At the point B (the stress upon which the creep loads are based) where fibres are fully engaged to control the crack opening, the bond between the matrix and the aggregate at the cracking plane has been completely broken. Debonding and some form of fibre pullout is expected to have taken place at a crack width of 0.6 mm, hence, the stress-crack width relationship is then taken to be controlled by the frictional shear between the fibre and the matrix during fibre pullout. RILEM TC 162-TDF (2002) alluded to the fact that beyond a crack opening of 0.2 mm, the stress-crack width is only controlled by the fibre contribution. This phenomenon is also observed during the pre-cracking of all specimens that were later subjected to creep loads. It is acceptable to say that the pre-cracking of specimens introduced an initial damage to the fibre/matrix interface which is expected to have some effect on the time-dependent behaviour under sustained loading.

The extensive crack opening displacements experienced after the first cracking point may also be attributed, in a sense, to the high loading rate (0.01 mm/s) used. Steel FRC cylinders tested under uniaxial tensile loading at much lower speed sequence, 5-500 $\mu\text{m}/\text{min}$ up to a displacement of 2 mm, gave a better crack opening control without the sudden dissipation of energy (Barragán et al., 2003). Conversely, steel FRC tested in uniaxial tensile loading at a high loading rate of 0.017 mm/s showed a sudden dissipation of energy similar to that observed for the macro synthetic FRC investigated in this study (Mouton & Boshoff, 2012). The differences in response between the work of Barragán et al. (2003) and this study could be due to the control of the test.

The sudden energy released after the first crack (point A) has been reported to have a significant influence on the load-displacement graph (Banthia & Trottier, 1995). Since the fracture energy of cement based materials is calculated as the area under the stress-crack width graph, they reported that it will be misleading to assume fracture energy performance based on the area under such curve. This is particularly true when dealing with the area under the load-displacement curve of triangle ABC shown in Figure 4.1.

Beyond Point B as mentioned in the results, the residual stresses at defined crack widths increase up to a crack width of 2.5 mm showing a slight pseudo-hardening response in the strain softening branch. The increased toughness shows that the macro synthetic fibre used in this research proves to be structurally effective in transferring stresses between cracked planes under uniaxial tensile load. A number of reasons could be attributed to the pseudo-hardening behaviour observed in the strain softening portion. One reason is the increasing number of effective fibres crossing the cracked plane as cracks widens (Cunha et al., 2011). Due to the flexible nature of the macro synthetic fibres, fibres inclined at various angles to the cracked plane eventually become aligned to the direction of the applied load as the crack opening displacement increases (Carnovale, 2013). This phenomenon could thereby have contributed to the pseudo-hardening behaviour at a significant crack opening. Figure 4.3 shows this phenomenon by presenting a photo showing fibres aligned in the direction of the load at significant crack width.



Figure 4.3: Fibre aligned in the direction of loading

The stress-crack width relationship in this study is important as the flexural creep of cracked macro synthetic FRC are modelled using the material parameters obtained from the uniaxial tensile test. Though the flexural test is usually preferred to the uniaxial tensile test, the flexural test represents the structural performance whereas the uniaxial tensile test gives the material characteristics (Boshoff, 2007; Kanakubo, 2006). The stress-crack width relationship has been acknowledged to be useful in predicting the post cracking behaviour of concrete reinforced with short discrete fibres (Cunha et al., 2011; Cunha et al., 2012). It is estimated that when the material model parameters obtained from the uniaxial tensile test is directly used in the finite element modelling for the prediction of the flexural stress-crack opening displacement relationship, an overestimation is likely to be obtained due to the extensive crack widening discussed above. A number of modifications were made to the experimental average stress-crack width relation of the uniaxial tensile test to adequately predict the flexural response. This is fully discussed in Chapter 7 of this dissertation.

4.2.3 Experimental Observation during test

As already mentioned in the Chapter 3, two LVDT's were placed adjacent to each other to measure the crack mouth opening displacement over the notched area of the specimens. For specimens subjected to uniaxial stresses, it would have been assumed that stress distribution would have been uniform over the cracked plane, however, researches have shown otherwise (Barragán et al., 2003; Rots, 1988; van Mier & van Vliet, 2002). During the uniaxial tensile test of specimens, it was evident

in one instance that out-of-plane propagation of crack occurred. This observed phenomenon has also been reported by other authors (Barragán et al., 2003; Carnovale, 2013; Dupont, 2003). At the onset of the test, deformation of the matrix is linear with displacement up to the ultimate strength of the matrix just before first cracking. Soon after the first crack, non-symmetrical crack opening begins to ensue for one of the three specimens tested while the other cases displayed symmetrical propagation (Figure 4.4).

One reason for the out-of-plane propagation of crack in the specimen could be as a result of uneven distribution of fibres in the cracked planes (Carnovale, 2013). This however did not influence the response as shown in Figure 4.1. It is also worth noting that this phenomenon could not be observed for specimens that were pre-cracked and unloaded before being taken to the uniaxial creep frame where they were subjected to permanent loads.

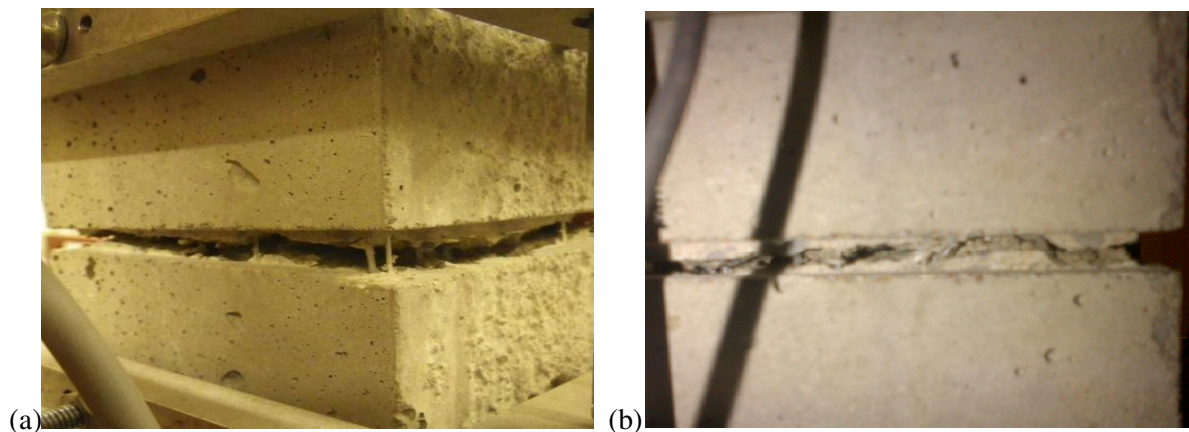


Figure 4.4: Propagation of crack (a) out-of-plane bending (b) symmetrical propagation

4.3 Uniaxial Tensile Creep

The uniaxial tensile creep of cracked macro synthetic FRC was investigated under five stress levels, 30 %, 40 %, 50 %, 60 % and 70 % of the ARS as previously mentioned. The results of the time-dependent propagation of the crack width and discussions of the results are presented in this section.

4.3.1 Results

Tensile creep loads were based on percentages of the average residual uniaxial tensile strength (Table 3.5) at the point where fibres are fully engaged as previously mentioned. Figure 4.5 shows the response of a specimen that was loaded, unloaded and reloaded up to a crack opening of 2 mm to investigate the reloading behaviour of a sample tested under uniaxial tension. The result obtained shows that the reloading of the specimen has a similar load carrying capacity in the post-crack region with those tested without unloading up to 3 mm. Hence it is reasonable to base the stress levels of the time-dependent tests on the ARS. The reloading process is also representative of specimens that were pre-cracked, unloaded and taken to the creep frame where they were subjected to sustained loads.

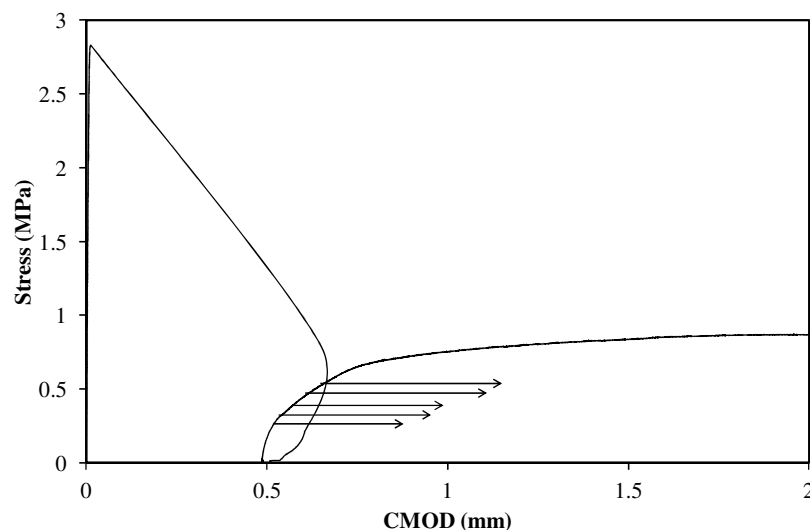


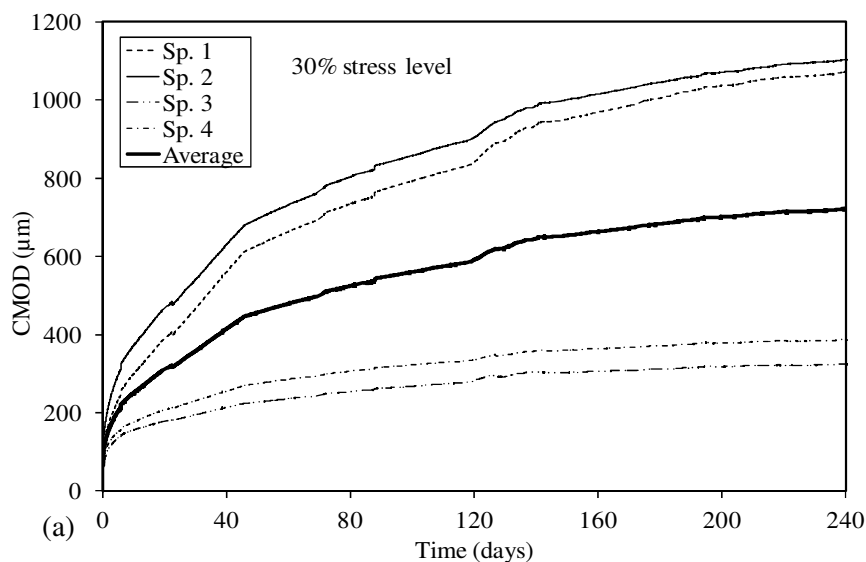
Figure 4.5: Unloading and reloading response under uniaxial tensile test

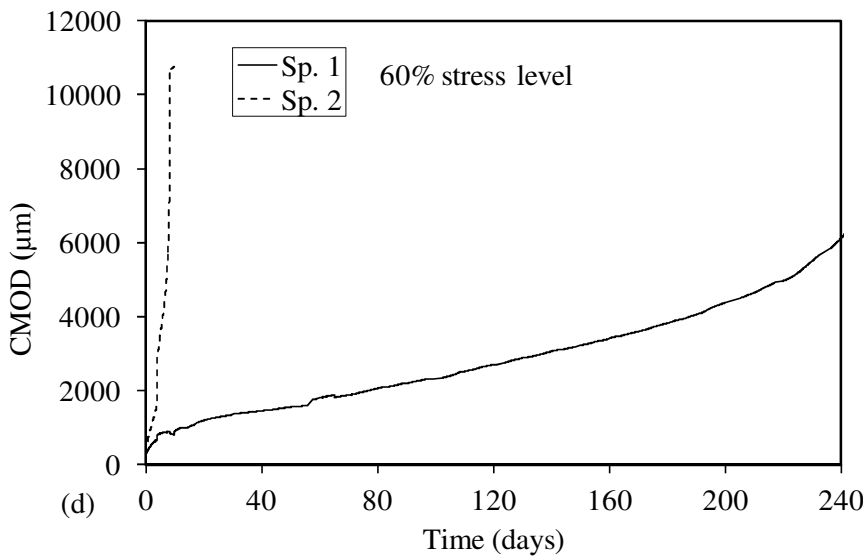
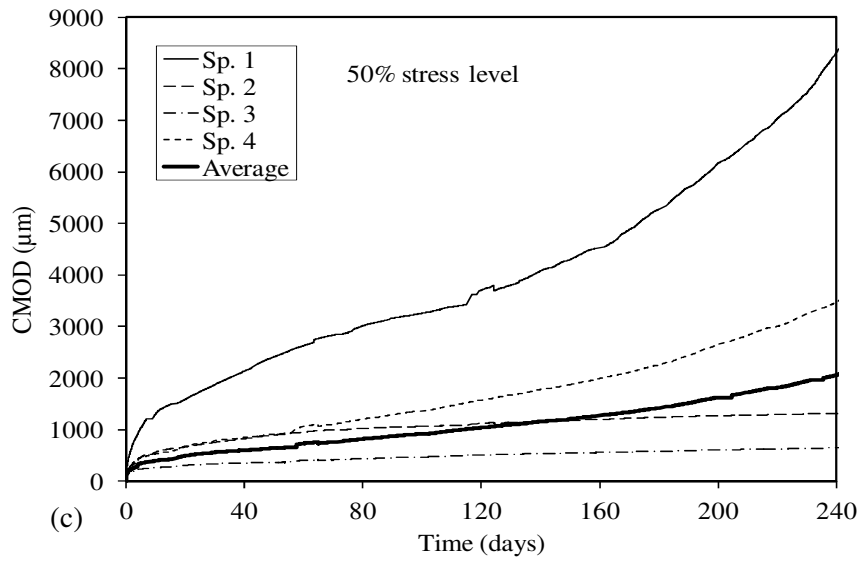
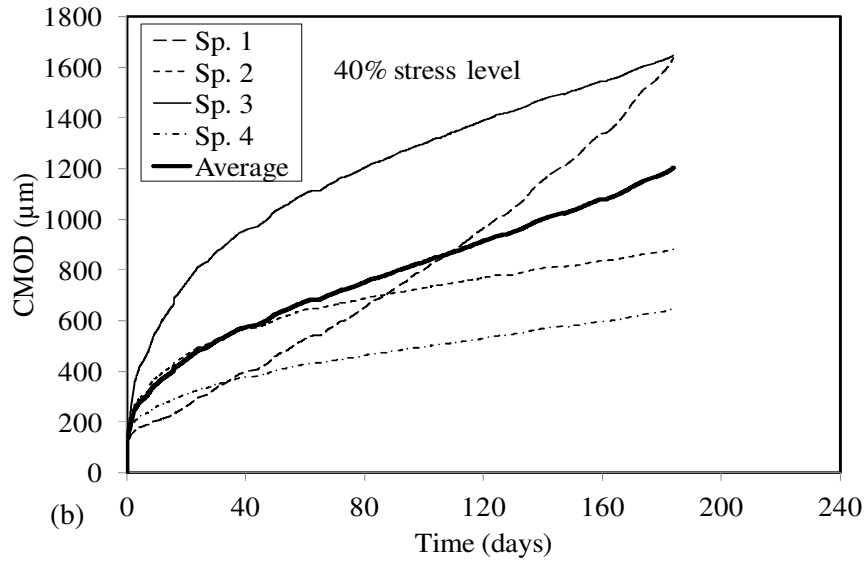
The response shows an irrecoverable crack opening of 0.5 mm upon fully unloading the specimen. The arrows indicated in Figure 4.5 represent the magnitude of the permanent loads applied to the specimens in the uniaxial tensile creep test. The arrows from bottom up represent the stress levels, 30 % to 70 % (in stepwise increase of 10 %) of the ARS respectively applied on the cracked specimens.

The total time-dependent CMOD of the specimens at the various stress levels investigated were measured as the cracking opening (w) from the irrecoverable crack width. It should be remarked that

during testing, drying shrinkage occurred in the specimens, hence an equivalent average shrinkage strain obtained from two unloaded specimens was deducted from the total creep strain. The result of the drying shrinkage is presented and discussed subsequently. After subtracting the drying shrinkage, the result gives the time-dependent CMOD of cracked macro synthetic FRC. The time-dependent deformation including the instantaneous deformation of the specimens at the various stress levels of the ARS measured as CMOD over a gauge length of 70 mm is presented in Figure 4.6 (a-g). Creep of the matrix over the gauge length is ignored as it is negligible for these relative small loads (less than 1 MPa) compared to the crack width increases.

Figure 4.6 shows the results of the uniaxial tensile creep tests. At all stress levels investigated, there was an initial increase in the CMOD as soon as the creep loads were applied. After two weeks of sustained loading, the specimens begin to show increase in cracking opening at a decreasing rate. On significant effect that can be established from the results is that, the time-dependent CMOD is sensitive to the applied stress level: the higher the sustained load, the higher the time-dependent CMOD. Stress level is a major factor influencing the time-dependent crack widening of cracked macro synthetic FRC.





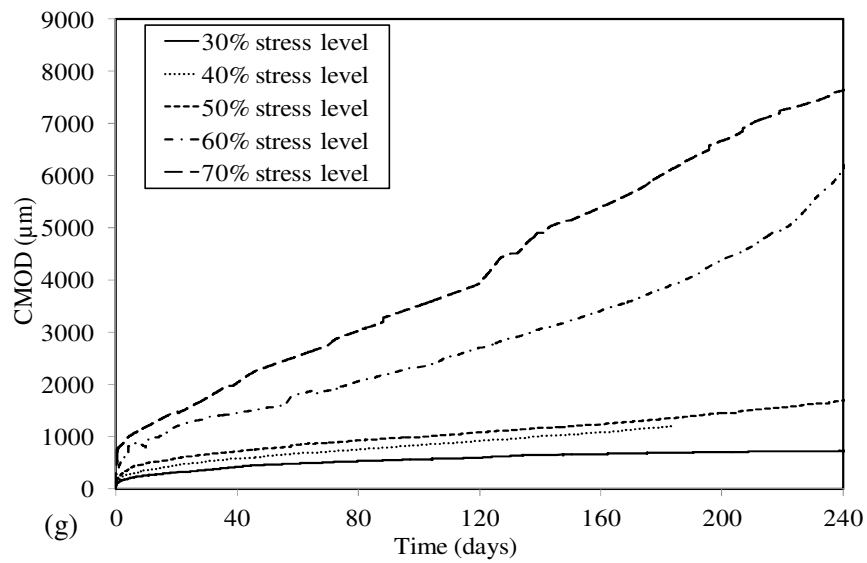
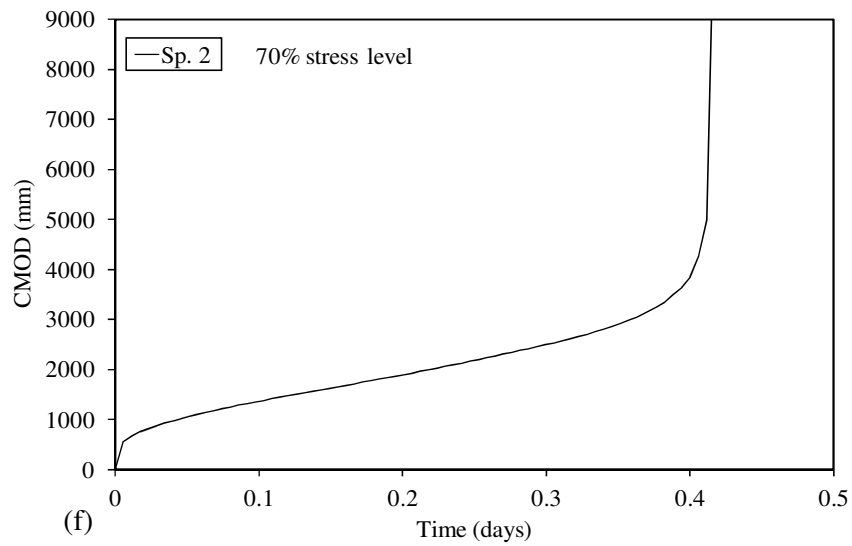
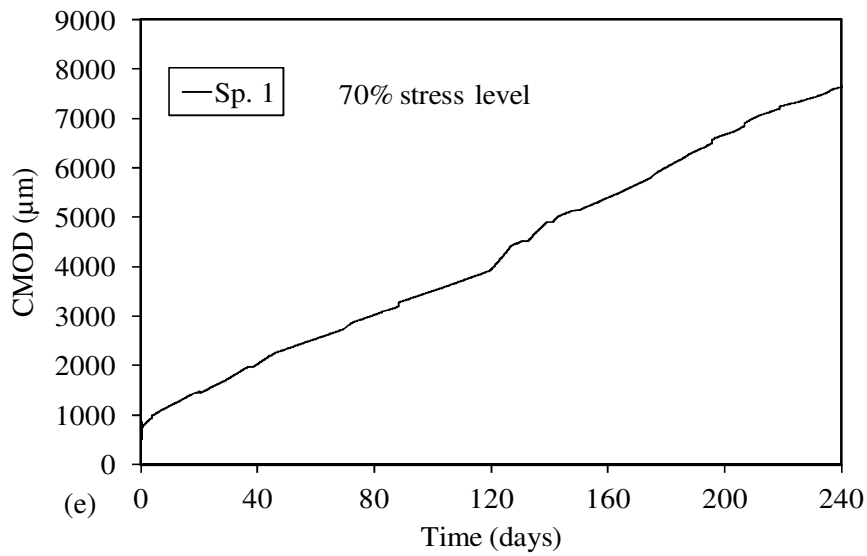


Figure 4.6: CMOD of tensile creep tests

4.3.2 Discussions

From Figure 4.6 a), specimens subjected to 30% stress level show similarity in the time-dependent CMOD for specimens tested in series (specimens 1 & 2-series 1; 3 & 4-series 2). However, significant variation can be seen when series 1 and 2 are compared. This could be due to the variation of fibre distribution on the cracked plane. This is discussed in Section for all observed variations. The total average time-dependent CMOD is calculated as:

$$CMOD_{tot} = CMOD_{irr} + CMOD_{inst} + CMOD_{creep} \quad (4.2)$$

where $CMOD_{irr}$ is the irrecoverable CMOD after unloading, $CMOD_{inst}$ is the instantaneous CMOD 1 minute after load application and $CMOD_{creep}$ is the actual creep.

Table 4.3 shows the total average time-dependent CMOD after 8 months of sustained loading at the various stress levels.

Table 4.3: Total average time-dependent CMOD after 8 months

Stress level (% ARS)	CMOD _{tot} (µm)
30	1200
40	1700
50	2100
60	6700
70	8300

The results of Table 4.3 are significant crack openings for the period investigated. While the four specimens at 30 % and 40 % were used to calculate the average CMOD, Specimen 1 was ignored in the determination of the average CMOD at 50 % stress level due to the high deviation of the result from the other specimens. Specimen 2 of 60 % stress level was also not used. At 40 % stress level, the result represented the time-dependent behaviour up to 6 months. Test could not be continued beyond 6 months due to unforeseen circumstances. An observation of Figure 4.6 g) gives an indication of sustainable stress up to 50% of the residual as this is yet to enter the tertiary creep stage.

At higher stress levels (60 % and 70 %), the time-dependent crack opening of macro synthetic FRC is more pronounced. Specimens exhibited the three stages of creep: primary, secondary and tertiary before failure. The specimens tested at 60 % stress levels had to be unloaded after 15 days of testing though fracture had not occurred. This was because CMOD of one of the two specimens had reached 10 mm (Figure 4.6 d), which is the maximum measuring capacity of the LVDT used. The specimen was removed from the creep frame and the other specimen was reloaded. Creep fracture however occurred for one of the two specimens at 70% stress level after 10 hours of loading. Both specimens (at 60 % and 70 % stress levels) had entered the tertiary creep stages before the unloading. The enlarged view of the time-dependent behaviour at 70 % stress level of one of the specimen at fracture is shown in Figure 4.6 f). The average CMOD at the different stress levels is presented in Figure 4.6 g).

It is evident from the average values, that none of the specimens attained an asymptotic limiting value. The above results indicate an alarmingly high CMOD of cracked macro synthetic FRC under sustained loading with fracture occurring at both 60 % and 70 % of the ARS of the specimens.

The CMOD-time relationship of cracked macro synthetic FRC at the various stress levels was further used to evaluate the creep performance by determining the coefficient of creep, defined as the ratio of creep strain to the instantaneous/elastic strain. However, some works have defined it in terms of crack width or deflection where strain values cannot be directly ascertained particularly for cracked FRC (Bernard, 2004; Blanco, 2013; Buratti & Mazzotti, 2012). In this work, the coefficient of creep, ϕ is defined in terms of the CMOD which is given as:

$$\phi(t) = \frac{CMOD_{creep}}{CMOD_{inst}} \quad (4.3)$$

The result of the creep at 30, 90 and 180 days represented as $CMOD_{cree(30)}$, $CMOD_{cree(90)}$ and $CMOD_{cree(180)}$ respectively and the instantaneous creep, $CMOD_{inst}$ is presented in Table 4.4. Also shown in Table 4.4 is the percentage difference in the CMOD between 30 and 90 days ($CMOD_{[30-90]}$),

90 and 180 days ($CMOD_{[90-180]}$). Six months is chosen for the purpose of comparison with specimens loaded at 40 % stress level. As previously stated, the specimens tested at 40 % had to be stopped after 6 months due to unforeseen circumstances.

Table 4.4: Uniaxial tensile creep parameters

Stress levels	$CMOD_{inst}$ (mm)	$CMOD_{creep(30)}$ (mm)	$CMOD_{creep(90)}$ (mm)	$CMOD_{creep(180)}$ (mm)	$CMOD_{(30-90)}$ (%)	$CMOD_{(90-180)}$ (%)	ϕ (30)	ϕ (90)	ϕ (180)
30%	0.017	0.357	0.546	0.65	53	19	21.06	32.18	38.24
40%	0.042	0.517	0.791	1.12	53	42	12.31	18.83	26.67
50%	0.070	0.655	0.960	1.25	47	30	9.36	13.71	17.85
60%	0.150	1.343	2.190	3.67	63	68	8.95	14.60	24.47
70%	0.280	1.737	3.280	5.71	89	74	6.20	11.71	20.40

From Table 4.4, the $CMOD_{inst}$ and $CMOD_{creep}$ increase with age and the creep load. The actual time-dependent deformation, $CMOD_{creep}$ shows to be several times higher than the instantaneous creep at each of the stress levels investigated. The percentage increases in the CMOD shows to be more significant between 30 and 90 days and increase at a decreasing rate. Marked decrease in the time-dependent crack width can be observed at 30 % stress level. Though decreases are also shown for other stress levels (except at 60 % which shows increase in creep), they are not as significant as the average CMOD at 30 %. At 60 % and 70 % stress level, the effect of the level of applied load is more pronounced on the creep even with increase in age. There seems to be no significant reduction between the two time periods reported above.

At each stress level, it is also seen that the creep coefficient increases with age (Table 4.4). Since the creep coefficient is known to be the capacity of concrete to creep (Gilbert & Ranzi, 2010), it therefore means that with increase in age, the specimens show more creep deformation at a decreasing rate for each stress level. While it is acknowledged that specimens with the lowest creep stress should show the least deformation tendency, the results in Table 4.4 and Figure 4.7 have shown otherwise. Similar observation has been reported by some authors (Blanco, 2013; Buratti & Mazzotti, 2012; MacKay & Trottier, 2004). While Table 4.4 shows the creep coefficient at specific times, Figure 4.7 shows the progression of the creep coefficient at each stress level until an age of 6 months.

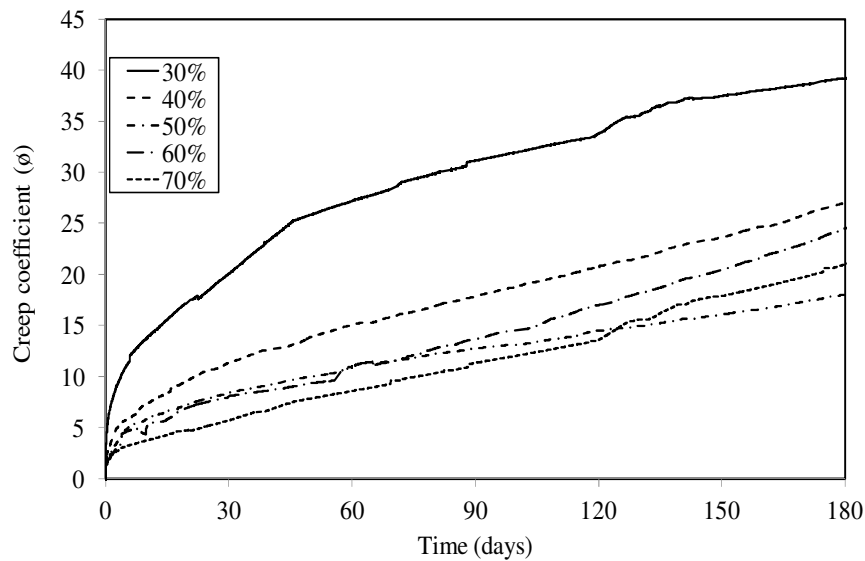


Figure 4.7: Creep coefficient of cracked FRC at different stress levels

4.3.3 Effect of cracked plane fibre count on the variability of CMOD

The results of the individual test specimen subjected to the same load level showed variability (Figure 4.6). It has earlier been suggested that the cracked plane fibre count of each sample could be responsible for the variation in the time-dependent CMOD behaviour at each stress level considered. To investigate this, un-fractured samples were separated into two at the end of the creep tests. Since the fibres are macro fibres, they were clearly visible, hence manual counting was done. The total numbers of fibres exposed, i.e. both sides added together, were counted. Note that there was no clear indication that any fibre fracture occurred. To verify this, the number of fibres protruding on the one side of the sample was compared to the holes left by the fibre pulling out on the other side of the sample. This study showed a good correlation between the number of fibres and number of holes, therefore it can be concluded that the fibres did not rupture and the fibre count is the actual number of fibres crossing the crack plane. All specimens have the same area of cracked plane (6400 mm^2).

The result of the fibre count on the cracked plane of the specimens tested under uniaxial tensile creep is presented in Table 4.5.

Table 4.5: Average fibre count on cracked plane of specimens at different stress levels

Stress levels	30 %				40 %				50 %				60 %		70 %	
Specimen No.	1	2	3	4	1	2	3	4	1	2	3	4	1	2	1	2
Fibre count	61	59	64	70	70	71	74	84	61	64	81	66	58	73	74	-
Average	63.5				74.75				68				65.5		74	

A careful consideration of the result reveals that the fibre counts on the cracked surface of each specimen within a stress level does contribute to the variability noticed in the time-dependent CMOD results previously discussed. For example, at 30 % stress level, Specimens 1 and 2 had lesser fibre counts compared to Specimens 3 and 4, hence they showed more time-dependent behaviour under sustained loading (see Figure 4.6 a). It will be noticed that Specimens 1 and 2 (Series 1) have almost equal fibre counts and their creep responses are almost the same just as Specimens 3 and 4 (Series 2) have close fibre counts and their responses are as well almost the same. However, the fibre counts of both series show significant time-dependent CMOD with Series 1 showing an average CMOD of 67 % higher than that of Series 2 (Figure 4.6 a). This is also reflected in the creep coefficient result discussed in the previous section. It is acknowledged that the variability in the fibre count only might not have been totally responsible for this significant difference. Other factors such as fibre orientation, fibre distribution on the cracked plane, fibre/matrix bond have been reported to affect the variability of the post crack behaviour in fibre reinforced cement composites (Ding, 2011; Li et al., 1990; Nguyen et al., 2014). It should here be remarked that the effect of fibre orientation is not considered in this work.

Similar pattern applies to specimens tested at all stress level. At 50 % stress level, Specimen 3 has the highest fibre count of 81 and hence, the lowest creep. This gives an indication that the more fibres there are on the cracked planes, the more active they are in bridging micro-cracks and the lesser the time-dependent CMOD. For the two specimens tested at 60 %, Specimen 1 shows far lesser fibre counts (58) compared to specimens 2 which have 73 fibre counts. As already mentioned, Specimen 1 with lesser fibre counts, experienced tensile creep failure after 15 days whereas Specimen 2 continues until 8 months, even though the creep shows significant CMOD at that period. Conclusively, it can be said that one of the factors that contributed to the variability of the time-dependent CMOD of

specimens in the same test group is the fibre count on the cracked planes. This is consistent with the fact that fibres/fibre counts have greater influence on the fracture properties of fibre reinforced cementitious composites than on their mechanical properties (Buratti & Mazzotti, 2012; Cifuentes et al., 2013).

4.4 Drying Shrinkage of Test Specimens

As already presented in Table 3.1, the drying shrinkage was measured on a $100\text{ mm} \times 100\text{ mm} \times 500\text{ mm}$ in conformity with the size of the specimens subjected to uniaxial tensile creep. The phenomenon of drying shrinkage in itself is known to be a complex phenomenon because of its sensitivity to many factors. The investigation of the drying shrinkage strain was carried out to distinguish between creep and drying shrinkage.

4.4.1 Results

The results of the drying shrinkage measured over a gauge length of 285 mm as described in Section 3.3.4 is presented in Figure 4.8 as shrinkage-time relationship over a period of 8 months. The time is reported in days commencing from the zero point which started at 28 days after curing by complete immersion in water.

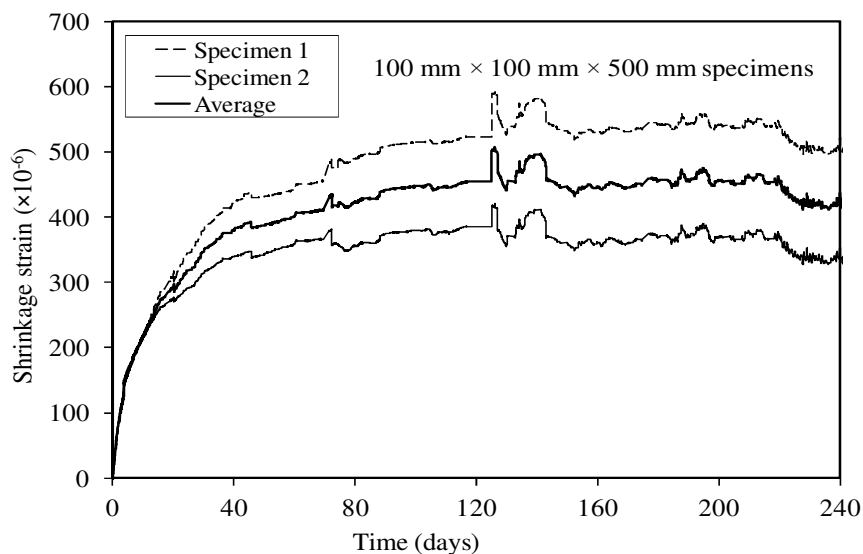


Figure 4.8: Drying shrinkage of macro synthetic FRC

The shrinkage deformation was calculated as the average displacement of the LVDT reading over the gauge length. Since this strain is subtracted from the actual creep deformation of specimens subjected to sustained uniaxial tensile loadings, the strain is converted to shrinkage displacement, δ_{sh} (mm) as:

$$\delta_{sh} = \frac{\text{Average LVDT reading}}{\text{Gauge length}} \times \text{gauge length of the creep specimen} \quad (4.4)$$

The drying shrinkage measured up to 120 days before an anomaly in the reading shows an average deformation of 440 μ strain. The anomaly is due to significant changes in the temperature/humidity of the climate controlled room where the test was carried out. The average shrinkage-time relationship tends to be approaching equilibrium with the test environment after about three months (150 days).

4.4.2 Discussion

The shrinkage response of the unsealed specimens shows a nonlinear rapid increase at the onset of the test up to 3 months. This agrees with the postulation that the drying shrinkage of Portland cement materials majorly occurs within the first 3 months and then continues at a decreasing rate (Neville, 2012). An anomaly in the strain-time relationship is observed at two instances when the humidity and temperature in the climate room became unstable due to the malfunctioning of the control unit. However, as soon as this was rectified, the shrinkage deformation can be observed to again assume its initial trend. The rapid increase in the shrinkage within the first three months indicates an increase in the loss of water from the specimen to the environment (evaporation) and begins to decrease as equilibrium is approached.

The effect of the macro synthetic fibres on the drying shrinkage of normal concrete was studied by comparing experimental results with the prediction model of the final draft of Model Code 2010. Figure 4.9 shows that the macro fibres increase the drying shrinkage of concrete. In FRC, macro fibres are known to create more voids in concrete as reported in this research. Since drying shrinkage is reported to depend on the size and type of voids in concrete (Pelisser et al., 2010), these voids could

have caused increase in the drying shrinkage of macro fibre concrete. However, on the overall, it can be concluded that the fibres have no significant effect on reducing the drying shrinkage of concrete. It is however acknowledged that the shrinkage was not compared to that of the same concrete without fibres. Some authors have also presented this view (Amin et al., 2014; Mesbah & Buyle-Bodin, 1999).

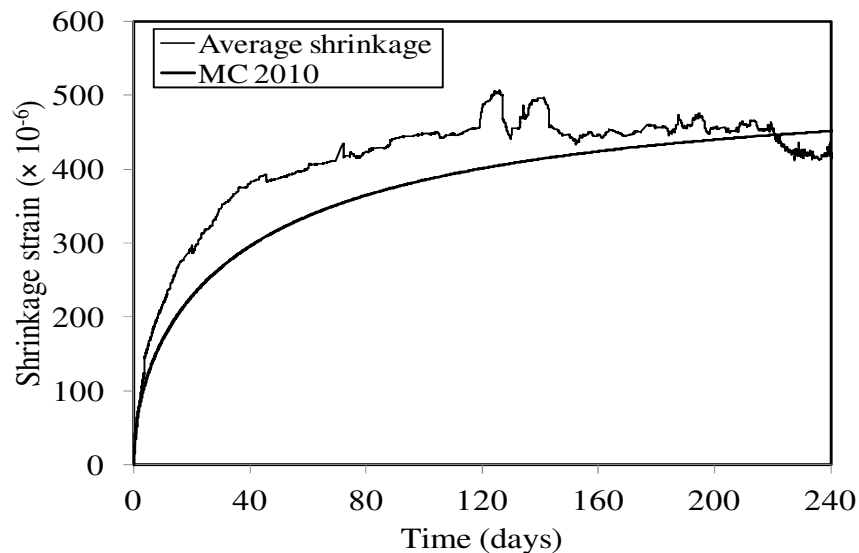


Figure 4.9: Time-dependent development of drying shrinkage

4.5 Summary

Experimental tests to study the behaviour of macro synthetic FRC subjected to compression, uniaxial tension, uniaxial tensile creep and drying shrinkage (macro level investigation) have been carried out.

The compressive strength test carried out for plain concrete and macro synthetic FRC at a fibre content of 9.1 kg/m^3 has shown that the addition of macro synthetic fibres to plain concrete lowers its strength by about 8 %. It is supposed that due to the balling tendency of fibres, increase air content could be trapped leading to reduced density of the FRC and invariably, the compressive strength.

Macro synthetic FRC specimens have also been investigated in uniaxial tensile test. Strain softening response is reported with significant CMOD before the fibres were fully engaged. The significant CMOD could be related to the significant difference between the elastic modulus of the fibre to the concrete matrix. However, significant toughness with a slight pseudo-hardening behaviour

is observed in the post crack region. Macro synthetic fibres are known to be flexible in nature. Inclined fibres at the cracked plane tend to eventually become aligned to the direction of the applied load with increase in the crack opening displacement, hence producing the pseudo-hardening response.

Specimens subjected to uniaxial tensile creep at varying stress level from low to high have shown significant creep even at a low stress level of 30 % average residual tensile strength. Tensile failure of specimens after 10 days and less than 1 day were also recorded at 60 % and 70 % post crack strength respectively. Increase in creep loads have generally led to increase in the time-dependent CMOD. Some variability found in the results have been attributed to the fibre counts on the cracked plane; the more the fibre counts, the lesser the creep response.

The drying shrinkage of macro synthetic FRC has shown to be close to the typical response of concrete modelled using Model Code 2010.

Chapter 5

Single Fibre Level Investigation

The nature of the interface between the matrix and fibre of a FRC has a significant effect on the quasi-static response of the material under load (Scheffler & Mäder, 2011; Zhandarov & Mäder, 2005). The nature of this interface, commonly referred to as the interfacial transition zone (ITZ) determines the load transfer mechanism from matrix to the fibre and hence, the reinforcing character of the fibre. Several attempts have been made in improving the interfacial shear resistance between the fibre and matrix by adopting fibres of different geometrical configurations, aspect ratios, fibre surface treatments and modification to the concrete mixes. Modification to the surface geometry of fibres from straight to a deformed configuration has been reported to increase the shear resistance between fibre and matrix (Oh et al., 2007; Singh et al., 2004; Wille & Naaman, 2012; Zile & Zile, 2013). The 'X' profile of the macro polypropylene (PP) fibre used in this study is designed to enhance the mechanical bond between the fibre and the matrix. A study of the interaction between the fibre and matrix using the single fibre pullout test will help to simulate the crack bridging capability of macro fibres. Again, an understanding of the pullout response can be correlated to the material behaviour of macro synthetic FRC.

In this chapter, an understanding of the mechanism causing the time-dependent crack widening of cracked macro synthetic FRC on the structural level is presented. To understand this mechanism, single fibre pullout (SFP) is studied by performing series of time-dependent SFP tests at different sustained stress levels. Furthermore, the creep of a single PP fibre subjected to sustained loading is also investigated as these types of fibres are known to show a time-dependent behaviour. However, the presentation of results in this chapter begins with the results of the uniaxial tensile response of single PP fibres subjected to quasi-static loading at different rates.

The evaluation of the short term pullout behaviour of single PP fibre is carried out with emphasis on studying the interfacial shear resistance due to pullout. The effects of rate and embedment length on pullout behaviour are particularly studied. A Scanning Electron Microscopy (SEM) investigation was also carried out on pulled out fibres to investigate the effects of the pullout rate on the surface of the fibres.

Finally, the results and discussions of the time-dependent single fibre pullout and macro fibre creep under sustained loadings are then presented.

5.1 Uniaxial Tensile Strength of PP Fibres

The effect of loading rate on the tensile strength of the macro synthetic PP fibres under four loading rates is reported. The uniaxial tensile response was investigated using three PP fibres at each loading rate considered. The tensile strength of the fibre was investigated to study to response of the fibre under direct tensile load at different loading rates and to determine the exact fibre strength (see Section 3.5.2).

5.1.1 Results

The macro synthetic fibre tested has a nominal diameter of 0.8 mm, fibre length of 40 mm and cross-sectional area of 0.55 mm². Since the fibre does not have a round surface area, the effective diameter was computed and used for the analysis of the results as discussed in Section 3.1.2. The effective diameter, d_e was calculated to be 0.794 mm.

The result of the direct tensile tests on the fibres presented as breaking load, P in (N) versus fibre elongation, e_f in (mm) is shown in Figure 5.1. The fibres were tested in a controlled environment under constant temperature of 23 ± 1 °C and a relative humidity of $65\pm 5\%$.

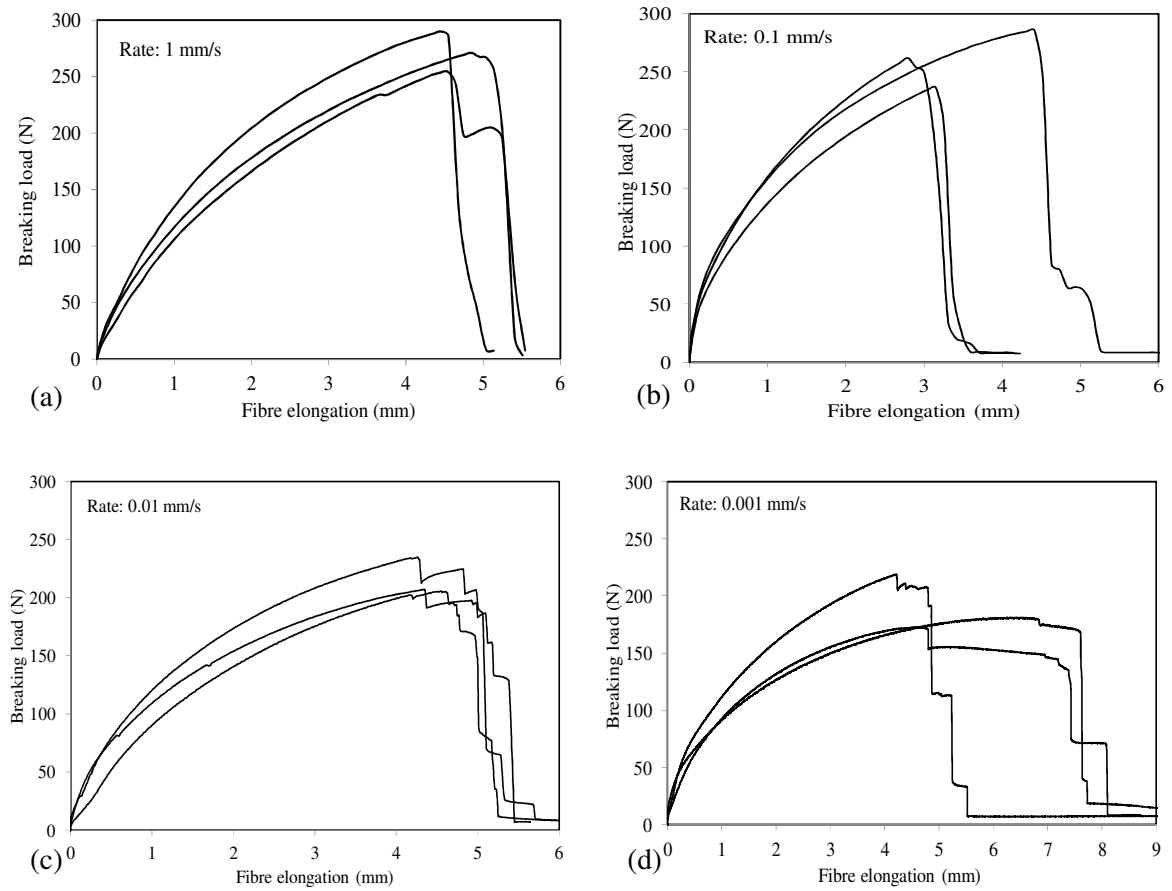


Figure 5.1: Single fibre tensile test result at different loading rate

The output of the average breaking loads at the various loading rates is presented in Table 5.1.

Table 5.1: Average breaking load of PP fibre

Loading rates (mm/s)	Average breaking load (N)
1	271.74
0.1	261.14
0.01	214.45
0.001	192.96

These average breaking loads give average maximum tensile strengths of 549 MPa, 527 MPa, 433 MPa and 390 MPa at loading rates of 1 mm/s, 0.1 mm/s, 0.01 mm/s and 0.001 mm/s respectively as shown in Figure 5.2. The effect of loading rate is seen on the tensile behaviour of the macro PP fibres.

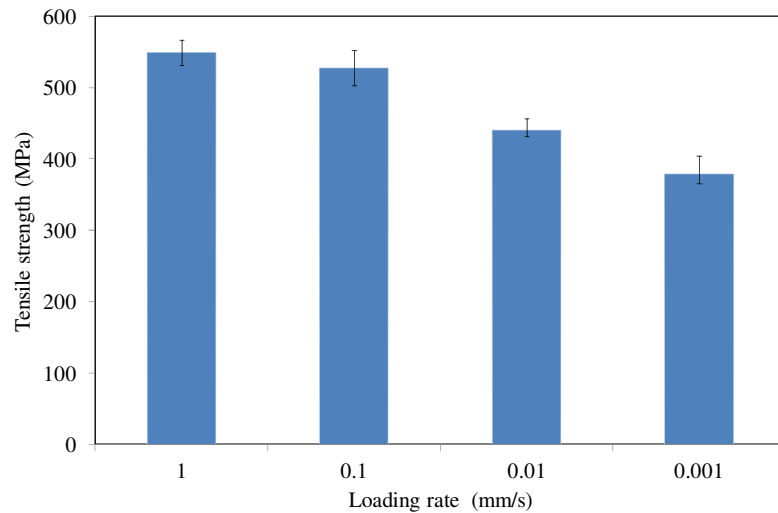


Figure 5.2: Average maximum tensile strength of macro PP fibre

5.1.2 Discussion

The response of the macro synthetic fibre under direct tensile test shows a typical non-linear material behaviour from the start of the test with parabolic curves up to fibre breakage. The breaking load-elongation graphs (Figure 5.1 a-d) show the fibre responding in a similar way at all the loading rates, hence the loading rate does not influence the non-linear response. From high to very low loading rate, the behaviour shows no elastic response before entering a non-linear regime. The single fibre subjected to creep load at 30 % of the average tensile strength which is discussed later, also exhibited the same non-linear behaviour.

The increase in the breaking load of the fibre with increase in the loading rate over and above the breaking load at 0.001 mm/s is shown in Table 5.2.

Table 5.2: Percentage increase in average breaking load

Loading rate (mm/s)	Percentage increase
0.001	-
0.01	11
0.1	35
1	41

The result of Table 5.2 indicates that better usefulness of the fibre is achieved when the tensile capacity of the fibre is enhanced. In this light, some recent publications have reported better concrete

composite behaviour with macro synthetic fibres of higher tensile strength and elastic modulus (Carnovale, 2013). However, care must be taken to ensure that in improving the tensile capacity of this type of fibre, the mechanism of fibre pullout which is desirable in the composite behaviour is not altered. As expected during the direct tensile tests of the fibres, failure occurred at maximum load by fracturing as shown in Figure 5.3.

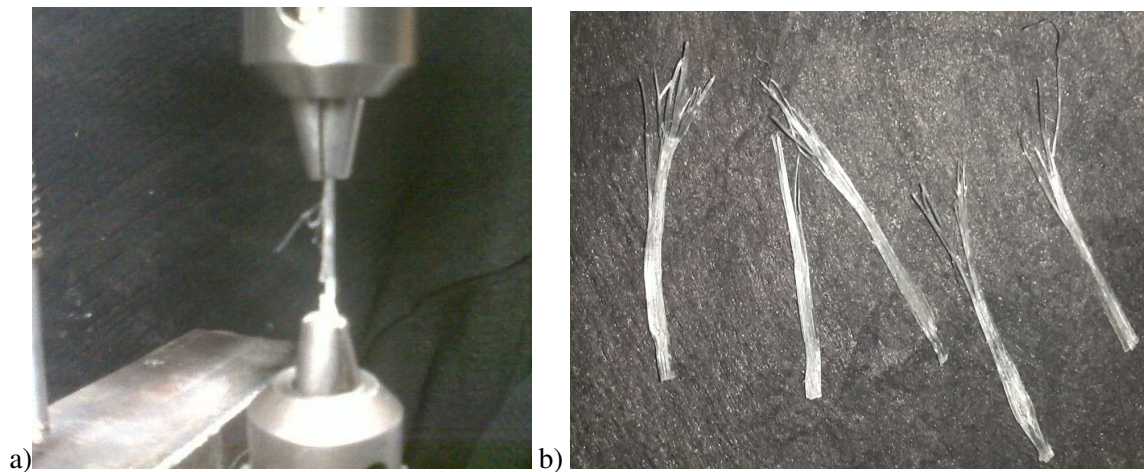


Figure 5.3: Fractured macro synthetic fibres

5.2 Single Fibre Pullout Rate Test

A number of scholarly articles have been published on the pullout behaviour of fibres (steel and synthetic) under static loading. While the evaluation of loading rates effect on the pullout behaviour of steel fibres is being given much attention lately due to consideration for seismic and impact loading (Wille & Naaman, 2012; Yang & Li, 2014), less is reported for macro synthetic fibres. The fibre pullout test will help to characterise the interface parameters based on the embedment lengths and the loading rates investigated. At least three specimens were tested at each loading rate and averages were computed based on the number of specimens.

5.2.1 Results

Figure 5.4 a-d) presents the results of the single fibre pullout behaviour of macro synthetic fibre from concrete matrix at an embedment length, E_L , of 10 mm. The pullout rate was varied over four orders of magnitude from 0.001 mm/s to 1 mm/s. The pullout force is expressed as interfacial shear

resistance by dividing it by the surface area of the embedment length of the fibre in contact with the matrix according to Equation 3.2 using the effective fibre diameter. For the purpose of comparison with the pullout behaviour at other embedment lengths, the pullout displacement has been normalised according to Equation 3.3.

The stress-pullout displacement curve at all loading rates show similar softening pattern. The result presented in Figure 5.4 shows softening pullout behaviour at the loading rates investigated. This response is consistent with the behaviour of macro synthetic FRC tested under uniaxial tensile loading reported in Chapter 4. It should be remarked that all fibres pulled out of the concrete matrix at the end of the test. This is also consistent with the results of specimens tested on the macro level (see Chapter 4) where specimens that fractured under short and time-dependent uniaxial tensile loadings show complete pullout of fibres in all cases. Similar response of PP fibres pulled out from mortar samples has been reported (Gokoz & Naaman, 1981).

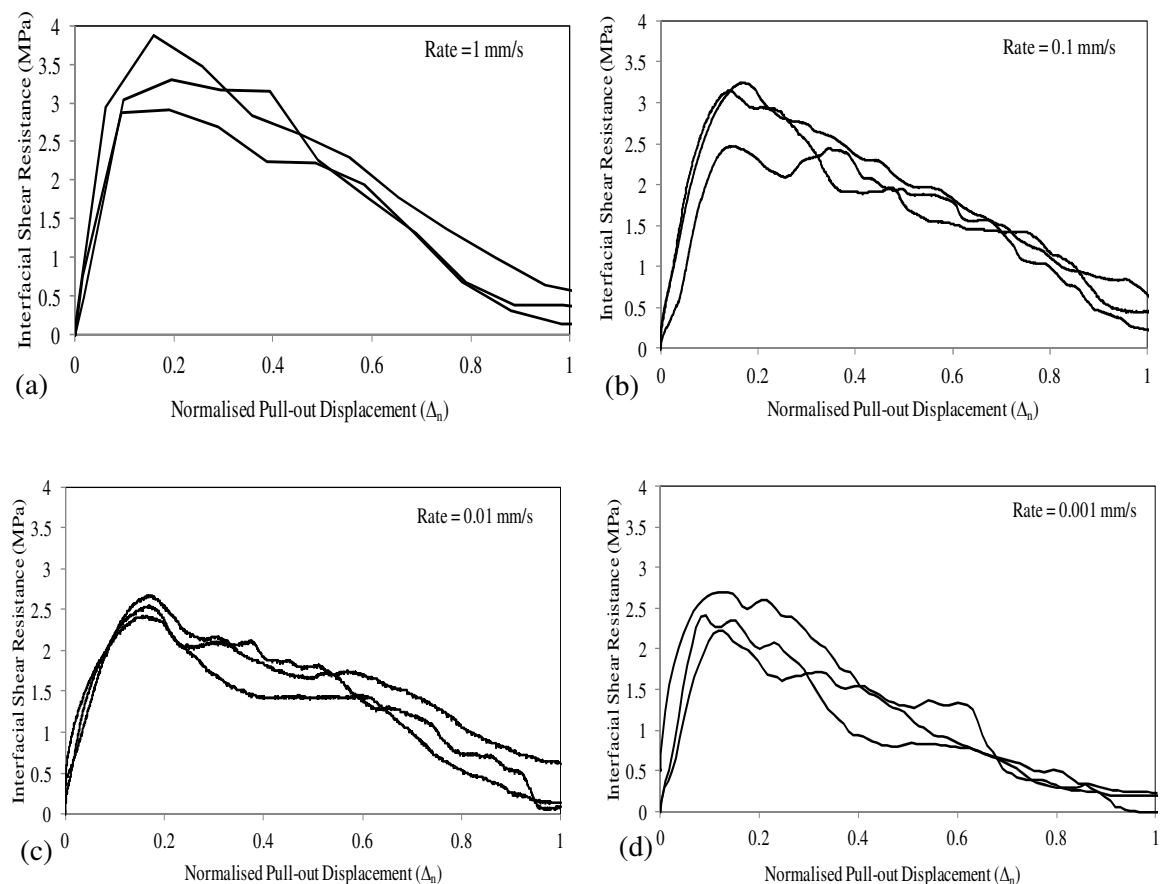


Figure 5.4: Rate dependence of single fibre pullout at embedment length, $E_L = 10$ mm.

At the highest loading rate investigated, 1 mm/s, the interfacial shear resistance shows a linear response before attaining the peak stress. At other much lower rates, this phenomenon is not so much evident as the pullout behaviour before peak stress is more of a non-linear response.

A consideration of the rate effect on fibre pullout for the four orders of magnitude tested (Figure 5.4) appears to fall into two categories: high and low rate response. Output of maximum average interfacial shear stress (τ_{\max}) between 0.1 mm/s to 1 mm/s is regarded as Series 1 while between 0.001 mm/s to 0.01 mm/s are taken as Series 2 due to shear resistance difference of less than 10 % in both series. Beyond peak stresses, the bond decreases significantly with decrease in the embedment length as the fibre pulls out.

Figure 5.5 a-d) shows the result of the single fibre pullout rate test at an embedment length, $E_L = 15$ mm.

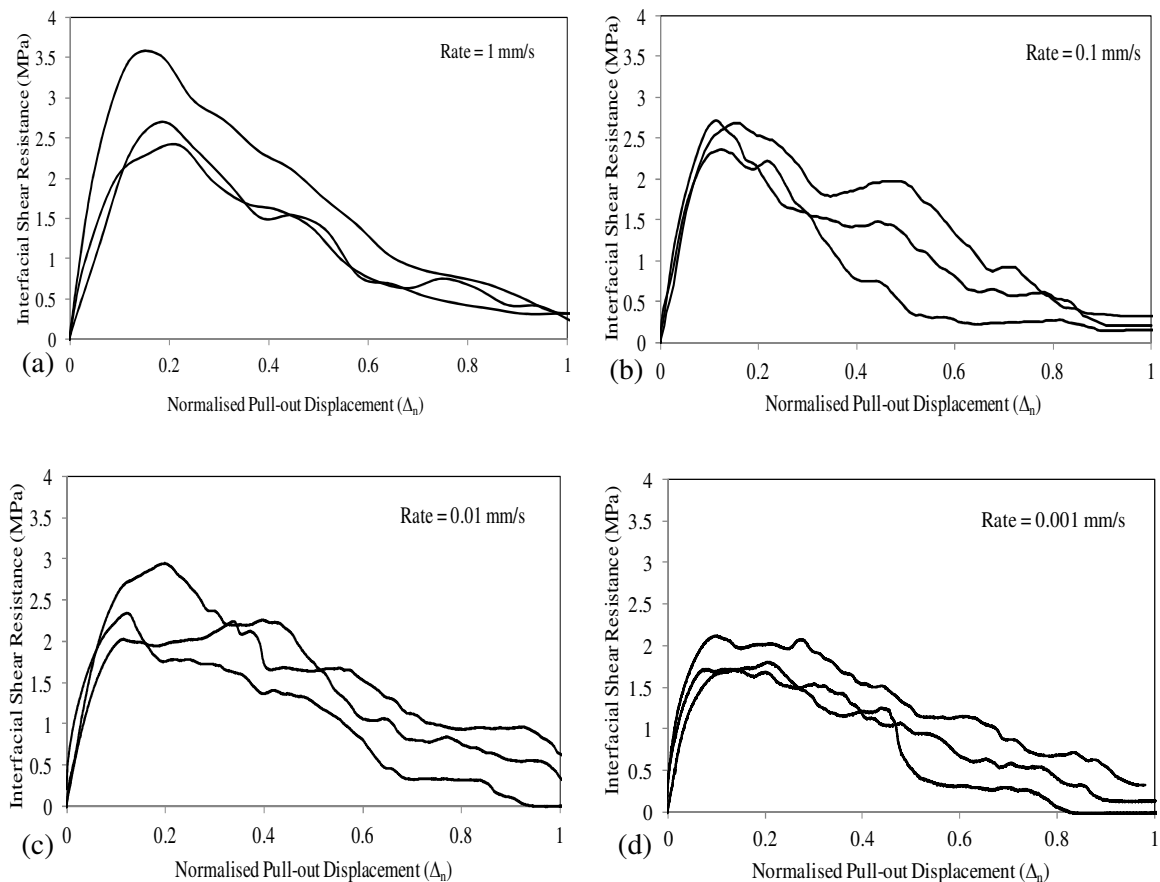


Figure 5.5: Single fibre pullout tests results at embedment length, $E_L = 15$ mm

The pullout behaviour shows similar stress-displacement response to those tested at $E_L = 10$ mm. However, lower values of τ_{\max} are obtained at the various loading rates when compared with results presented in Figure 5.4. The loading rate response of the τ_{\max} can also be said to fall into the two series mentioned at fibre $E_L = 10$ mm. However, a slightly higher variation is observed with increase in the embedment length. The τ_{\max} differs one from another at the various loading rates tested: 0.1 mm/s differs from 1 mm/s by about 11 % while 0.001 mm/s differs from 0.01 mm/s by about 14 %.

For specimens tested for pullout at $E_L = 25$ mm, the result is presented in Figure 5.6 a-d). The mechanism of the pullout behaviour follows similar pattern exhibited at fibre $E_L = 10$ mm and 15 mm.

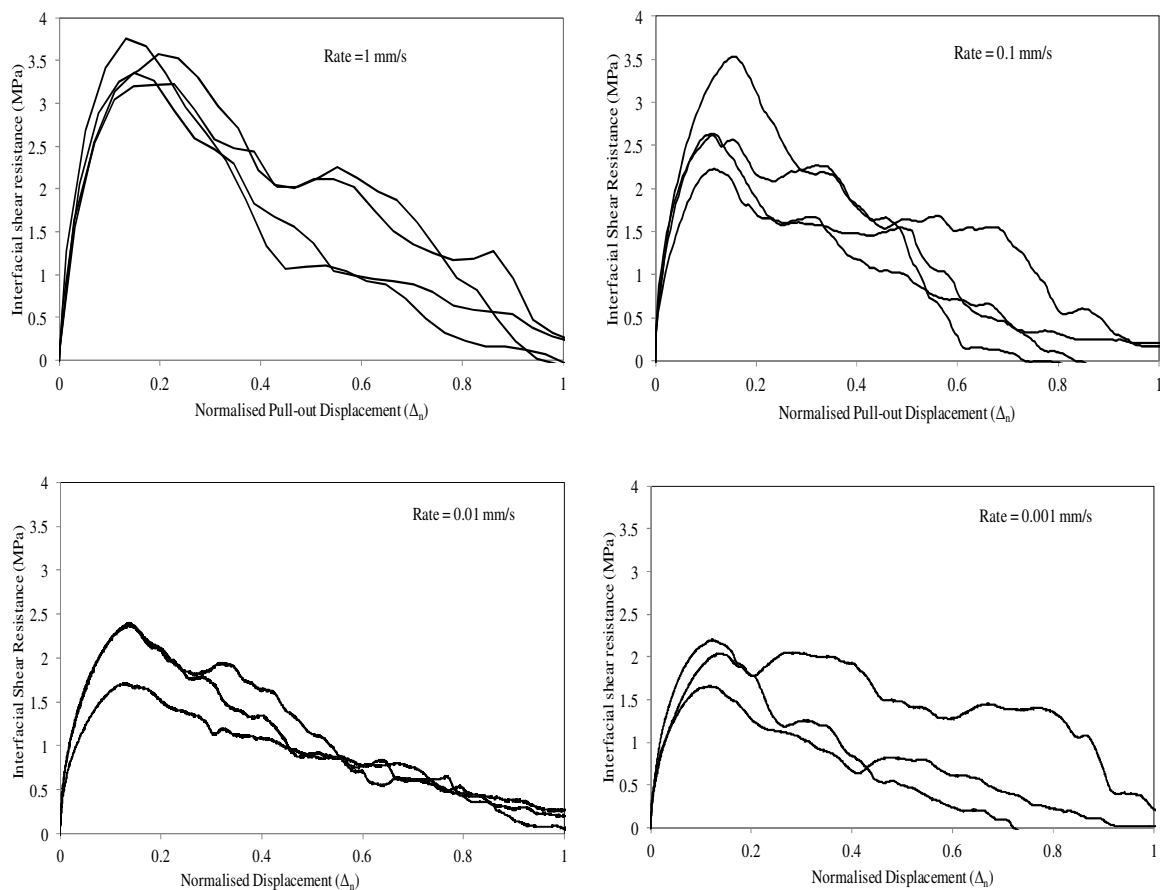


Figure 5.6: Single fibre pullout tests results at embedment length, $E_L = 25$ mm

The embedment length tends not to have any significant influence on the shape of the stress versus pullout displacement curve. As with other embedment lengths, the highest loading rate also shows

better linear response before peak load compared to the lower rates. This phenomenon is consistent irrespective of the embedment length investigated.

The variation of the τ_{\max} between the loading rates tested also shows to increase with increase in the embedment length. At $E_L = 25$ mm, while the lower rates (0.01 mm/s and 0.001 mm/s) differ in shear resistance by 11 %, it is more pronounced between 0.1 mm/s and 1 mm/s, that is, 42 %.

The pullout load of the fibres from the concrete matrix is rate sensitive. A plot of the maximum average pullout load against the loading rates at the different embedment length is presented in Figure 5.7. The pullout load evidently increases with increase in the embedment length of the fibre and also increases with increase in the pullout rate.

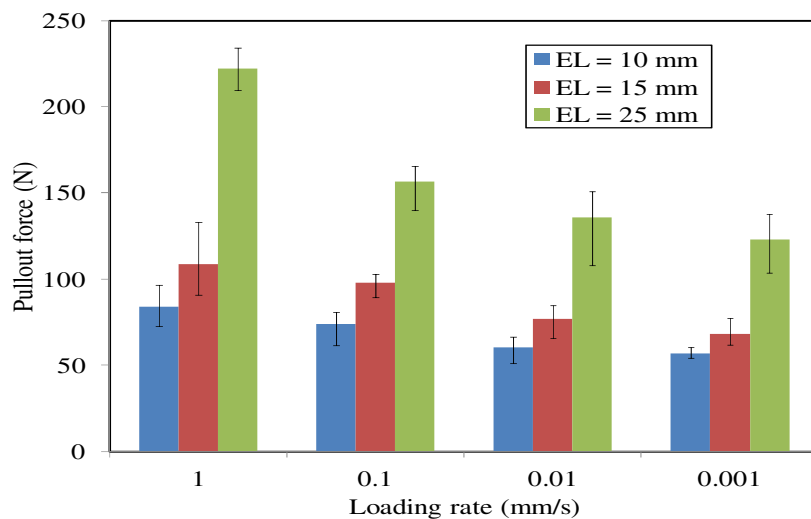


Figure 5.7: Effect of loading rate and embedment length on the pullout load of single embedded fibres

Conversely, the τ_{\max} however decreases with increase in the embedment length except at loading rate of 1 mm/s as presented in Figure 5.8. While it has been said that the interfacial shear stress decreases with increase in the embedment lengths and increases with increase in pullout rate, the effects on the deformation of the fibre surface were also studied using scanning electron microscopy (SEM). It should be remarked that one fibre pullout rate (1 mm/s) was evaluated for effect of embedment length and one embedment length (15 mm) for effect of pullout rate. They were examined to investigate the damage to the surface of the fibre in comparison to an untested fibre which serves as the control.

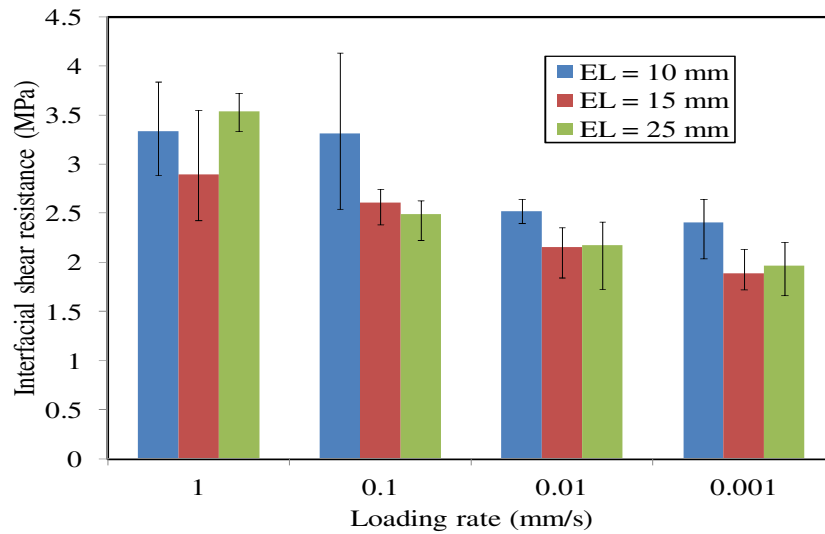


Figure 5.8: Effect of loading rate and embedment length on τ_{\max}

Figure 5.9 shows the SEM photos starting with the untested fibre and surface damage to fibres at the three embedment lengths. In Figure 5.10, the surface damage due to effect of loading rate at embedment length of 1 mm/s is depicted.

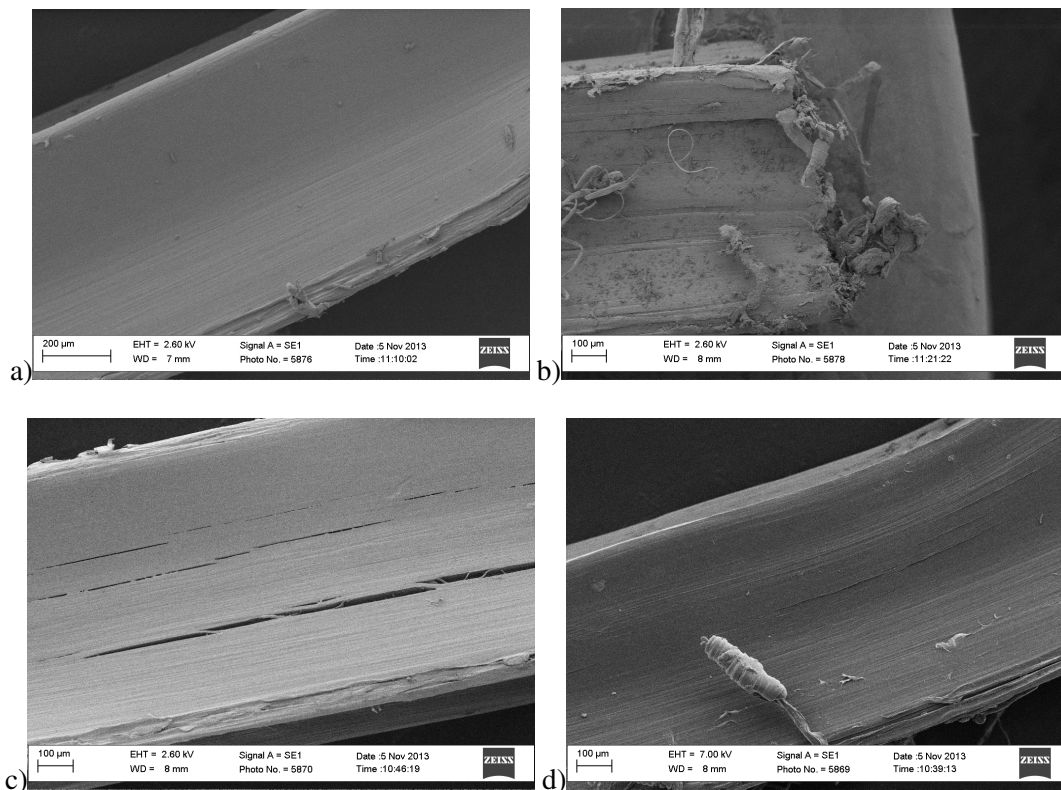


Figure 5.9: Macro PP fibre surface damage with varying fibre embedment length. a) SEM photo of unused fibre. b) $E_L = 10$ mm; c) $E_L = 15$ mm; d) $E_L = 25$ mm

Since all the fibres pulled out from the concrete matrix, it was considered unnecessary to examine the grooves created in the matrix for possible trace of fractured fibre. The photos shown in Figures 5.9 and 5.10 reflect different degrees of damage on the surface of the fibres due to frictional effect between the fibre and the matrix during pullout when compared to the unused fibre.

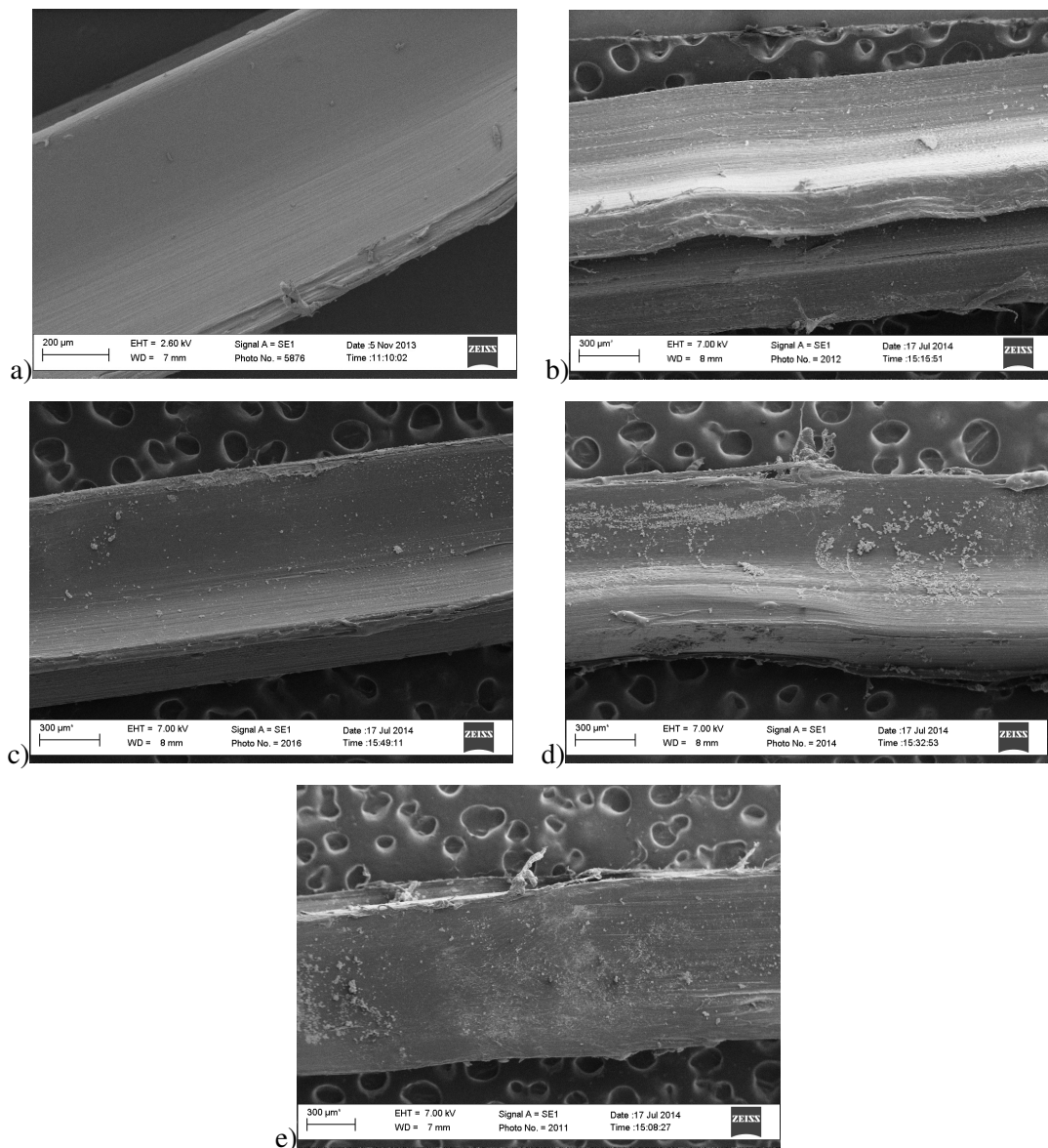


Figure 5.10: Effect of pullout loading rate on macro PP fibre surface. a) SEM photo of unused fibre. b) Loading rate, LR = 1 mm/s; c) LR = 0.1 mm/s; d) LR = 0.01 mm/s; e) LR = 0.001 mm/s

5.2.2 Discussion

The nature of failure for all fibres tested at all loading rates and embedment lengths has been complete pullout. As remarked by earlier authors, this is characteristic of macro PP fibres and it

indicates that the adhesion between the fibre and the matrix at the ITZ is weaker when compared to the strength of the matrix and that of the fibre (Richardson, 2005; Singh et al., 2004). It should be noted that this type of behaviour is desirable unlike micro synthetic fibre such as PVA (hydrophilic in nature) where fibres are reported to have ruptured during fibre pullout test due to the high chemical bond between the fibre and the matrix (Boshoff et al., 2009b; Kanda & Li, 1998; Lin et al., 1999). With the complete fibre pullout mechanism of macro synthetic fibres from the concrete matrix, sudden failure in structures where such fibres are utilized could be prevented as would the case if fibre failure occurs by rupturing. This is demonstrated in the results of the macro synthetic FRC specimens tested under uniaxial tensile and flexural loadings showing considerable post cracking ductility.

The response of the maximum fibre stresses at pullout under different loading rates shows similar pattern of increase except for pullout rate between 0.1 to 1 mm/s at embedment length of 25 mm. The pullout fibre stress increases up to 450 MPa from 0.1 to 1 mm/s (Figure 5.11). The maximum fibre stresses was obtained by dividing the maximum load at pullout by the effective fibre area. When these results are compared with the direct tensile stresses of the fibre at the same loading rate (Figure 5.2), the maximum fibre pullout stresses show lower values. So, the complete fibre pullout behaviour is predicated on the fact that the maximum fibre tensile stresses at pullout are less than the experimental direct tensile stresses of the PP fibre.

The complete pullout phenomenon of macro PP fibres can also be evaluated on the basis of the critical fibre length. Beyond the critical length, fracture is expected to occur (Boshoff et al., 2009b; Fu et al., 2000). The critical fibre length (l_c) is presented as:

$$l_c = \frac{d_f \sigma_{f,max}}{2\tau_{avg}} \quad (5.1)$$

where d_f is the effective diameter of the fibre, $\sigma_{f,max}$ the maximum pullout fibre tensile stress and τ_{avg} is the mean interfacial shear resistance obtained from the single fibre pullout experiments.

At all three embedment lengths, the critical length are greater than the fibre length and is apparently twice the fibre length.

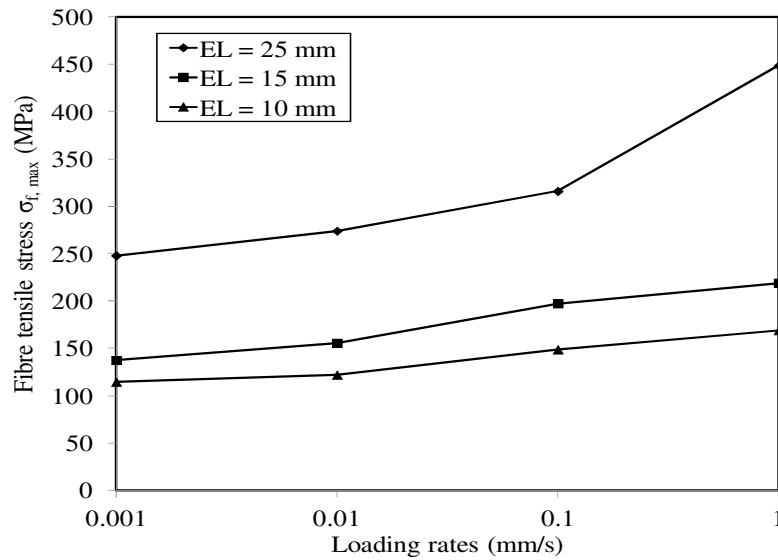


Figure 5.11: Effect of pullout rate on the fibre tensile stress

On the average, the critical fibre length obtained at embedment lengths of 10 mm, 15 mm and 25 mm are 20 mm, 30 mm and 50 mm, respectively (Figure 5.12).

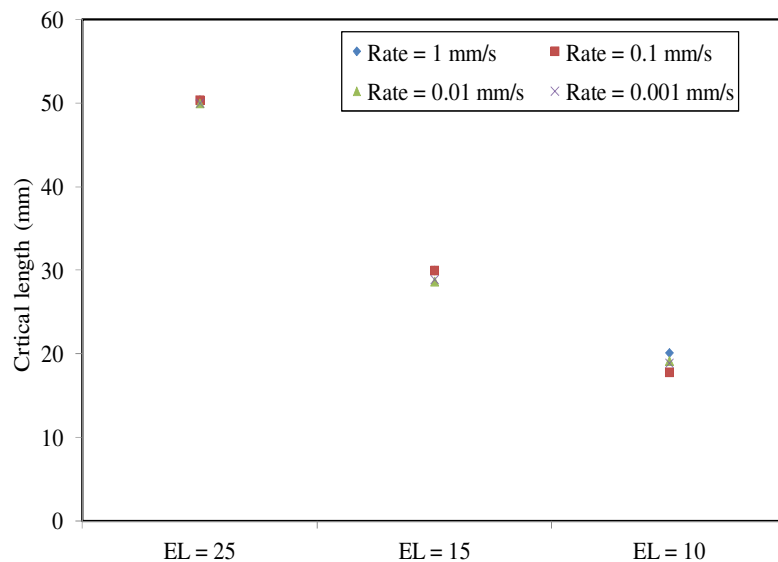


Figure 5.12: Critical fibre length at different embedment length

The interfacial shear stress is a good indicator of load transfer ability between the matrix and the fibre. It has been mentioned that this parameter was calculated from the load output as a function of the embedment length and the effective diameter of the fibre. For the Rocstay macro PP fibres tested in this research, the average maximum interfacial shear stress ranges from 2.0 to 3.4 MPa for the

various loading rates and embedment lengths investigated. This result agrees well with the bond strength results for deformed/short crimped PP fibres reported by Carnovale (2013) and Richardson (2005). As reported, the interfacial shear resistance is influenced by the loading rate and the fibre embedment length. The test results indicate that the higher the pullout rate, the higher the interfacial shear resistance. This phenomenon is caused by the clamping pressure exerted on the surface of the fibre by the acceleration of material points surrounding the fibre (Tran & Kim, 2013), hence increasing the frictional coefficient.

Generally, effect of loading rate on pullout response of fibres embedded in cement matrix is reported to be produced from micro cracking within the specimen in the vicinity of the fibre embedment (Kerans & Parthasarathy, 1991; Kim et al., 2008). At embedment length of 10 mm, the sensitivity of fibre pullout between 0.1 mm/s and 1 mm/s is insignificant. In fact, the maximum average interfacial shear resistance is almost the same. The insensitivity of the interfacial shear resistance to loading rate is believed to be caused by the shorter loading time due to the small embedment length of the macro fibre and this has also been corroborated by Tran & Kim (2013). For lower loading rates, 0.001 mm/s and 0.01 mm/s, micro cracking would have significantly occurred due to longer pullout time. However, the embedment length could still be a factor that resulted in a similar output at both loading rates. When a greater embedment length is considered, such as 15 mm and 25 mm, the interfacial shear resistance is seen to be more sensitive to the loading rate. With fibre embedment lengths of 15 mm and 25 mm, more surface contact is made between the matrix and the fibre, hence the rate effect is more pronounced. Increases in the average maximum interfacial shear stresses at the various loading rates over the lowest loading rate, 0.001 mm/s are shown in Table 5.3.

Table 5.3: Increase in τ_{\max} at different loading rates and embedment lengths

Loading rate (mm/s)	% Increase in τ_{\max}		
	$E_L = 10$ mm	$E_L = 15$ mm	$E_L = 25$ mm
0.001	-	-	-
0.01	1700	14	11
0.1	2100	39	28
1	8300	54	81

These increases establish that the fibre embedment length is a critical factor for consideration with respect to the bond strength between the matrix and the fibre. Since it has also been reported that the pullout behaviour of fibres in a single fibre pullout test has a direct relation to the behaviour of specimens tested at structural levels (Kim et al., 2008; Tran & Kim, 2013; Tran & Kim, 2014), it is believed that the uniaxial tensile and flexural responses of macro synthetic FRC will also be rate sensitive though not covered in this work.

Whereas the interfacial shear resistance increases with increasing pullout rate at the various embedment lengths considered, the reverse is the case with increase in embedment length. Similar phenomenon has also been reported for micro synthetic fibre (Boshoff et al., 2009b). Earlier works on fibre pullout behaviour had assumed a uniform distribution of shear stress along the ITZ between the fibre and the matrix. However, this is not true as the results of this investigation shows (Figure 5.8) and other works have proven (Fu et al., 2000). It has been described above that with a shorter pullout time for shorter embedment length, a confining pressure builds around the fibre from the surrounding leading to higher interfacial shear resistance. This confining pressure builds up around the fibre at application of the pullout load to prevent debonding. However, as the load continues to be applied, the confining pressure begins to reduce due to the Poisson's ratio of this type of fibre. With longer pullout time, the reduction of the confining pressure also leads to a reduction in the interfacial shear resistance as the fibre tends to debond from the matrix. This is particularly critical as the fibre embedment length increases, hence the reduced interfacial shear resistance with increase in fibre embedment length (Boshoff et al., 2009b; Simkins et al., 2005). It can therefore be concluded that, at longer fibre embedment length, the interfacial shear resistance is lower compared to shorter embedment length due to reduced surface frictional effect during pullout.

To investigate this assertion, the frictional effect on the pulled out fibre surfaces tested at different embedment lengths were visually evaluated as presented in Figure 5.9. One loading rate was considered while Figure 5.10 shows the effect of loading rates at one embedment length. The result presented in Figure 5.9 shows that fibres tested at lower embedment length show lesser surface

damage compared to the untested fibre. The higher the embedment length, the lesser the surface damage due to a reduction in the confining pressure leading to a reduced frictional surface effect.

With regards to the effect of loading rates on macro PP fibre surface damage, photos presented in Figure 5.10 shows that the higher the loading rate, the higher the surface damage caused. Pulled out fibres generally tend to show grooves on the surface. This could have been caused by the aggregates tearing through the fibre surface during pullout. This is also reported for crimped synthetic macro fibres pulled out from cement mortar (Won et al., 2006).

In all cases of the SEM images taken, the pulled out fibre surfaces did not reflect adhesion of cement hydrates. This confirms that due to the hydrophobic nature of the polypropylene fibres, no chemical adhesion occurred between the fibre and the matrix, hence only mechanical damage can be observed. The mechanical damage (frictional effect during pullout) has been attributed to the mechanism of interlock between large crystal of CH formed around the fibre during hydration and the fibre (Pakravan et al., 2013). While the mechanical damage on fibre surface might be limited to the frictional effect between crystals of CH and the fibre in cement mortar, the presence of coarse aggregate in concrete matrix (as used in this work), also causes damage to the fibre surface.

5.3 Time-Dependent Behaviour

Significant creep behaviour of macro synthetic FRC under sustained uniaxial tensile loadings has been reported in this dissertation. To gain insight into the mechanisms causing this time-dependent crack opening, investigation was conducted at the single fibre level as already described in Chapter 3. This section discusses the results of the time-dependent test carried out at the single fibre level embedded in concrete matrix and the fibre creep behaviour of a single fibre subjected to sustained loading.

5.3.1 Single fibre pullout

The result of the time-dependent pullout of the single PP fibres embedded in concrete matrix against time (minutes) in log scale is presented in Figure 5.13. All the fibres were tested at embedment length of 25 mm as described in Chapter 3. The specimens were subjected to sustained loads at percentages of the average maximum interfacial shear stress (2.5 MPa) of specimens tested in the single fibre pullout test at a loading rate of 0.1 mm/s. Lower percentages were not investigated.

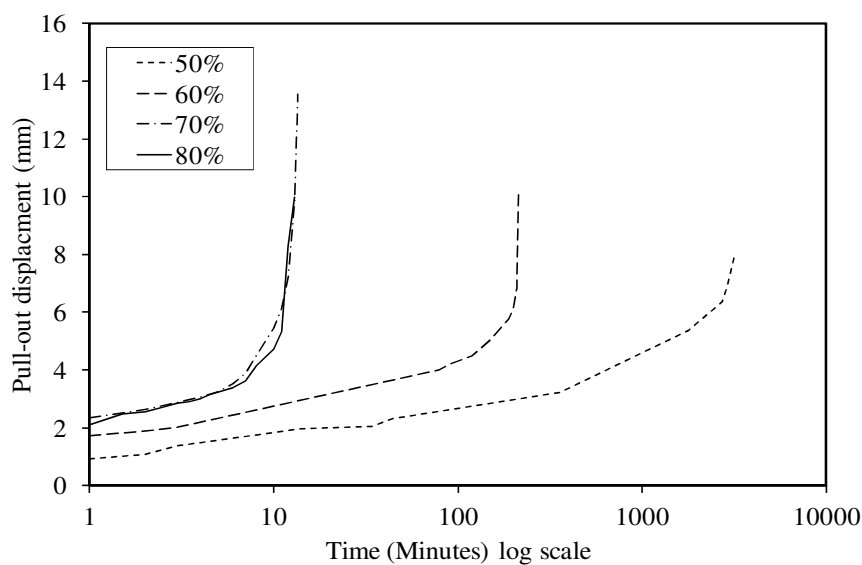


Figure 5.13: Fibre pullout displacement against time

From the time-dependent pullout test, all the fibres pulled out from the matrix without any fracture over the period tested. The complete pullout happened shortly after the last readings were taken. Figure 5.13 shows that the time-dependent pullout of the single fibres was dependent on the magnitude of the stress applied: the higher the stress, the quicker the pullout. The result shows an initial instantaneous pullout displacement of the fibres as soon as the loads were applied. The instantaneous pullout displacement also depends on the magnitude of the applied load. Specimens loaded at 70 % and 80 % show almost the same instantaneous pullout displacement of about 2.2 mm while those loaded at 50 % and 60 % show displacements of 1.0 mm and 1.8 mm respectively. All the test specimens show three stages of pullout behaviour: primary, secondary and tertiary pullout responses (refer to Figure 2.10). At the primary stage, the pullout is rapid and soon enters the

secondary stage where the rate of pullout decreases with increasing pullout displacement. Beyond this stage, the fibres pulled out rapidly and led to complete sudden pullout from the matrix (tertiary stage), hence images could not be captured.

The mechanism of pullout can be described as follows: at the onset of the applications of the pullout force, the matrix/fibre interface can be described as perfectly bonded where chemical bond (adhesion) is said to be active for a short time (Dupont, 2003). After a while, a critical force level is exceeded and the adhesion is broken and the debonding phase is entered. It should however be noted that at this stage, the fibre is partly bonded and debonding at the same time.

A possible explanation for the complete and sudden pullout of the fibre from the matrix at certain pullout displacement before the full embedment length of the fibre can be described as follows; As the fibre debonds, a tunnel shape crack forms around the fibre/matrix interface and the pullout is controlled by friction between the fibre and the matrix (Dupont, 2003). At some pullout length of the fibre, complete contact is lost between the fibre and the matrix and hence, the sudden pullout.

The time-dependent crack width increase of specimens subjected to uniaxial tensile loading can be attributed to fibre pullout from the matrix though about two ruptured fibres are observed (Figure 5.14).



Figure 5.14: Tensile creep failure of specimen showing pulled out fibres

Evidently, the time-dependent fibre pullout behaviour at the macro and single fibre level show failure pattern by complete pullout, hence time-dependent fibre pullout is one of the mechanisms responsible for the time-dependent crack widening of the tensile creep specimens.

It is acknowledged that the single fibre pullout test is not a true reflection of the actual condition where the fibres are randomly distributed in the matrix and at different angles of inclination to the cracked plane. A consideration of orientation might show that the fibres are each transferring different amount of stresses and the orientation of fibres to the stress direction has an effect on the tensile properties of FRC (Al-Khaja, 1995). However, an identification of one of the mechanisms responsible for the time-dependent crack widening of cracked specimens is obtained from the presented tests.

5.3.2 Single fibre creep

MacKay & Trottier (2004) reported that fibre creep is one of the mechanisms causing the time-dependent crack widening of macro synthetic FRC under sustained loading. The strength and stiffness of synthetic fibres do have the tendency to vary over time due to a host of factors such as temperature, stress level, strain rate, etc. (Brinson & Gates, 1995; Drozdov, 2010; Ebert et al., 2011; Muliana, 2014). A single fibre was subjected to sustained load of 30 % of the fibre capacity to give an indication of the elongation over time. The result of the time-dependent fibre creep under sustained tensile loading is presented in Figure 5.15.

The deformation is scaled as fibre elongation in percentage against duration of loading. Figure 5.15 clearly shows a time-dependent creep of the fibre under sustained load over 4 days. At the instance of loading, the fibre shows an instantaneous deformation of about 12 %. After over 3.5 days, the time-dependent creep has shown an elongation of about 40 % which indicates a significant fibre creep. While the intent of this study is not to study the creep of the fibre over a prolonged period of time, at the second stage of deformation, it is observed that the fibre begins to show whitening colouration as with specimens tested under uniaxial tensile creep. This whitening of the fibres has been described to be the result of accumulation of damage to the fibre (Pawlak & Galeski, 2008).

Beyond the secondary creep phase, other authors have reported that the deformation is said to get into the tertiary phase which is characterised again by non-linear deformation with time (Drozdov, 2010).

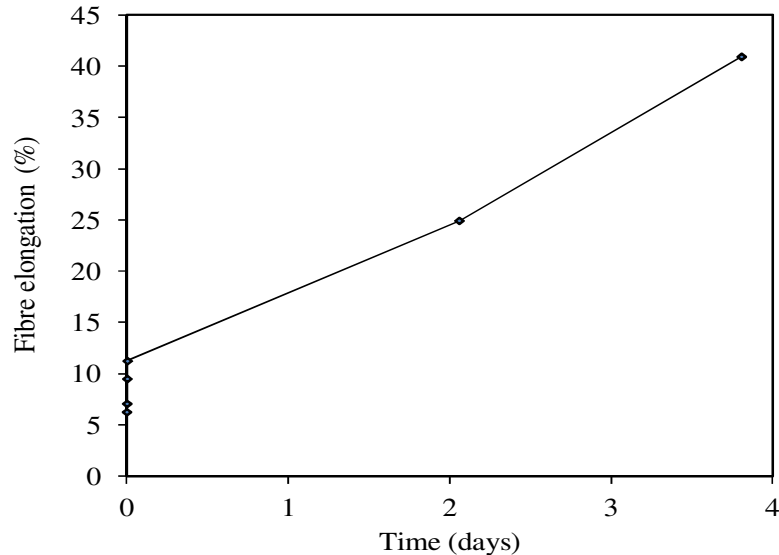


Figure 5.15: Time-dependent PP fibre creep

The significant creep of flexible macro synthetic fibre is attributed to the lengthening of fibres. When they are subjected to permanent loads, they behave viscous and the deformation maybe significantly large (MacKay & Trottier, 2004). While reported that the synthetic fibre used in their investigation (micro synthetic fibrillating) did not show any significant creep after 20 days at 20 % of the tensile strength. However, at 40 %, MacKay & Trottier (2004) reported creep of the fibrillating fibre. The macro synthetic fibre investigated in this research shows significant creep at 30 % load level at only 4 days.

It is expected that the fibres will be subjected to different stresses on the cracked plane. This could be due to their orientation, distribution and properties of the interfacial transition zone (ITZ) between the fibre and the matrix. The surface geometry of different type of macro synthetic fibre is expected to give different results. This is however not investigated in this study.

5.3.3 Mechanisms causing time-dependent crack widening

The time-dependent behaviour of cracked macro synthetic FRC shows continued crack widening under sustained tensile loading. The mechanisms causing this phenomenon have been identified in this research as fibre creep and fibre pullout. As shown in the previous section, the polypropylene fibres do lengthen over time when subjected to sustained loading. Due to Poisson's effect, this will result in the fibre's cross section reducing over time. The deformation leading to dimensional instability has been attributed to the motion of the molecules activated by high stresses (Lv et al., 2014). The transfer of load between the fibre and the matrix when the matrix is cracked is dependent on the frictional bond and mechanical interlock between the fibre and the matrix. When the fibre contracts laterally, both the frictional bond and the mechanical bond will weaken and this will result in partial fibre pullout. This process will continue until this debonding stabilises or the fibre pulls out completely which in turn leads to failure.

Though this research project did not consider the micromechanics of this time-dependent fibre pull-out, this is an important aspect that requires further investigation so that the mechanism responsible for this time-dependent pullout is fully understood. This will pave the way to finding solutions to this concerning behaviour.

5.4 Summary

The experimental response of single macro synthetic fibres pulled out from concrete matrix at varying loading rates and embedment lengths has been investigated and reported. Also presented at the single fibre level are the results of the tensile behaviour of fibres tested at different loading rates and the results of the time-dependent fibre pullout and fibre creep tests. The time-dependent behaviour was studied to understand the mechanisms causing the time-dependent crack opening of macro synthetic FRC.

Single fibres tested under direct tensile tests have shown to be rate sensitive with fibre tensile strength giving higher value with increase in the loading rate. Average maximum fibre tensile strength

of 549 MPa has been obtained for the Rocstay macro PP fibre employed in this study at a loading rate of 1 mm/s. Tensile response was typically non-linear and independent of the loading rate.

Single fibre pullout of macro synthetic fibres from concrete matrix has been found to be sensitive to pullout rate. The higher the pullout rates, the higher the pullout force and invariably the interfacial shear stress at all the embedment lengths investigated. All the fibres pulled out without any fracture occurring as is the case in the time-dependent single fibre pullout test.

The complete fibre pullout mechanism may majorly characterise failure of specimens tested at macro and structural levels as found in this study. However, this could be influenced by the mix design and other factor, hence requiring further investigation. It should be remarked that the critical length is independent of pullout rate but dependent on the embedment length.

The strength of the bond between the macro PP fibre and the concrete matrix lies between 2.0 to 3.4 MPa. This bond strength (interfacial shear resistance) has been shown to be sensitive to pullout rate and fibre embedment length. It increases with increase in fibre pullout rate and decreases as the embedment length of the fibre increases indicating a possibility that not all the fibre length is engaged in stress transfer.

Embedded fibres at 25 mm subjected to time-dependent pullout test under sustained loadings between 50 % and 80 % of its tensile strength pulled out completely from the concrete matrix. The load level dictated the rate of pullout as specimens tested at 50 % pulled out after about 4 days while those subjected to 80 % pulled out after 15 minutes. It is important to remark that all fibres pulled out suddenly at less than half the embedment length. This could have been caused by the dimensional instability of PP fibres when subjected to creep.

Creep of PP fibres has shown to be significant even at four days under sustained load reaching up to 40 % elongation. The two major mechanisms that caused the time-dependent crack opening of crack macro synthetic FRC have been identified as time-dependent fibre pullout and fibre creep.

Chapter 6

Structural Response of Macro Synthetic FRC

The behaviour of macro synthetic FRC at the macro and single fibre level has been reported in Chapters 4 and 5 of this dissertation. However, when dealing with the mechanical and fracture properties of fibre reinforced concrete (FRC) for structural optimisation at the structural level, flexural test is usually used (Bencardino et al., 2013). Structures are also known to deform with time under sustained loading, hence the need to also evaluate the structural performance of FRC under time-dependent loading.

This chapter presents and discusses the result of the short term behaviour of macro synthetic FRC when subjected to three point loading. The evaluation of the material behaviour is based on the recommendation of Model Code 2010 and the European standard, EN 14651 (2005). The time-dependent flexural creep of macro synthetic FRC is also evaluated. Though few scholarly articles have been published on the flexural creep of crack steel FRC, fewer have been reported for macro synthetic FRC. The creep is investigated at two stress levels, 30 % and 50 % of the residual flexural strength retained at a crack mouth opening displacement (CMOD) of 0.2 mm. The time-dependent crack widening and coefficient of creep are discussed.

6.1 Flexural Tensile Behaviour

It should be recalled that for the structural applications of FRC, the material classification is usually based on the post cracking residual strength. The emphases of performance specification of FRC at the structural level based on the final draft of the Model Code 2010 are the class, residual strength ratio and the material of the fibre. This section focuses on these criteria at the structural level. The discussion is focused on the evaluation of the structural performance based on the final draft of the Model Code 2010 and the European Committee recommendations. Tests were performed in a Zwick Z250 Universal Testing Machine.

6.1.1 Results

The purpose of this test is to determine the material properties of concrete reinforced with macro synthetic fibres at a volume V_f , of 1 % (9.1 kg/m^3). The specimens were notched at mid-span to a depth of 25 mm on the bottom side and tested by controlling the CMOD displacement with a linear variable displacement transducer (LVDT). The result of the three point bending test for three specimens tested is presented in Figure 6.1. The load is expressed as flexural strength and the actual CMOD calculated according to the requirement of EN 14651 (2005) as:

$$CMOD = CMOD_y \frac{h}{h + y} \quad (6.1)$$

where h is the total depth of the specimen, $CMOD_y$ is the measured crack mouth opening displacement (mm) during the test and y is the distance of the LVDT to the bottom surface of the beam. In this case, y was maintained as 20 mm for all tests.

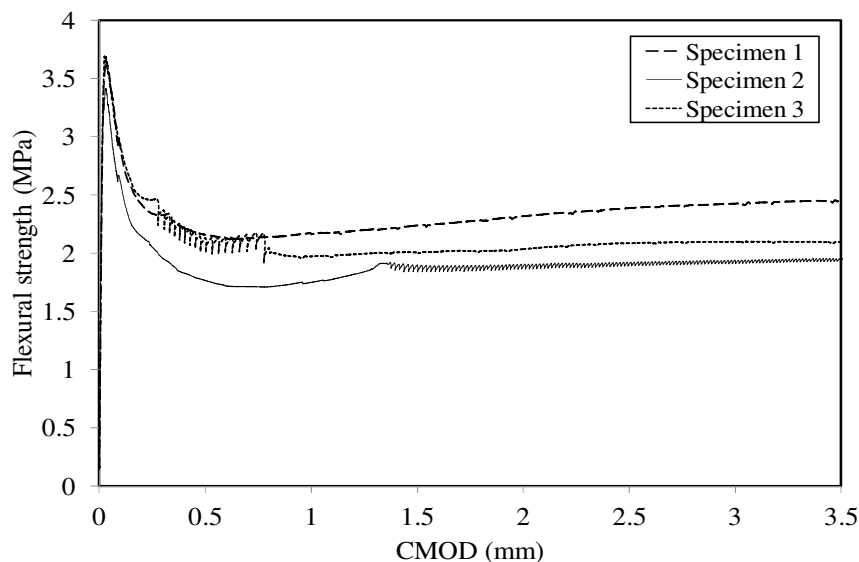


Figure 6.1: Flexural behaviour of beams under three point bending test

The load at the limit of proportionality, F_L , the stress at the proportionality limit, f_L (at CMOD of 0.05 mm) and the residual strengths f_{R1} , f_{R2} , f_{R3} and f_{R4} at 0.5, 1.5, 2.5 and 3.5 mm CMOD were determined according to the requirement of EN 14651 (2005). According to EN 14651 (2005), the

stress at the limit of proportionality (LOP) and the residual flexural tensile strength parameters, $f_{R,j}$ are given as:

$$f_{R,j} = \frac{3 \times F_{R,j} \times l}{2 \times b \times h_{sp}^2} \text{ in (MPa)} \quad (6.2)$$

where $f_{R,j}$ is the residual flexural tensile strength corresponding with $\text{CMOD} = \text{CMOD}_j$ ($j = 1, 2, 3, 4$) in (MPa), $F_{R,j}$ is the load corresponding with $\text{CMOD} = \text{CMOD}_j$ ($j = 1, 2, 3, 4$) in (N), l is the span length of the specimen in mm (used as 450 mm), b is the width of the specimen in (mm) and h_{sp} is the distance between the tip of the notch and the top of the specimen in (mm). It should be remarked that in calculating the stress at limit of proportionality, F_L , the load at the limit of proportionality is substituted for $F_{R,j}$.

The post peak behaviour reflects a strain softening response at a fibre volume of 1 %. Results of the pre- and post cracking strength characteristics are presented in Table 6.1. The Table shows the average maximum flexural strength ($f_{\sigma,\max}$), the stress corresponding to the LOP (f_L) and residual flexural tensile strength parameters corresponding to the CMOD at 0.5, 1.5, 2.5 and 3.5 mm. Insignificant scatter of the average first crack stress, $f_{\sigma,\max}$ and the stress corresponding to the LOP can be observed. The mean residual flexural stresses, $f_{R,j}$ at different CMOD however showed more scatter but was highest at a CMOD of 3.5 mm having a coefficient of variation of 12 %.

Table 6.1: Residual flexural tensile strength parameters for 3-point test

Residual strength	$f_{\sigma,\max}$	f_L	f_{R1}	f_{R2}	f_{R3}	f_{R4}
Mean	3.60	3.37	2.24	2.27	2.36	2.40
CoV (%)	4.31	4.75	10.97	8.57	11.42	12.09

*CoV is the coefficient of variation

Significant energy absorption capacity of the beam is observed up to a crack width of 3.5 mm. The high energy absorption capacity of macro synthetic FRC was further investigated beyond a CMOD of 3.5 mm. One specimen was cracked, unloaded and reloaded up to a CMOD of about 6 mm and the result is shown in Figure 6.2.

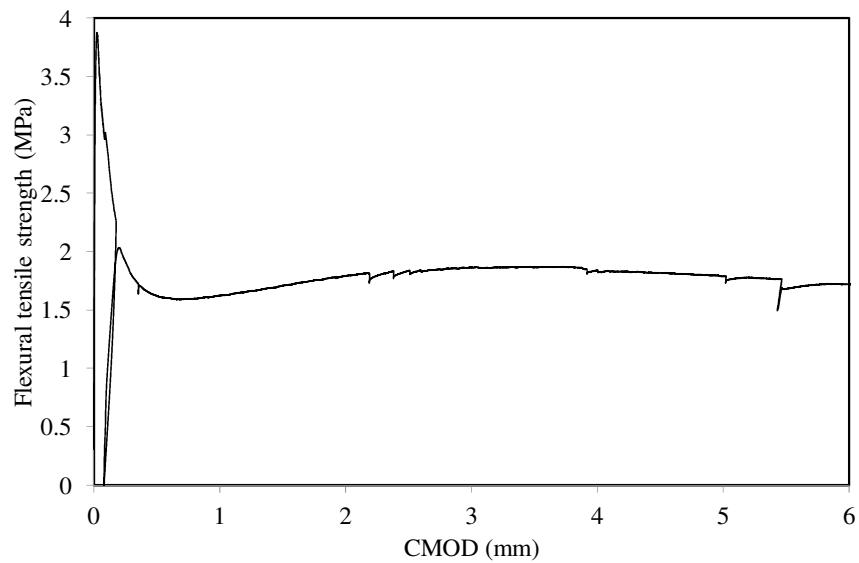


Figure 6.2: Extensive energy absorption capacity of cracked macro synthetic FRC

The result of the cracked, unloaded and reloaded specimen shows that concrete reinforced with synthetic macro fibres displays an extensive toughness and energy absorption capacity even at larger crack width. This is a great advantage in the prevention of sudden collapse in concrete structures.

6.1.2 Discussions

The results of the flexural tensile behaviour of the macro synthetic FRC presented above show a linear response of the composite under load up to some point before the first cracking stress, $f_{\sigma, \max}$ (see Figure 6.3).

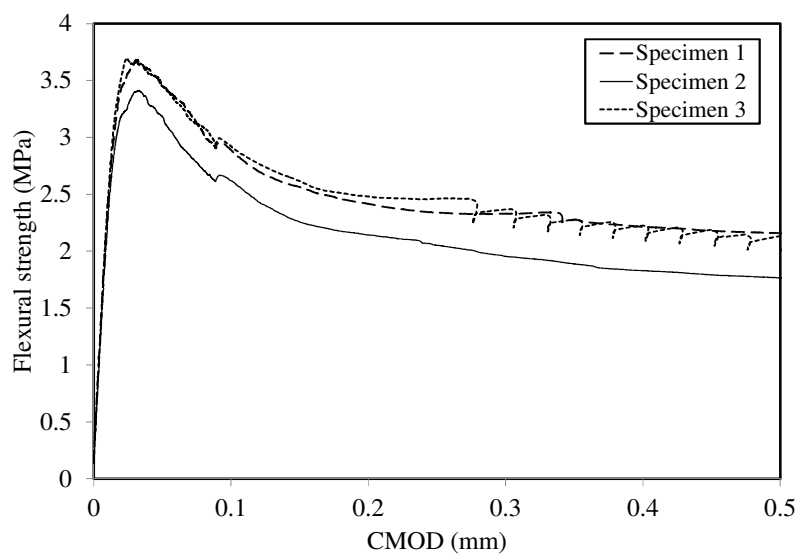


Figure 6.3: Graph showing linear response before ultimate strength

This is unlike the response of the specimens tested in uniaxial tension where linear behaviour is observed up to the first cracking strength. The mean maximum flexural strength is 3.60 MPa whereas the mean maximum uniaxial tensile strength is 2.90 MPa. This shows an increase of 24 % in the flexural tensile strength over the uniaxial tensile strength. One reason for this observed phenomenon can be attributed to the fact the MOR is calculated based on elastic theory which assumes perfectly elastic behaviour up to the maximum stress (Boshoff, 2007; Raphael, 1984). However, this is not the case as the gradient of the load-CMOD is only perfectly elastic (linear) to some point before the maximum stress where fracture occurs as earlier mentioned. It can therefore be said that the computation of the MOR is an overestimation and results in a value greater than the uniaxial tensile strength. The flexural strength-uniaxial tensile strength relationship obtained therefore is consistent with the results obtained by Raphael (1984) for conventional concrete, that is, the tensile strength is about 0.75 of the MOR.

Beyond the maximum strength of the composite, a gradual drop in stress is observed as the crack mouth widens unlike the sudden drop with specimens tested in uniaxial tensile stress. This initial drop could be adjudged to have been caused by the great disparity in the elastic modulus of the matrix and the fibre as explained with the uniaxial tensile test results. However, the post peak behaviour shows a pseudo-strain hardening behaviour in the softening branch with increase of the crack bridging capacity as the crack width widens. This is reflected in the average residual stresses that continue to increase in the post crack region up to a CMOD of 3.5 mm. When compared with the residual stresses obtained in the uniaxial tensile test at the same crack width, the mean residual flexural strengths (f_{R1} , f_{R2} , f_{R3}) are larger.

The residual strengths tend to stabilise as soon as the CMOD increases beyond 0.5 mm with a gradual increase in flexural toughness. In a similar test under 3-point bending, stable sustained flexural toughness of macro synthetic FRC have also been reported with increase in CMOD (Buratti et al., 2011; Soutsos et al., 2012). However, the residual flexural strength decrease at a CMOD of 3.5 mm is about 33 % of the stress at LOP.

For the specimens that were cracked and reloaded to a CMOD of about 6 mm (Figure 6.2), the decrease in the residual stresses compared to the mean maximum flexural strength is still in the range of 33 %. This indicates sustained flexural toughness of macro synthetic FRC over large crack width. This stable and increased flexural toughness over extensive CMOD can be attributed to a good interphase matrix-fibre interaction in the tensile zone (Ding, 2011).

To further describe the post cracking strength characteristics of FRC, the Model Code 2010 stipulates that designers should specify the class, residual strength ratio and the fibre material. In this regards, a consideration of the characteristics residual strengths significant for serviceability (f_{R1k}) and ultimate (f_{R3k}) conditions can be defined assuming a linear elastic behaviour. According to the code, two parameters denoted by f_{R1k} (representing strength interval) and a letter a, b, c, d or e (representing the ratio f_{R3k}/f_{R1k}) are normally used. The strength interval is defined by two subsequent numbers in the series: 1.0, 1.5, 2.0, 2.5, 3.0, 3.5, 4.0 ... [MPa] while the letters a, b, c, d, e corresponds to the residual strength ratios as shown in Table 6.2.

Table 6.2: Classification of residual flexural strength ratio (Model code 2010)

Designation	Residual strength ratio
a	$0.5 \leq f_{R3k}/f_{R1k} \leq 0.7$
b	$0.7 \leq f_{R3k}/f_{R1k} \leq 0.9$
c	$0.9 \leq f_{R3k}/f_{R1k} \leq 1.1$
d	$1.1 \leq f_{R3k}/f_{R1k} \leq 1.3$
e	$1.3 \leq f_{R3k}/f_{R1k}$

For the macro synthetic FRC investigated in flexure, the material (based on the results in Table 6.1) shows a classification denoted as “2c”. This means that the FRC has a strength, f_{R1k} ranging between 2 and 2.5 MPa and residual strength ratio, f_{R3k}/f_{R1k} ranging between 0.9 and 1.1. The simplified constitutive laws governing the post cracking behaviour of a bending test as defined by the code is presented in stress-crack width relationship: the plastic rigid behaviour or a linear post cracking behaviour (hardening or softening) as shown in Figure 6.4. f_{Fts} represents the serviceability residual strength, defined as the post-cracking strength for serviceability crack openings, and f_{Ftu} represents the ultimate residual strength (fib, 2010).

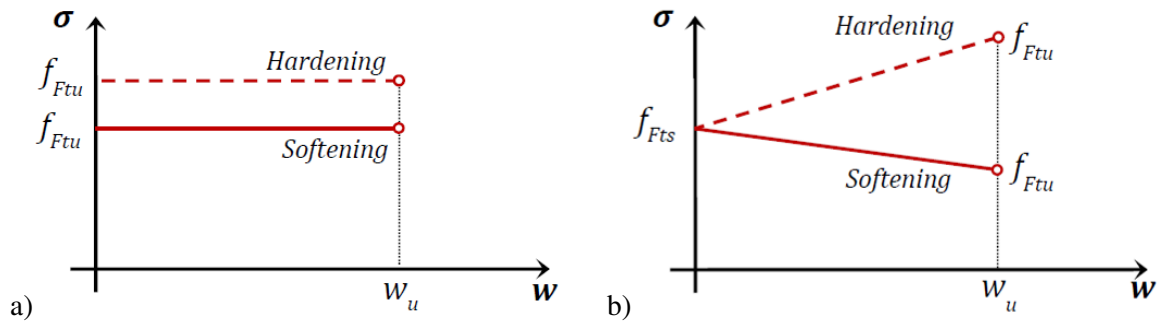


Figure 6.4: Simplified post cracking stress-crack opening diagrams (a) rigid plastic behaviour
b) linear post cracking behaviour (fib, 2010)

The ultimate residual strength, f_{Ftu} , when plastic rigid behaviour is assumed is given as:

$$f_{Ftu} = \frac{f_{R3}}{3} \quad (6.3)$$

Based on the results given in Table 6.1, the ultimate residual strength gives a value of 0.79 MPa.

When linear post cracking behaviour is assumed, the residual strength, f_{Fts} is defined as:

$$f_{Fts} = 0.45 \times f_{R1} \quad (6.4)$$

whereas, f_{Ftu} is given as:

$$f_{Ftu} = f_{Fts} - \frac{w_u}{CMOD_3} (f_{Fts} - 0.5f_{R3} + 0.2f_{R1}) \geq 0 \quad (6.5)$$

where w_u is the maximum crack opening accepted in structural design (max = 2.5 mm) and its value depends on the ductility required. Substituting $f_{Fts} = 1.008$ MPa, $w_u = 2.5$ mm, $CMOD_3 = 2.5$ mm, $f_{R1} = 2.24$ MPa and $f_{R3} = 2.36$ MPa, Equation 6.5 gives $f_{Ftu} = 0.73$ MPa. This shows that when linear behaviour is assumed, the post cracking behaviour of the macro synthetic FRC demonstrates a strain softening behaviour with a serviceability residual stress of 1 MPa and ultimate residual stress of 0.73 MPa.

Lastly, it should be remarked that even though macro synthetic FRC shows great post crack flexural toughness, these occurred at significant CMOD which might not be desirable where serviceability is critical. Due to the flexibility of these fibres, they have to stretch extensively before they are fully engaged to control a crack opening, hence the tensile properties of these fibres need to

be improved in terms of tensile strength and E-modulus before they can be suitably used for structural purposes and in structures where water tightness or durability is required.

6.2 Flexural Tensile Creep

The time-dependent behaviour of macro synthetic FRC under flexure has been investigated for two purposes. The first is to understand its response under sustained flexural loadings when compared to the uniaxial tensile creep result and for the purpose of the verification of the finite element modelling (FEM) of the flexural creep. As previously mentioned in Chapter 3, the specimens for the flexural tensile creep were cracked in a three point bending test before they were transferred to the flexural creep frame where they were subjected to sustained loading in a four point bending test setup. The strength result obtained in the three point bending test was converted to an equivalent four point strength result (Zerbino & Barragan, 2012) using the relation given as:

$$\text{Flexural strength in four point} = \frac{\text{Flexural strength in three point}}{1.5} \quad (6.6)$$

where the flexural strength in three and four point bending are given respectively according to (BS EN12390-5, 2000) as:

$$f_{cf(3p)} = \frac{3 \times F \times l}{2 \times d_1 \times d_2^2} \quad (6.7)$$

$$f_{cf(4p)} = \frac{F \times l}{d_1 \times d_2^2} \quad (6.8)$$

F is the maximum load, l is the span of the supports, d_1 is the width and d_2 is the height. d_1 is used in this study as 150 mm whereas d_2 taken as 125 mm due to the notch. Two sustained stress levels were investigated: 30 % and 50 % of the residual flexural stress at a crack width of 0.2 mm.

6.2.1 Result

As previously discussed in the experimental methods for this investigation, two specimens were cracked, unloaded and reloaded to illustrate the position of the sustained applied stress levels as shown in Figure 6.5.

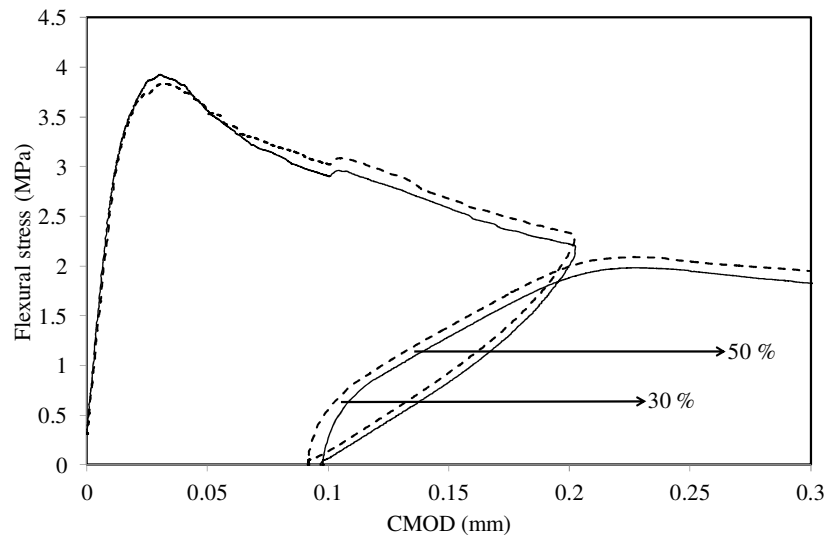


Figure 6.5: Unloading response and the sustained flexural load levels

The sustained loads were based on the residual flexural stress at a CMOD of 0.2 mm before unloading. After fully unloading, an average irrecoverable crack width of about 0.1 mm can be observed. The arrows indicate the typical response expected when permanent loads are applied to the specimens in the flexural tensile creep test.

The results of the creep of the cracked specimens subjected to sustained flexural loadings for a period of 8 months are shown in Figure 6.6. It should be mentioned that since the beams are stacked in column of three, the results are discussed based on the position of each beam; top, middle and bottom. The CMOD was measured as discussed in Chapter 3 using dial gauges attached to the specimens.

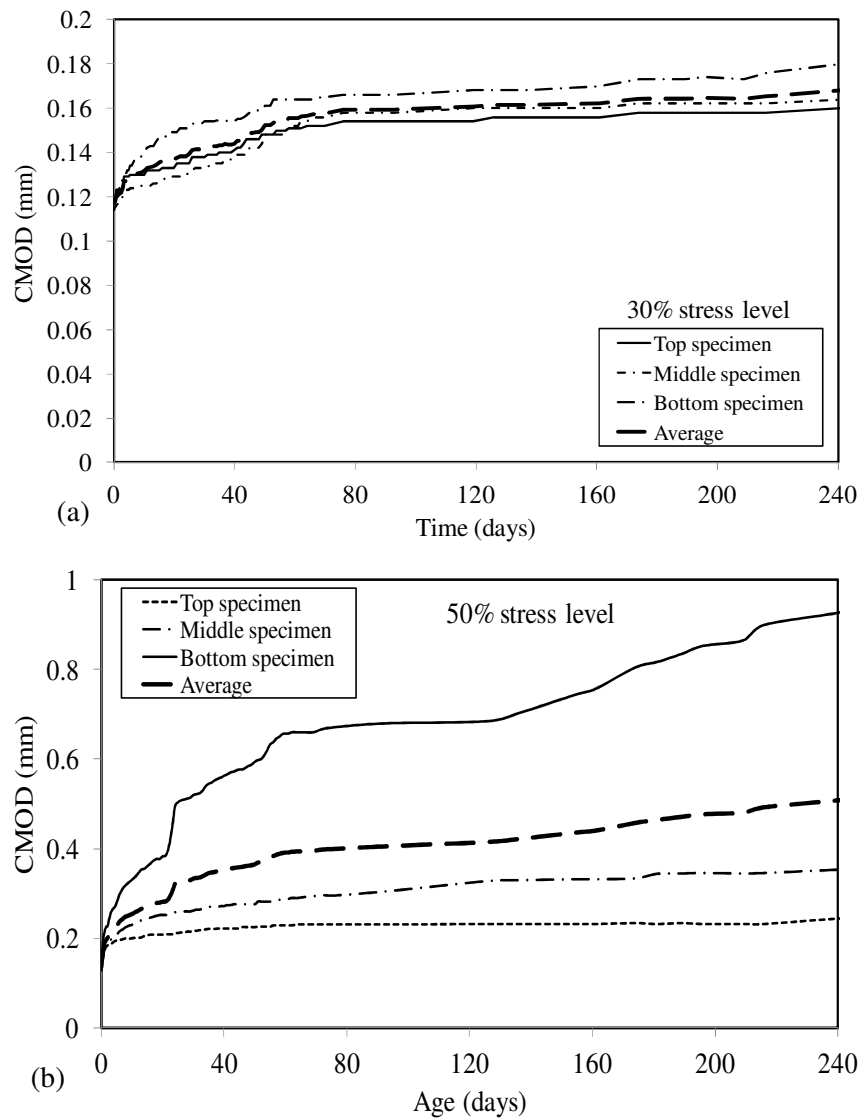


Figure 6.6: Flexural creep of cracked macro synthetic FRC

The evolution of the time-dependent CMOD with time for each column of arrangement under the two stress levels considered as presented in Figure 6.6 is a combination of the instantaneous crack opening and the crack opening due to creep after 8 months.

The creep parameters reported by García-Taengua et al. (2014) and Arango et al. (2012) have also been used to describe the flexural creep performance of cracked macro synthetic FRC. These are the crack opening rate, $COR(t_1-t_2)$, creep coefficients, $\varphi(j)$, and creep coefficient referred to the origin, $\varphi_o(j)$. They defined these parameters as follows:

- $COR(t_1-t_2)$: ratio between the increase in crack opening and the lapse of time from t_1 until t_2 .
This is evaluated for $COR(0-14)$, $COR(14-30)$, $COR(30-90)$ and $COR(90-240)$; indicating COR at 14, 30, 90 and 240 days.
- $\phi(j)$: defined at different j times as the ratio between the deferred crack opening at time j , $w_{cd}(j)$, and the initial crack opening at the beginning of the creep stage, w_{ci} . Creep coefficients at 14, 30, 90 and 240 days represented by $\phi(14)$, $\phi(30)$, $\phi(90)$ and $\phi(240)$ respectively are reported.
- $\phi_o(j)$: the ratio between the deferred crack opening at time j , $w_{cd}(j)$, and the crack opening at the beginning of the creep test in the complete curve, which is $w_{pr} + w_{ci}$.

In this study, these parameters have been considered for each specimen tested and averages flexural creep responses obtained at both stress levels. The idealised plot reported in García-Taengua et al., (2014) and Arango et al. (2012) has been adapted and presented in Figure 6.7 for strain softening macro synthetic FRC.

Based on Figure 6.7, the following parameters are further defined: F_L as the first crack load, w_p as the maximum CMOD at the pre-cracking process, F_a as the applied creep load, F_w load at w_p , w_{pr} residual CMOD after unloading at the pre-cracking process, w_{ci} the CMOD at the beginning of creep test (measured 1 min after load application), $w_{cd}(t)$ the CMOD when creep test was ended.

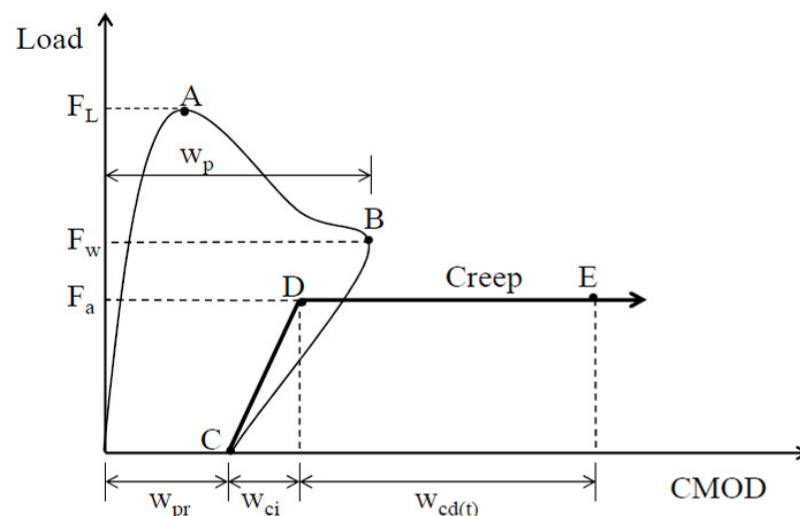


Figure 6.7: Idealised plot of pre-cracking and sustained creep load under flexure, adapted from [(García-Taengua et al., 2014) and (Arango et al., 2012)]

Table 6.2 reveals that the applied creep load has an effect on all the parameters considered: the initial cracking opening (w_{ci}), COR, $\varphi(j)$ and $\varphi_o(j)$.

Table 6.3: Parameters from experimental creep test

Test type	Stress level (%)	w_{ci}	$w_{cd}(240)$	COR ($\times 10^{-3}$)				$\varphi(14)$	$\varphi(30)$	$\varphi(90)$	$\varphi(240)$	$\varphi_o(14)$	$\varphi_o(30)$	$\varphi_o(90)$	$\varphi_o(240)$
				0-14	14-30	30-90	90-240								
Flexural creep	30	0.01	0.10	3.43	0.94	0.45	0.07	4.80	6.30	9.00	10.10	0.44	0.57	0.82	0.92
	50	0.04	0.40	12.93	4.56	1.38	0.72	4.31	6.05	8.02	10.60	1.27	1.79	2.37	3.13

6.2.2 Discussion

The time-dependent crack opening shows an instantaneous deformation in response to the applied creep load. The magnitude of this response is a function of the stress level applied: the higher the stress level, the higher the instantaneous deformation (see Table 6.2). The instantaneous deformation at 30 % and 50 % stress levels are 0.01 mm and 0.04 mm respectively. This indicates an increase of 300 % when the stress level increases from 30 % to 50 %. The result of the flexural creep after 8 months shows to be several times higher than the instantaneous deformation. At both stress levels, an increase of 900 % is recorded. However, the result does not seem to show any significant crack opening due to creep under sustained flexural loading for the period investigated. It should be remarked though, that the average time-dependent CMOD continues to increase but at a decreasing rate in both cases. This implies that the final crack width has not been reached.

Overall, the time-dependent crack widening is dependent on the applied stress levels: the higher the applied creep load, the higher the deferred CMOD. After 8 months under sustained creep load, specimens tested at 30 % stress level show an average total CMOD of 0.17 mm while those tested at 50 % stress levels show an average of 0.5 mm (this includes the irrecoverable CMOD, w_{pr}). The average time-dependent CMOD at 50 % stress level obtained shows to be almost 8 times more than the result of a similar test ($w_p = 0.2$ mm) carried out for steel FRC under a sustained flexural load of 52.3 % after 100 days (Blanco, 2013). It has been reported in this dissertation that one of the

mechanisms responsible for the time-dependent crack opening of macro synthetic FRC is the creep of the macro fibres. This is not the case for steel fibres as they do not undergo any creep.

The result presented in Figure 6.6 also reflects the effect of specimen's position in the test setup at both stress levels on the time-dependent crack widening: this is however more pronounced at 50% stress level. This effect has also been reported by García-Taengua et al. (2014) and Zerbino & Barragan (2012) for steel FRC. This variability in the result of one specimen from the other in a set of column specimens can be attributed to the additional beam load on lower specimens compared to the top specimen. It can be clearly seen from the result that bottom specimens show more crack opening under creep load followed by the middle specimens. Top specimens show the least crack opening in both cases. An accurate computation of the load applied when beam weights are added gives the following: at 30 % stress level, actual load is 30 % (top beam), 33 % (middle beam) and 36 % (bottom beam) whereas at 50 %, it is 50 % (top beam), 53 % (middle beam) and 56 % (bottom beam). At a much lower stress level (30 % to 36 %), the variability in the time dependent crack opening does not differ that much and the influence of specimen position is hardly observed. Conversely, between 50 % and 56 %, the effect is quite noticeable from the result (Figure 6.6b). It should be recalled that specimens tested under uniaxial tensile creep showed significant creep between 50 % and 60 % stress levels compared to 30 % and 40 % stress levels. Where enough space for placement of flexural creep frames and measuring instrument are available, it is advised that only a single specimen be placed on the creep frame to avoid this effect on the crack opening due to creep. Variability in the results could also be attributed to the number of fibres crossing the cracked plane as reported in the uniaxial tensile creep results and by other authors (Blanco, 2013; García-Taengua et al., 2014).

Furthermore, in assessing the time-dependent crack opening, a computation of the crack opening rate (COR) has been made and shown in Table 6.2. As expected, the COR is a function of the applied stress level: increasing with increase in creep load. In general terms, the result shows that the COR reduces with increase in age (from 0 to 240 days) with the rate of opening being more significant at earlier ages. The first two weeks of test shows a COR of 3.43×10^{-3} mm/day and 12.93×10^{-3} mm/day at

30 % and 50 % stress levels respectively (see Table 6.2), hence an increase of about 73 % at 50 % stress level over the rate at 30 % stress level. At 30 % stress level, opening rate continues to decrease up to 240 days from 3.43×10^{-3} to 0.07×10^{-3} and from 12.93×10^{-3} to 0.72×10^{-3} at 50 % stress level (Table 6.2). At 8 months, the COR is almost reduced to zero at a stress level of 30 %. This indicates that at 8 months of sustained loading, the crack widening is almost stabilised with no significant increase. When compared with specimens tested under uniaxial tensile creep at the same stress level (Figure 4.5 a), uniaxial tensile creep shows COR about 17 times more. Similarly, at a stress level of 50 %, average COR at 8 month shows that creep of uniaxial tensile specimen are about 7 times more than those under flexural creep. While the specimens tested in uniaxial tensile creep are subjected purely to tensile stresses, the same cannot be said of specimens under flexural creep where specimens in flexure experiences both compression (upper portion) and tension (lower portion) stresses at the same time. This leads to differences in the time-dependent CMOD under both test conditions. The observed phenomenon, lesser flexural creep compared to uniaxial tensile creep, shall be discussed in Chapter 7.

Creep coefficients, $\phi(j)$, and creep coefficient referred to the origin, $\phi_0(j)$ both increase with age of testing. The creep coefficient $\phi_0(j)$ clearly shows to be dependent on the applied stress level. Higher values in the coefficient is observed (Table 6.2) at 50 % stress level in comparison to the average values at 30 % stress level.

6.3 Summary

This chapter has examined the performance of macro synthetic FRC at the structural level when subject to bending in short term and time-dependent sustained loadings in the cracked state. The short term behaviour was evaluated under the three and four point bending test using the post cracking strength criteria spelt out in the Model Code 2010 (fib, 2010) and European standard, (EN 14651, 2005). Flexural creep of cracked specimens subjected to 30 % and 50 % stress level were also

investigated and results discussed. The following conclusions can be deduced from the aforementioned investigations:

- Significant post cracking energy absorption capacity of macro synthetic FRC under three and four point bending test have been observed. The residual flexural strength under three point test according to the requirement of Model Code 2010 and EN 14651(2010) at CMOD between 0.5 and 3.5 mm range from 2.24 MPa to 2.40 MPa.
- Specimen cracked and reloaded has also shown similar flexural toughness up to a crack opening of 6 mm with residual strength of about 1.8 MPa.
- Due to the flexibility of these fibres, they have to stretch extensively before they are fully engaged to control crack opening, hence might not be suitability where serviceability is an issue.
- According to Model Code 2010 requirement, the macro synthetic FRC is classify as '2c', that is, it has a strength ranging between 2 and 2.5 MPa and residual strength ratio between 0.9 and 1.1.
- Flexural creep results have shown that time-dependent crack opening increase with time at a decreasing rate. At 8 months of investigation, total crack opening were 0.2 mm and 0.5 mm at 30 % and 50 % stress level respectively.
- The creep coefficient, $\phi_o(j)$, is a function of the applied stress level and decreases with testing age. At 8 months, creep coefficients were 0.93 and 3.13 at 30 % and 50 % stress levels respectively.

Chapter 7

Modelling the Time-Dependent Behaviour

To adequately and efficiently predict the effects of creep in a structure, there must be the availability of reliable data of the creep characteristics of the particular concrete mix. This dissertation has initiated the availability of such data for cracked macro synthetic FRC. Analytical or numerical procedure for the inclusion of this time-dependent effect in the analysis and design of structures is also of necessity. Different prediction models for the creep of normal concrete have been developed over the years. These models have shown great variability in the prediction of the creep of concrete. Fanourakis & Ballim (2003) investigated the accuracy of eight International known models for predicting creep strain of concrete and compared model results with experimental results. Though the parameters which the codes considered were different, the results of their comparison reported that the Model B3 RILEM draft recommendation seems to be the most accurate among others with a coefficient of variation (CoV) of 25.9 %.

Similar investigation was reported by Goel et al. (2007). They compared five models used to predict the creep and shrinkage strains of concrete and related the results to experimental data. The creep and shrinkage strains prediction by GL 2000 model was said to best describe the experimental data. It should however be noted that even though GL 2000 model best describe the experimental data, the results of the specific creep and shrinkage strains were not accurate. These codes are basically addressed the prediction of the creep and shrinkage strains of conventional concrete and not FRC. A number of differences have been observed with these prediction models while some appear complicated. However, similarity in the exponential component which is a function of the material properties and environmental factors has been observed.

When discussing the creep of cracked FRC, these prediction models cannot be used since they are only applicable to uncracked concrete specimens. In the cracked state, the creep mechanism of macro

synthetic FRC is basically that of crack widening and time-dependent fibre creep under sustained load as shown in Chapter 4. The fracture response is usually described by a stress-crack width (σ - w) relationship (Löfgren, 2005; Wille et al., 2014). This relationship is said to be better captured using the uniaxial tensile test despite its attendant challenges as noted in Chapter 2. If the cracked specimens are subjected to permanent load, the time-dependent σ - w relationship shows non-linear viscoelastic behaviour as reported in Chapter 4. In this chapter, the viscoelastic model approach has been used to simulate the time-dependent crack opening of cracked macro synthetic FRC subjected to four-point sustained flexural loading using materials model parameters obtained from the uniaxial tensile test. The details of the implementation using a finite element analysis (FEA) from a commercially available software programme, DIANA version 9.5 are fully described in the subsequent sections.

7.1 Constitutive Model

The modelling of cement based materials has become a common practice in the field of engineering. The time needed for building and testing engineering structures/materials can now be saved by carrying out computational modelling (Boshoff, 2007). While elastic constitutive models are used for modelling the behaviour of materials when creep is not of importance, viscoelastic models are engaged for time-dependent behaviours under sustained loadings. Concrete is generally known to exhibit a non-linear time-dependent behaviour under load. The constitutive model describing its time-dependent response under sustained load has been described in Figure 2.8. Once load is applied to the material, an elastic deformation is experienced which is recoverable if the load is removed. If the load is sustained with time, the behaviour is non-linear with deformation reducing with time. This has been fully described in Section 2.2.4. With regards to FRC in the cracked state, the creep of the matrix is negligible as the fibres are the main material bridging the cracked plane.

It has been shown in this dissertation that the mechanisms responsible for the time-dependent crack widening of cracked macro synthetic FRC is the time-dependent fibre pullout and fibre creep. While these could be modelled separately to predict the creep behaviour of macro synthetic FRC, this

study has taken a phenomenological approach. A rheological model (Kelvin chain model) designed to model the elastic (using spring elements) and the viscous (using dashpots) behaviour is used. The viscoelastic curves obtained were then curve fitted to the experimental results of the uniaxial tensile creep to obtain the material model parameters for implementation in FEA programme to predict the time-dependent crack opening response under flexure.

7.2 Rheological Creep Model

A number of rheological models (Kelvin-Voigts model, Maxwell model, Standard Linear Solid, etc.) have been developed over time to describe the behaviour of materials considering different internal (composition) and external (environment, time history) factors. The Kelvin model is favoured for the description of the viscoelastic behaviour of materials undergoing creep while the Maxwell model is used for relaxation. When the Maxwell model is used for the creep, it predicts that strain increases linearly with time which is not the case. With the Kelvin model for the prediction of creep, the model parameters are accurately predicted and predicts that strain tend to σ/E as time approaches infinity. The Kelvin model uses simple mechanical elements such as the springs and the dashpots/dampers. Figure 7.1 a & b) shows the description of the Kelvin element and the Kelvin chain respectively.

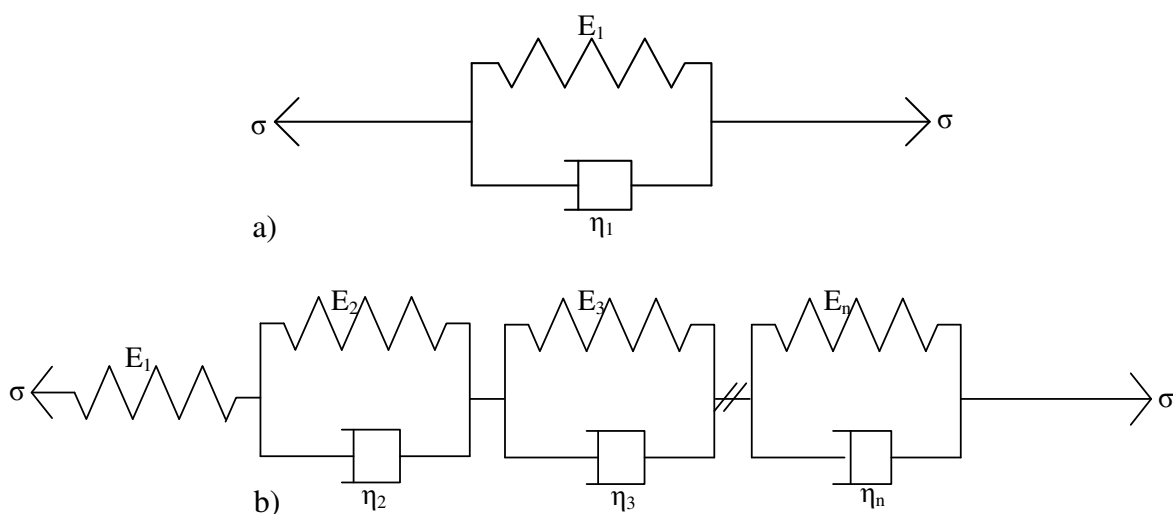


Figure 7.1: Viscoelastic model for creep a) Kelvin element b) Kelvin chain

The Kelvin element is designed to have a spring, characterised by linear stress-strain relation and a dashpot connected in parallel while elements connected in series gives the Kelvin chain. Element 1 (spring only) models the instantaneous deformation of the material while other elements simulate the time-dependent deformation. The total stress in the Kelvin element can be represented as:

$$\sigma = \sigma_s + \sigma_D \quad (7.1)$$

where σ_s and σ_D are the stresses in the spring and dashpot respectively and they are defined as:

$$\sigma_s = E \varepsilon_s \quad (7.2)$$

$$\sigma_D = \eta \frac{d\varepsilon}{dt} \quad (7.3)$$

where E is the elastic modulus (analogous to the spring constant, k), ε_s the strain, is the analogous to the displacement in the spring and η is the viscosity of the material. It should be noted that the displacement in the spring is equal to that in the dashpot, hence,

$$\varepsilon = \varepsilon_s = \varepsilon_D \quad (7.4)$$

and

$$\dot{\varepsilon} = \frac{d\varepsilon}{dt} = \dot{\varepsilon}_s = \dot{\varepsilon}_D \quad (7.5)$$

The coefficient of viscosity can be written as:

$$\eta = \tau E = \frac{\sigma_D}{\dot{\varepsilon}} \Rightarrow \sigma_D = \tau E \dot{\varepsilon} \quad (7.6)$$

Note that the change in stress, $\delta\sigma = \sigma - \sigma_0 = 0$, change in strain, $\delta\varepsilon = \varepsilon - \varepsilon_0$ and change in time $\delta t = t - t_0$. $t = \tau$ is the relaxation time.

Now, substituting Eqns. (7.2) and (7.3) into (7.1) and solving gives the change in strain in the Kelvin element as:

$$\delta\varepsilon = \frac{\sigma_0 - E\varepsilon_0}{\frac{\tau E}{\delta t} - E} \quad (7.7)$$

For the Kelvin chain,

$$\sigma = \sigma_1 = \sigma_2 = \dots \sigma_n \quad (7.8)$$

and the time-dependent strain, ε is given as:

$$\varepsilon_{t,m} = \varepsilon_{1,m} + \varepsilon_{2,m} + \dots + \varepsilon_{n,m} \quad (7.9)$$

$$= \varepsilon_{t,m-1} + \delta\varepsilon_{1,m} + \delta\varepsilon_{2,m} + \dots + \delta\varepsilon_n \quad (7.10)$$

where n is the time step and m is the element number.

At time Step 0 (instantaneous deformation), the strain in the spring becomes:

$$\varepsilon_{t,0} = \frac{\delta\sigma}{E} \quad (7.11)$$

Since only the spring (Element 1) is active, the change in Elements 2 and 3 will be zero.

At time Step 1, strain becomes:

$$\varepsilon_{t,1} = \varepsilon_{t,0} + 0 + \frac{\sigma - E_2\varepsilon_{2,0}}{\frac{\tau E_2}{\delta t} + E} + \dots + \frac{\sigma - E_n\varepsilon_{n,0}}{\frac{\tau E_n}{\delta t} + E_n} \quad (7.12)$$

while at time Step 2, the strain is

$$\varepsilon_{t,2} = \varepsilon_{t,1} + 0 + \frac{\sigma - E_2\varepsilon_{2,1}}{\frac{\tau E_2}{\delta t} + E} + \dots + \frac{\sigma - E_n\varepsilon_{n,1}}{\frac{\tau E_n}{\delta t} + E_n} \quad (7.13)$$

The number of steps depends on the number of Kelvin elements adequate for proper curve fitting to experimental result in any given case. In this study, four component elements have been used.

7.2.1 Viscoelastic material model parameters

Equation (7.10) gives the generalised form of the Kelvin chain model. As earlier mentioned, four elements were used in the determination of the Young's moduli of elements two to four in the chain and their respective relaxation time by curve fitting to the experimental data of the uniaxial tensile creep. This was done at two stress levels (30 % and 50 %) which is equivalent to those tested for the flexural creep. It should however be mentioned that due to some scatter in the tensile creep results (which had been discussed in Chapter 4), modelling has been done for each specimen and not the average behaviour. Whereas Specimens 1 to 4 were modelled at 30 % stress level, only Specimens 2 and 3 were modelled at 50 % stress level. The Young's modulus, E_1 , for the first element (spring) was calculated from the recommendation of Model Code 2010 given as:

$$E_{ci} = E_{c0} \cdot \alpha_E \cdot \left(\frac{f_{cm}}{10} \right)^{\frac{1}{3}} \quad (7.14)$$

where α_E is a factor dependent on type of aggregates and it is taken as 1.0 for quartzite aggregates, E_{c0} is the modulus of elasticity at concrete age of 28 days, given as 21.5×10^3 in MPa while f_{cm} is the compressive strength.

It should be remarked since the beam elements were notched at mid-span and pre-cracked, non-linear behaviour will be localised at that region. Hence, simulation of time-dependent CMOD was focussed on the columns of mesh elements at the notch while other elements were assigned linear elastic behaviour. Therefore, the viscoelastic material model parameters for the elements were determined by relating the crack opening to strain. This was done by dividing the crack width by the mesh element size (3 mm), hence the FEA is invariably dependent on the element size.

7.2.2 Results

Figures 7.2 shows an example of the curve fitting performed and Tables 7.2 and 7.3 show the analyses material model parameters obtained from the uniaxial tensile creep results of cracked macro

synthetic FRC. These parameters were later used to simulate the time-dependent CMOD of the beams subjected to flexural creep.

The results of the viscoelastic model parameters presented in Tables 7.2 and 7.3 at the stress levels indicated show that the spring stiffness (represented by E) has been kept constant for Element 1. This represents the elastic modulus of the concrete and the relaxation time is zero since no dashpot is attached to the first element. The curve fitting operation has been used to determine the stiffness of the other elements and their respective relaxation time at the cracked state, hence smaller values.

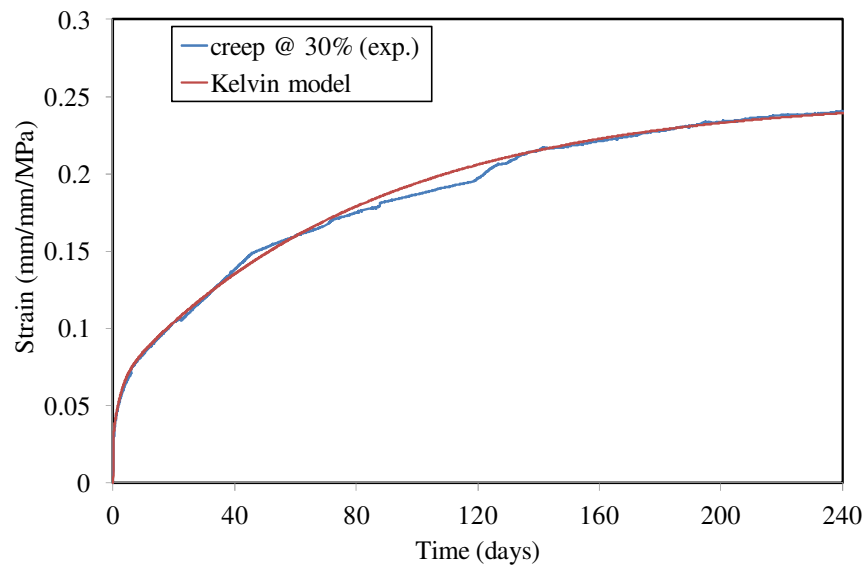


Figure 7.2: Example of Kelvin chain curve fitted to experimental creep result at 30 % stress level

Table 7.1: Viscoelastic material model parameters at 30 % stress level

Specimen no.	E_1 [MPa] (τ_1 [/day])	E_2 [MPa] (τ_2 [/day])	E_3 [MPa] (τ_3 [/day])	E_4 [MPa] (τ_4 [/day])
1	28802.83 (0)	20.887 (0.261)	12.066 (222.683)	3.410 (152.778)
2	28802.83 (0)	14.483 (0.517)	12.090 (21.116)	03.839 (134.234)
3	28802.83 (0)	23.966 (0.869)	30.181 (41.816)	18.503 (252.149)
4	28802.83 (0)	25.616 (0.400)	41.336 (15.365)	13.559 (104.419)

Table 7.2: Viscoelastic material model parameters at 50 % stress level

Specimen no.	E_1 [MPa] (τ_1 [/day])	E_2 [MPa] (τ_2 [/day])	E_3 [MPa] (τ_3 [/day])	E_4 [MPa] (τ_4 [/day])
2	28802.83 (0)	31.206 (0.033)	20.924 (22.540)	5.721 (167.731)
3	28802.83 (0)	7.713 (1.279)	5.898 (30.178)	2.221 (634.201)

7.3 Finite Element Modelling

The simulation of the structural behaviour of cracked macro synthetic FRC in flexure from material model parameters obtained from the macro (uniaxial tensile) test was carried out as previously mentioned. Nonlinear constitutive behaviour of concrete has been simulated severally by the finite element approach even though it poses a number of difficulties compared to the linear elastic analysis (Özcan et al., 2009; Palacio, 2013). There abound numerous studies on the response of FRC using different simulation approach (Casanova & Rossi, 1997; de Montaignac et al., 2012; Lok & Xiao, 1999; Nour et al., 2011; Zhang & Stang, 1998). It should however be remarked that the simulation of the time-dependent CMOD of cracked FRC in flexure from material model parameters obtained from the uniaxial tensile test is only a matter of recent interest (García-Taengua et al., 2014). This stems from the fact that only few studies are available on the time-dependent behaviour of cracked FRC. The following section discusses the approach to modelling the time-dependent CMOD of macro synthetic FRC.

7.3.1 Constitutive law of FRC: stress-crack width relationship

For the flexural behaviour of FRC to be understood and predicted, it has been reported that the characterisation of the fracture in terms of strain distribution, stress-crack width (σ - w) relation and deflection of the beam (where appropriate) must be given due consideration (Carnovale, 2013; Jones et al., 2008). Since FRC is usually investigated in the cracked state, the focus of a constitutive model for FRC in tension is to describe the post cracking behaviour in terms of σ - w or stress-strain (σ - ϵ) relation. For such a description, the σ - w relation must be linear up to the peak load in a uniaxial tensile test (Zhang & Stang, 1998). Results of σ - w relation from uniaxial tensile test have been

successfully used to obtain the constitutive tensile behaviour of FRC (Barragán et al. 2003; de Oliveira e Sousa et al. 2006; Stang & Bendixen, 1998). While many studies have obtained the corresponding σ - w constitutive material properties from experimentally notched beam using inverse analysis, this study uses the σ - w material properties obtained from the uniaxial tension test reported in Chapter 5.

Continuum damage mechanics approach of numerical modelling as against the continuum elasto-plasticity model has been chosen for the simulation of the time-dependent behaviour. This was then implemented as a smeared cracking approach which requires that the strains generated during the crack opening be added to the total strains at a material point as against the discrete approach. The discrete approach requires that the position of crack propagation be known beforehand which is not the actual case with FRC. Since the constitutive property from the uniaxial tensile test is obtained in the form of σ - w curve, it can be approximated using the Total Strain crack model which describes the tensile and compressive behaviour of a material with one σ - ϵ relationship. This could either be a Total Strain Rotating crack model or Total Strain Fixed crack model. The Rotating model is used in this study because the σ - ϵ relationship is evaluated in the principal direction unlike the Fixed model where the relationship is evaluated in a fixed coordinate system which is fixed upon cracking. The advantage of this approach is that, it can be directly combined with input of Kelvin chain viscoelastic properties presented in Tables 7.2 and 7.3. Similarly, this model is said to be well suited for serviceability state (SLS) and ultimate limit state (ULS) analyses which governs the cracking or crushing of concrete materials (TNO Diana, 2009).

7.3.2 Tensile behaviour

The tensile behaviour of a Total Strain crack model may be implemented in Diana software package for finite element analysis in a number of ways. The tensile model parameters of the material can be specified by direct input from a uniaxial tensile test (as done in this study) or from predefined properties in the analysis software. Depending on the softening response during the uniaxial tension

test, any of the tensile responses shown in Figure 7.3 can be engaged for the Total Strain crack model. This model describes the tensile and compressive behaviour of a material with one stress-strain relationship (TNO Diana, 2009).

The cracking behaviour obtained for the specimens tested in uniaxial tension in study mostly resembles that shown in Figure 7.3 g) with a multi-linear response. The multi-linear tension softening model has been used for this study. However, this behaviour is given as σ - ε relationship, hence the σ - w relationship obtained from the uniaxial tensile test has been related to a σ - ε relationship as already mentioned in Section 7.3.1. Implementation using the multi-linear diagram shown in Figure 7.3 g) does not require the use of the tensile strength of the material. It should however be remarked that the input for the Total Strain crack model in Diana requires basic material properties such as the Young's modulus, Poisson's ratio and the tensile behaviour (cracking material response).

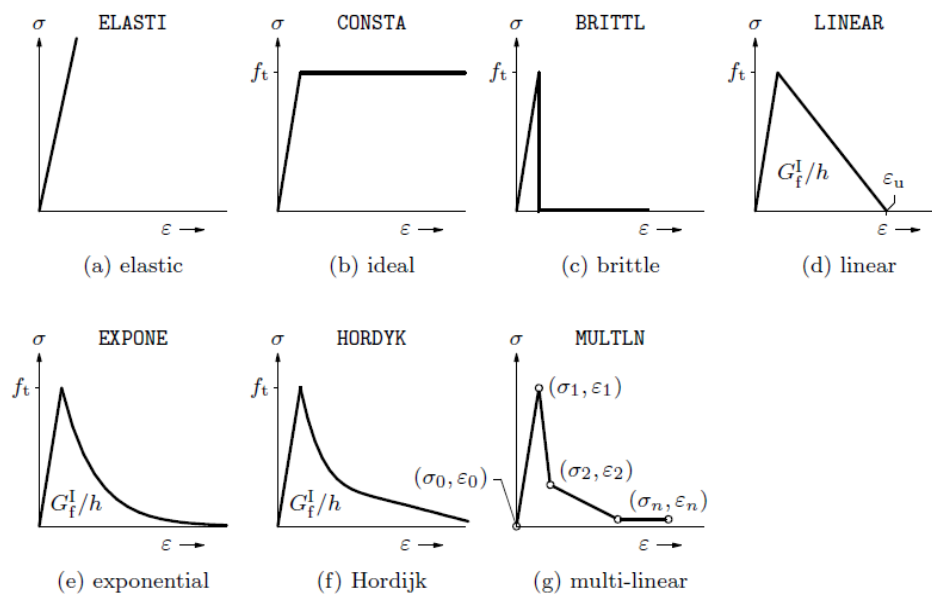


Figure 7.3: Predefined tension softening for Total Strain crack model (TNO Diana, 2009)

In this study, the Young's modulus as previously mentioned was determined using Eqn. 7.14 while the Poisson's ratio was taken as 0.15.

The post cracking tensile response was presented in Section 4.2.1. The average tensile material model parameters obtained from the uniaxial tension test is presented in Table 7.4. It should be noted

that the elastic strain of the material has been included to the result presented in Figure 4.1 to obtain the total strain (ϵ). Again, at ultimate tensile strength, the strain had been obtained by dividing the ultimate stress by the Young's modulus of the material. Note that as mentioned before, the other strain values are calculated by dividing the crack width by 3, the element size in mm, in the perpendicular direction to the intended crack plane.

Table 7.3: Actual tensile parameters obtained from test

Stress (σ) (MPa)	Crack width (w) (mm)	Strain (ϵ)
0	0	0
2.90	0.01	1.007e-04
0.78	0.61	0.203
0.85	1.00	0.333
0.91	1.50	0.500
0.94	2.00	0.667
0.94	3.00	1.000

7.3.3 Model description

To perform the finite element analysis for the prediction of the time-dependent CMOD of macro synthetic FRC beams subject to sustained flexural loadings, a beam model was first developed. A beam of the same size as those subjected to creep described in Chapter 6 under four point loading and having the same boundary conditions was used for the simulation. Figure 7.4 shows the finite element mesh of the beam, the boundary conditions and the applied load. The beam has a geometry cross-sectional area of 150 mm \times 150 mm and a span of 450 mm with the load applied at a third point. Since the actual test specimens were notched, the beam for the analysis was also notched at mid-span to a depth of 25 mm and notch width of 3 mm which is the thickness of the saw cut blade.

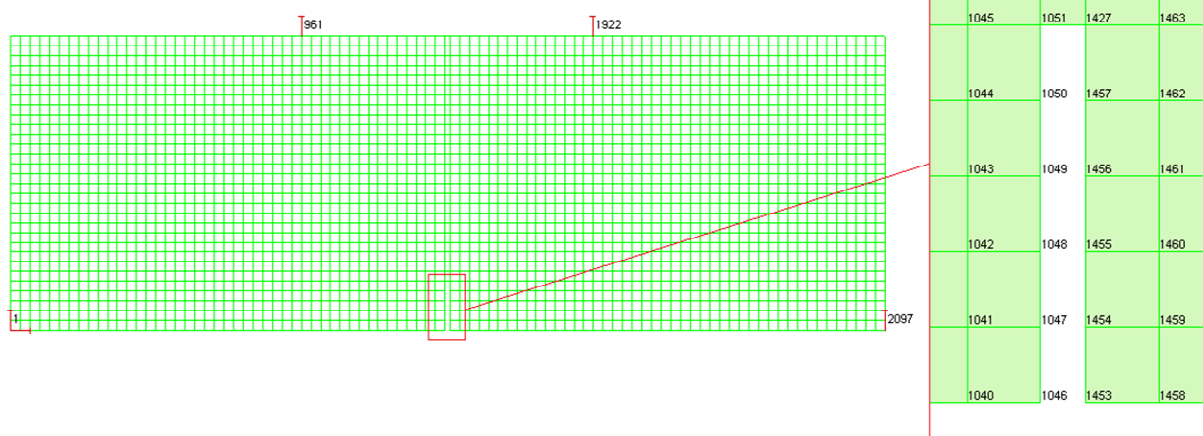


Figure 7.4: The finite element mesh of the beam subjected to four point bending

The finite element mesh size was chosen as 5 mm × 5 mm for satisfactory results to be obtained except at the middle of the beam where they were made 3 mm × 5 mm to conform to the width of the notch. The focus of the analysis is to investigate the time-dependent CMOD over the vertical column of elements at the notched area, hence two material properties were chosen. The column of elements across the notch was assigned the viscoelastic materials properties. This approach which focuses on the area of interest helps to simulate the instantaneous and time-dependent crack opening over the notched area of the beam. Other elements were assigned linear elastic material properties. The beam was modelled using linearly interpolated, four node plane stress elements (quadrilaterals) having a plane stress thickness of 150 mm which is equivalent to the actual specimen tested. A 2-dimensional (2D) analysis was performed.

7.4 Static Analyses

Prior to performing the analysis for the prediction of the time-dependent CMOD in flexure, an initial analysis to model the short-term flexural response was carried out. It should be reiterated that the beams subjected to the time-dependent tests had been cracked to a width of 0.2 mm and upon unloading showed an average irrecoverable crack width of 0.1 mm as explained in Chapter 6 before been subjected to sustained flexural loading. Hence, the initial analysis was set to accomplish two

objectives: predictions of the short term response under four-point loading and the time-dependent response.

It should also be mentioned that the damage mechanic approach which exhibit full unloading of the material (secant unloading) was implemented. This is not the true behaviour of the material under investigation as residual crack opening will not become zero (completely close up) as the case for the model. However, this approach assumes that internal damage during loading-unloading-reloading is not recoverable, hence stiffness degradation occurs as shown in Figure 7.5. Specimens were loaded to a crack width of 0.2 mm, unloaded by displacement control to a load corresponding to the stress level investigated and then kept constant as presented in Figure 7.6.

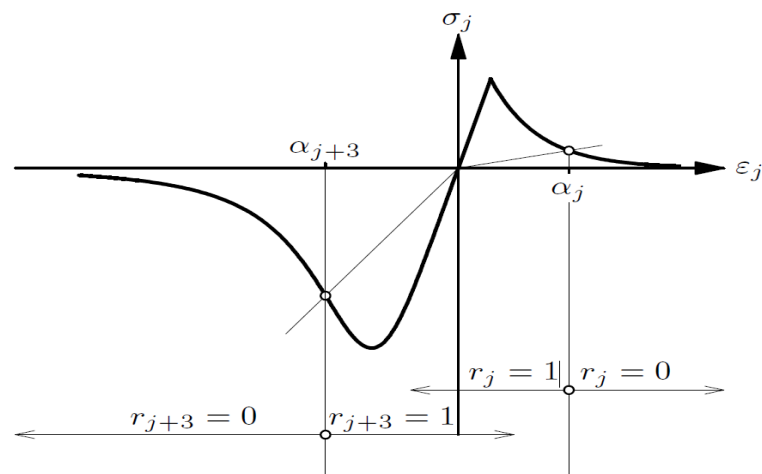


Figure 7.5: Loading-unloading (TNO Diana, 2009)

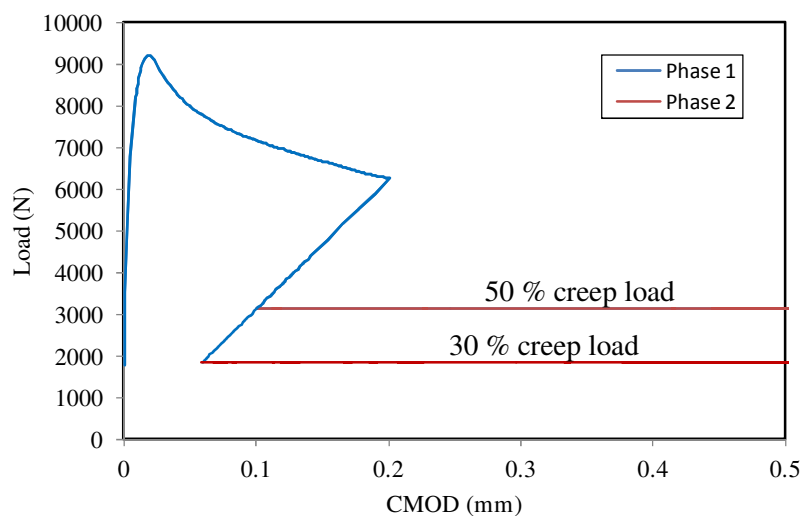


Figure 7.6: Modelled loading, unloading and applied creep load

7.4.1 Non-linear analysis procedures

Non-linear finite element analysis is usually a difficult operation to carry out, hence requires a good understanding of the problem at hand and appropriate knowledge of available solutions. Failure in the accurate definition of the model and the solution procedure can become a complex task particularly in achieving convergence (Palacio, 2003). Appropriate procedure for the initial analysis mentioned in Section 7.3.4 and the prediction of the time-dependent crack opening was ensured. Phase analysis was implemented for two cases: Phase 1 deals with the loading and unloading while Phase 2 of the analysis deals with the time-dependent analysis under sustained loading.

With regards to the applied load to the finite element model, incremental-iterative procedure solution was employed in a series of load/time steps. A number of available options are the force control, displacement control, arc-length control, arc-length method with indirect displacement control and automatic incremental procedure. The detailed description of these methods can be found in Palacio (2003).

The finite element analysis has been conducted in two categories. The first category of analysis is the prediction of the short term response of notched beams in flexure under four point loading. This has been performed using the displacement control incremental-iterative procedure. In the displacement control method, prescribed displacements increase step by step in the direction of a degree of freedom of a reference point on the structure and the unloading followed (Palacio, 2003).

Secondly, in modelling the time-dependent CMOD (Phase 2), force control was used for the application of the creep load. The load was kept constant throughout the analysis to obtain the deferred crack opening.

While a number of options are available for obtaining solutions to the non-linear system equilibrium equations, the Newton-Raphson (Regular) iteration method has been employed throughout the analysis. Convergence criteria have been based on force with a convergence tolerance limit of 5 %.

7.4.2 Prediction of four point flexural response

The result of the short term response of the analysis is presented in this section. The flexural behaviour of beams tested under four point loading were simulated as already mentioned using the tensile material model parameters obtained directly from the uniaxial tensile tests without any modification (Table 7.3).

The result of the analysis using the direct input shows to overestimate the flexural response: the maximum flexural strength of the analysis indicates an increase of 83 % above the experimental average (Figure 7.7). Beyond the peak stress, the analysis also overestimated the average experimental results by 164 %, 46 %, 34 % and 28 % at CMOD of 0.5 mm, 1.5 mm, 2.5 mm and 3.5 mm respectively. It can be observed that the difference is particularly more significant up to 1.5 mm.

The extensive crack opening after first crack in the uniaxial tensile tests (Figure 4.1) leading to significant reduction of the residual stress at average crack width of 0.6 mm could be adjudged to be responsible for this significant overestimation. It has been reported in Chapter 4 that such jump after first crack is influenced by the lack of stiffness of test setup. In addition, it should be mentioned that some form of overestimation may be expected because specimens in flexure and uniaxial tension are subjected to difference loading conditions. This will be further discussed in subsequent section. However, overestimation from FE results for similar kind of analysis using different approaches has been reported by Carnovale (2013) and Löfgren (2005).

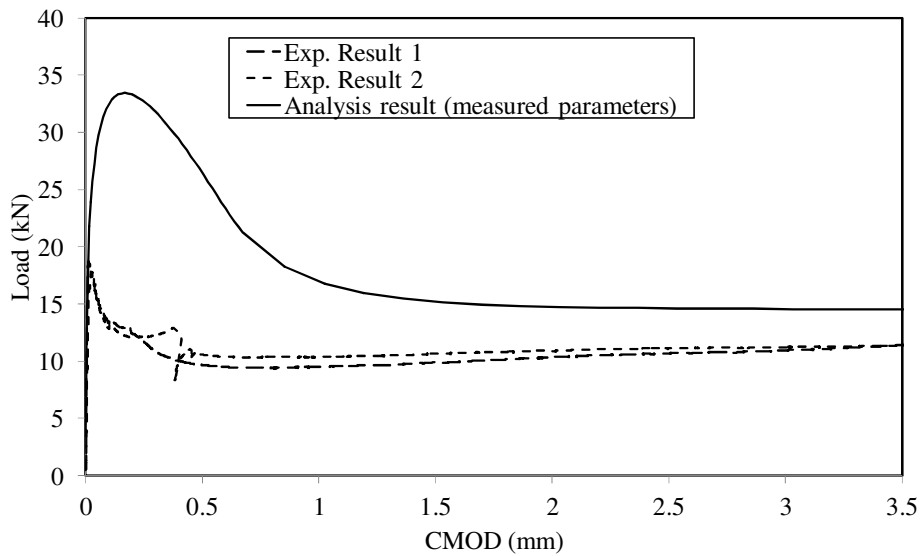


Figure 7.7: The analysis of result compared to the experimental flexural results

It is supposed that with a stiffer machine test setup and servo-controlled closed loop control, the sudden jump after first crack could be avoided and a steeper descending slope after first crack could contribute to be result output. The importance of a proper slope representation in the descending branch of the stress-crack width relation for successful analysis has been stressed (Löfgren, 2005). The measured tensile model parameters in Table 7.3 were then adjusted to reflect a steeper slope with two new points introduced, see Table 7.5 and Figure 7.8.

Table 7.4: Cases of adjusted tensile model parameters with the additional points highlighted

Case 1			Case 2			Case 3		
Stress (σ) (MPa)	crack width (w) (mm)	Strain (ϵ)	Stress (σ) (MPa)	crack width (w) (mm)	Strain (ϵ)	Stress (σ) (MPa)	crack width (w) (mm)	Strain (ϵ)
0	0	0	0	0	0	0	0	0
2.90	0.01	1.01e-04	2.9	0.01	1.01e-04	2.9	0.01	1.01e-04
1.00	0.024	0.008	1.00	0.024	0.008	1.00	0.024	0.008
0.72	0.30	0.100	0.72	0.18	0.060	0.72	0.12	0.040
0.78	0.10	0.203	0.78	0.10	0.203	0.78	0.10	0.203
0.85	1.00	0.333	0.85	1.00	0.333	0.85	1.00	0.333
0.91	1.50	0.500	0.91	1.50	0.500	0.91	1.50	0.500
0.94	2.00	0.667	0.94	2.00	0.667	0.94	2.00	0.667
0.94	3.00	1.000	0.94	3.00	1.000	0.94	3.00	1.000

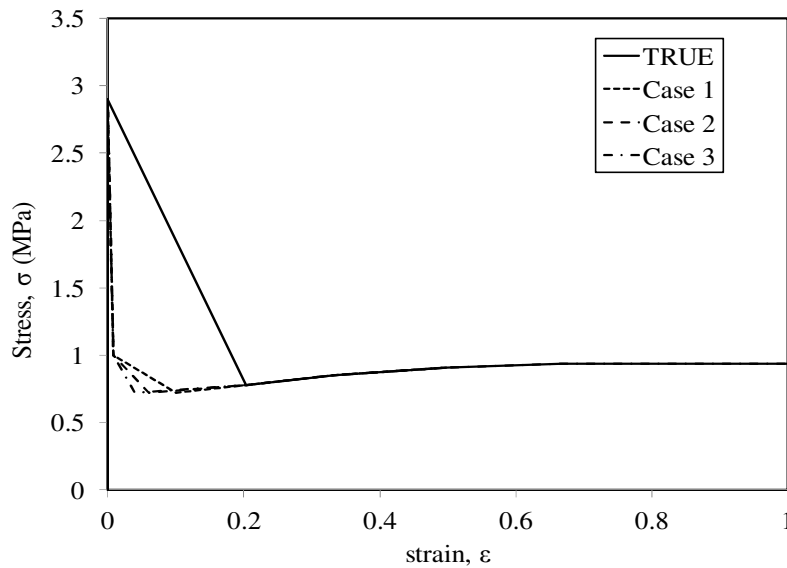


Figure 7.8: Stress-strain graph showing true and adjusted tensile parameters

While two additional points have been introduced to conform to Figure 7.3 g), the post cracking parameters obtained from the actual experiment have not being altered. The FEA result of the three adjusted cases in comparison to the experimental results is presented in Figure 7.9. The results of the three cases analysed show similarity with the experimental results. This confirms that the slope of descending branch of the curve after the peak load does have an influence on the analysis output. The analysis predicts the ultimate strength well and the shape is similar to the experimental response. Significant deviation (about 20 %) is still observed in the post cracking region from the two experimental results (see Figure 7.9).

Significant scatter in the post cracking response of FRC in flexure than in tension has been reported (Löfgren, 2005). The high variability in the post cracking behaviour of specimens tested under flexure is connected to high variability of the numbers of fibres crossing the cracked plane and the orientation of the fibres (di Prisco et al., 2009).

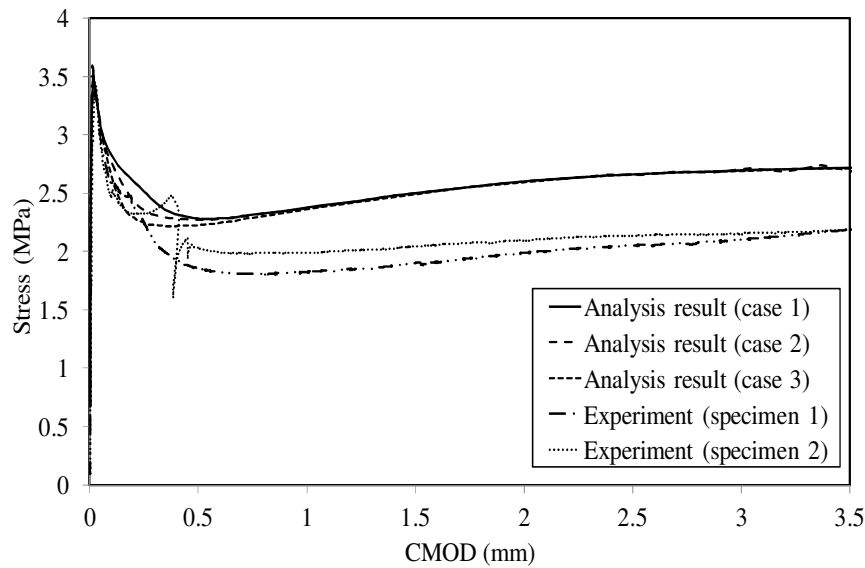


Figure 7.9: Parametric analysis of result compared to the experimental flexural results

7.5 Prediction of Time-Dependent CMOD

The prediction of the time-dependent crack widening of notched beams subjected to sustained flexural loading at 30 % and 50 % stress levels have been carried out. The Total Strain Rotating crack model (evaluation of stress-strain in the directions of the principal strain vector) was used with focus on the elements where cracking occurs (notched area). The behaviour of beams in flexure is known to be a complex phenomenon due to action of compressive and tensile stresses at the same time. As previously mentioned, the viscoelastic parameters were only applied to the elements at the notch to simulate the time-dependent crack opening in the area where cracking occurred. Before the viscoelastic material model parameters were applied to the elements at the area of interest, analysis was performed to distinguish elements subjected to tensile stresses from those in compression. Figure 7.10 shows the distribution of the stresses at point of application of the creep load. It should be remarked that the neutral axis did not differ significant at 30 % stress level from 50 %, hence the same elements were given the same viscoelastic material model parameters at both stress levels.

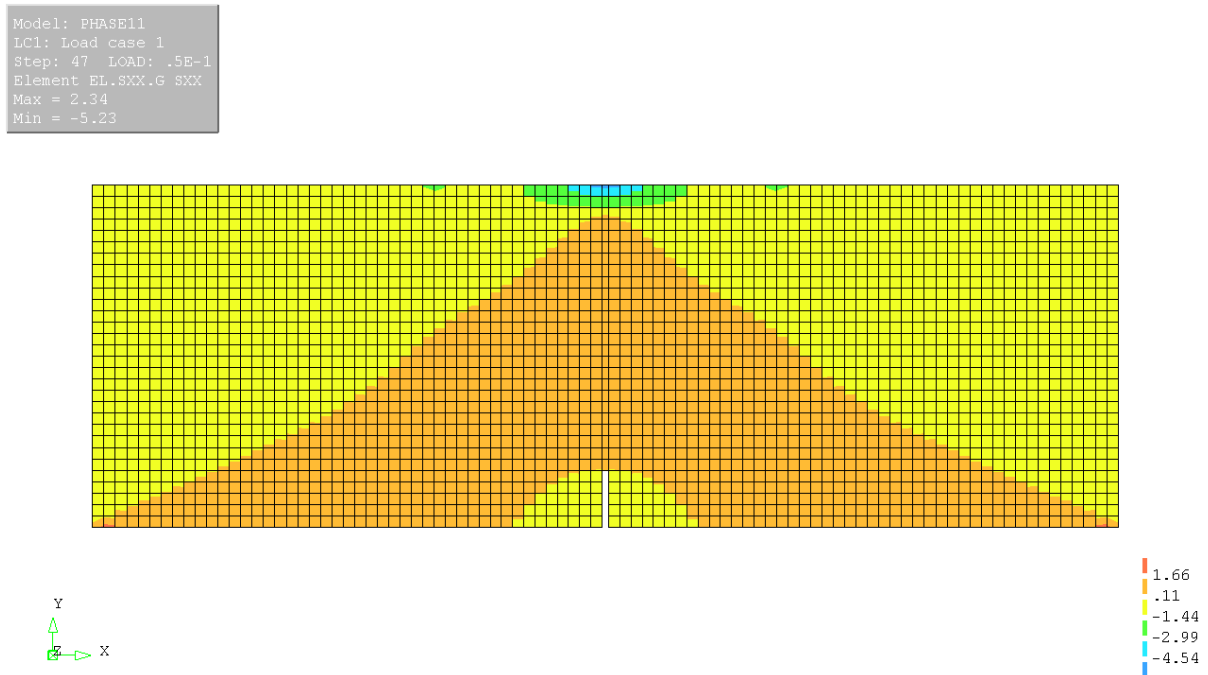


Figure 7.10: Compressive and tensile stress distribution

7.5.1 Results and discussion

The result of the prediction of the time-dependent CMOD in comparison to the experimental results for a period of 8 months at 30 % and 50 % stress levels are presented in Figures 7.11 and 7.12 respectively. It has been mentioned that rather than modelling the average behaviour at both stress levels, individual specimen behaviour has been modelled.

In Figure 7.11, four analyses output obtained by implementing material properties for each uniaxial tensile creep specimen are presented. The analyses results are compared to experimental flexural creep results. Results of analyses labelled 1 and 2 show an overestimation of the time-dependent CMOD at 30 % stress levels with an average CMOD of 0.3 mm after 8 months. Conversely, analysis results labelled 3 and 4 show good correlations with all the experimental results. However, within the range of the four analyses, good prediction is observed.

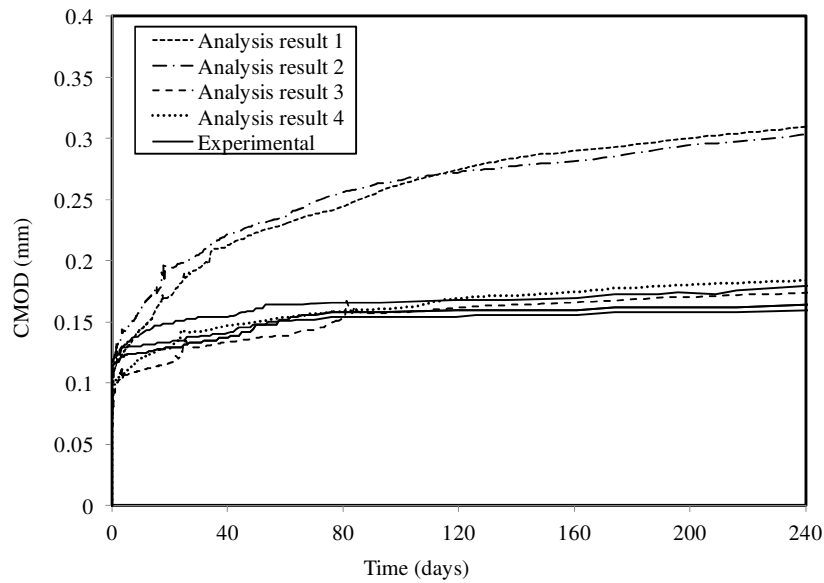


Figure 7.11: The analysis result compared to experimental creep result at 30 % stress level

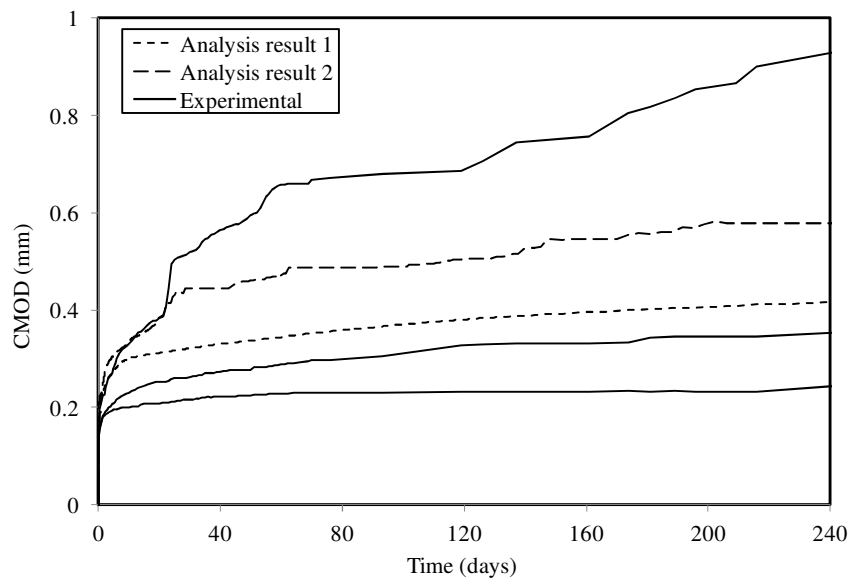


Figure 7.12: The analysis result compared to experimental creep results at 50 % stress level

At 50 % stress level, using material properties from the two tensile specimens simulated, the analyses results fall within the bounds of experimental variation showing a good prediction (Figure 7.12).

Overall, it can be said that the implementation of material model parameters (tensile and viscoelastic) from uniaxial tensile and tensile creep test in the Total Strain crack model could predict reasonably the time-dependent CMOD of specimens subjected to sustained flexural loading. This however is still a subject of further research. As proposed in Chapter 4, the use of test setup with

higher stiffness could reduce significantly the sudden drop in stress after the first crack which led to the large crack opening. Similarly, in Chapter 6, it has been suggested that where enough space is available for the placement of flexural creep frames, one specimen should be placed on a frame rather than the column of three specimens. This will eliminate the possible discrepancies in results due to specimen's position.

7.5.2 Relation between uniaxial tensile and flexural creep

Little or no attention has been given to the relation between FRC creep in tension and flexure in literature. This chapter has attempted to relate the uniaxial tensile creep of cracked FRC to the behaviour at the structural level.

Since the time-dependent crack opening under sustained uniaxial tensile and flexural loadings cannot be directly compared due to the different mechanisms of load transfer, FEA has been performed. This has been carried out using a constitutive model based on Total strain crack model in combination with Kelvin chain viscoelasticity. True material properties can only be obtained from the uniaxial tensile test. The FEA results have shown that the tensile material model properties (σ - w) from a uniaxial tensile test have a direct relationship to the beam response at the structural level of investigation. The analysis was able to predict the average ultimate strength, the shape of the load-CMOD curve and the post cracking residual response of the beams subjected to four point bending tests. Though about 20 % deviation in the post cracking response has been reported, FRC are general known to show such significant scatter in the post cracking behaviour.

With the combination of the viscoelastic material model parameters to the Total Strain crack model, the time-dependent CMOD of a cracked macro synthetic FRC beam subjected to sustained flexural loading on structural level has also been predicted within the bounds of experimental variations. The time-dependent CMOD response at the structural level is greatly influenced by the viscoelastic material model parameters. Viscoelastic material model parameters obtained by curve

fitting to experimental uniaxial tensile creep results with larger time-dependent CMOD predicts larger CMOD and vice versa.

However, in general, the FEA has shown a direct relationship between material model parameters obtained from a uniaxial tensile creep test and the time-dependent CMOD of a cracked FRC subjected to sustained flexural loading.

As briefly mentioned above, specimens in uniaxial tensile loading are subjected to pure tensile stresses even though stress distribution in fibres at cracked surface may not be purely uniform as argued by Rots (1988). Fibres are however all subjected to tension at the same time, hence significant crack widening by fibre pullout and fibre creep mechanism as presented in Section 5.3. For specimens in flexure, when the crack opens, the fibres at the tip of the notch resist the crack opening, and with time undergo creep. Under sustained loading, as the outer fibres at the notch creep, they are only able to bear less stress, while the upper layer of fibres bear higher stress to again resist further crack opening at that level. The distribution of stresses in a cracked FRC is presented in Figure 7.13.

This transfer of stress across the crack is continued from one layer to the other over time, hence, reducing the crack width propagation and the rate of crack opening. Figure 7.13 show the propagation and transfer of stress in four phases.

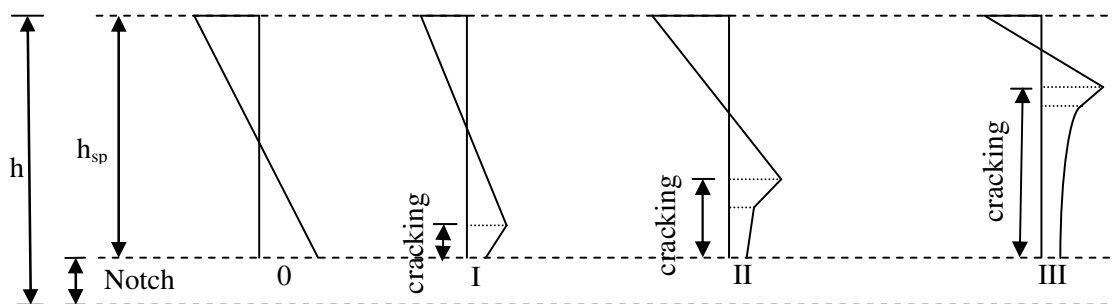


Figure 7.13: Stress distribution over the height of a hinge during crack evolution (Adapted from Olesen, 2001; Buratti et al. 2011)

At Phase 0, crack is yet to be initiated and the diagram shows the state of stress. With the initiation of crack, Phases I to III show different state of stress with the propagation of the crack. Away from the tip of the notch, the tensile stress in the fibres reduces and fibres at the neutral axis experiences

zero tensile stress (MacKay & Trottier, 2004). This phenomenon in flexure differs in specimens subjected to sustained uniaxial tensile loading, hence the crack opening differs and more pronounced in the uniaxial tensile creep specimens.

7.6 Summary

The time-dependent crack opening of macro synthetic FRC subjected to sustained flexural loading has been modelled using finite element analysis approach. The following conclusion can be made:

- The modelling of the short term behaviour of macro synthetic FRC was successful carried out using tensile material parameters obtained from the uniaxial tensile test. However, post cracking behaviour is overestimated by about 20 % for the adjusted tensile material model parameters.
- The viscoelastic approach was successful implemented in finite element analysis using the Total Strain crack model to predict the time-dependent CMOD of beams subjected to sustained loadings. Results of analyses correspond well with experimental results at both 30 % and 50 % stress levels.
- A direct relation has been established between uniaxial tensile and flexural creep test results by finite element analysis. Tensile material model parameters from uniaxial tensile test and viscoelastic material model parameters from curve fitting to experimental tensile creep results can be used to predict the time-dependent flexural response under sustained loading.

Chapter 8

Conclusions and Recommendations

This dissertation has investigated the time-dependent crack mouth opening displacement of cracked macro synthetic FRC subjected to different stress levels of uniaxial tensile loading. An experimental investigation was carried out at three levels: macro level (compression tests, uniaxial tensile tests, uniaxial tensile creep tests, drying shrinkage); single fibre level (single fibre tensile tests, single fibre pullout tests, time-dependent fibre pullout tests) and structural level (flexural tests, flexural creep tests). The mechanism responsible for the time-dependent cracking widening of cracked macro synthetic FRC has been investigated at the single fibre level.

Another goal of this dissertation is the modelling of the time-dependent crack mouth opening displacement of specimens subjected to sustained flexural loading. Tensile and viscoelastic material model parameters obtained from the uniaxial tensile and uniaxial creep results were implemented in the Total Strain crack model using finite element analysis software, Diana version 9.5. The conclusions from experimental investigations and the verification of the finite element modelling are presented in the following sections.

8.1 Macro Level

- The tensile creep response of cracked macro synthetic FRC is stress dependent: the higher the creep load, the higher the time-dependent crack opening. After 8 months of investigation, significant creep is recorded without crack widening stabilising. Average crack opening at 30 % to 70 % stress levels are 1200 μm , 1700 μm , 2100 μm , 6700 μm and 8300 μm respectively.

- Creep fracture of specimens occurred at 60 % and 70 % of the post peak resistance after 10 days and less than 1 day respectively. This shows that the creep loads are not sustainable, hence creep fracture should be taken into consideration when using macro synthetic FRC.
- The distribution and number of fibres crossing the cracked plane have shown to be responsible for variability on the behaviour of the time-dependent crack opening. The higher the fibre counts on a cracked surface, the lower the time-dependent crack opening and vice versa.
- Up to the points where tests were stopped, failure mechanism is by fibre pullout. However, only two ruptured fibres were observed in specimens that fractured at 60 % and 70 %, hence are not considered a major failure pattern.

8.2 Single Fibre Level

- Macro PP fibre tensile response is influenced by loading rate: the higher the loading rate, the higher the breaking load.
- Average maximum fibre tensile strength obtained from test at 1 mm/s, 0.1 mm/s and 0.01 mm/s showed to be higher than the manufacturer's recommendation (400 MPa) except at a rate of 0.001 mm/s, which is 390 MPa.
- While the interfacial shear resistance at pullout has shown to be influence by loading rate, the effect is less significant with lower fibre embedment length, e.g., 10 mm. Interfacial shear resistance however decreases with increasing fibre embedment length and increased with higher loading rate. The strength of the bond between the macro PP fibre and the matrix range from 2.0 to 3.4 MPa.
- Mechanism of fibre failure in all cases is by complete pullout. This is influenced by the fact that the pullout strength is lesser than the fibre tensile strength.

- At the stress levels investigated (50 % to 80 % of τ_{\max} of specimens tested at 25 mm embedment length), the time-dependent pullout is dependent on the load level: the higher the load, the quicker the pullout. Pullout at 50 % took about 4 days while at 80 %, complete pullout occurred after only 15 minutes.
- As in the single fibre pullout test, all fibres failed by complete pullout establishing it as one of the mechanisms responsible for the time-dependent crack widening of specimens subjected to creep loads.
- Significant creep of single macro fibre occurred for a period of 4 days investigated. Elongation of 40 % was recorded for a creep load as low as 30 % of the tensile strength of the fibre. Hence, it is concluded that fibre creep is also another mechanism responsible for the time-dependent crack widening of specimens under creep loading.

8.3 Structural level

- After 8 months under sustained creep load, specimens tested at 30 % stress level show an average total CMOD of 0.17 mm while those tested at 50 % stress levels show an average of 0.5 mm.
- The creep coefficient, $\phi_o(j)$, is a function of the applied stress level and decreases with testing age. At 8 months, creep coefficients were 0.93 and 3.13 at 30 % and 50 % stress levels, respectively.

8.4 Time-dependent CMOD modelling

- The prediction of the time-dependent CMOD for specimens loaded under sustained flexural loadings at 30 % and 50 % of the average residual strength was successfully carried out using the Total Strain crack model. Tensile material model parameters are obtained from the uniaxial tensile test while the viscoelastic material model parameters using the Kelvin chain is obtained by curve fitting to the experimental results of the uniaxial tensile creep.

- The results of the analyses at 30 % stress level corresponds well experimental results whereas at 50 %, analyses results fall within the boundary of experimental results for the three flexural creep specimens.

8.5 Recommendation

Based on experimental insight gained during the course of carrying out this research work, the following areas have been identified for further studies:

- Significant level of variability has been identified for the results of the uniaxial tensile creep test. While uneven distribution of fibres at the cracked plane has been established as one of the causes of this variability, it is anticipated that variability in the crack width of pre-cracked specimens could also have had some influence on the results.
- In Chapter 6, the effect of specimen's position on the flexural creep result was identified particularly at higher stress level. Where possible, single specimen should be placed on the creep frame to eliminate this effect.
- Since the stress distribution in the cracked plane of flexural creep samples are not uniform, it will be a worthwhile study to group and model the stresses for comparison with uniaxial tensile test specimens subjected to sustained loading.
- Test machines with higher stiffness and a servo-controlled closed loop control should be used for uniaxial tensile test to obtain true tensile material parameters without modification.

References

- Alhozaimy, A. M., Soroushian, P., & Mirza, F. (1996). Mechanical properties of polypropylene fiber reinforced concrete and the effects of pozzolanic materials. *Cement and Concrete Composites*, 18(2), 85-92. DOI:10.1016/0958-9465(95)00003-8
- Alizadeh, R., Beaudoin, J. J., & Raki, L. (2010). Viscoelastic nature of calcium silicate hydrate. *Cement and Concrete Composites*, 32(5), 369-376.
- Al-Khaja, W. A. (1995). Mechanical properties and time-dependent deformation of polypropylene fibre reinforced concrete. *Journal of King Saud University, Engineering Science*, 7(1), 67-76.
- Altoubat, S. A., & Lange, D. A. (2001). Tensile basic creep: Measurements and behavior at early age. *ACI Materials Journal*, 98(5), 386-393.
- Altoubat, S. A., & Lange, D. A. (2003). A new look at tensile creep of fiber-reinforced concrete. *ACI Special Publication*, 216, 143-160.
- Aly, T., Sanjayan, J., & Collins, F. (2008). Effect of polypropylene fibers on shrinkage and cracking of concretes. *Materials and Structures*, 41(10), 1741-1753.
- Amin, N., Kirk, V., Garo, A., & Bijan, S. (2014). Drying shrinkage behaviour of fibre reinforced concrete incorporating polyvinyl alcohol fibres and fly ash, *Advances in Civil Engineering*, 2014 DOI:10.1155/2014/836173
- Arango, S. E., Serna, P., Marti-Vargas, J., & Garcia-Taengua, E. (2012). A test method to characterize flexural creep behaviour of pre-cracked FRC specimens. *Experimental Mechanics*, 52(8), 1067-1078. DOI:10.1007/s11340-011-9556-2
- Babafemi, A. J., & Boshoff, W. P. (2015). Tensile creep of macro-synthetic fibre reinforced concrete (MSFRC) under uni-axial tensile loading. *Cement and Concrete Composites*, 55, 62-69.

- Balaguru, P. N., & Shah, S. P. (1992). *Fiber-reinforced cement composites*. New York: Mc-Graw Hill.
- Banik, K., Karger-Kocsis, J., & Abraham, T. (2008). Flexural creep of all polypropylene composites: Model analysis. *Polymer Engineering & Science*, 48(5), 941-948.
- Banthia, N., & Gupta, R. (2006). Influence of polypropylene fiber geometry on plastic shrinkage cracking in concrete. *Cement and Concrete Research*, 36(7), 1263-1267.
- Banthia, N., & Trottier, J. (1995). Test methods for flexural toughness characterization of fiber reinforced concrete: Some concerns and a proposition. *ACI Materials Journal*, 92(1), 48-57.
- Barnett, S. J., Lataste, J., Parry, T., Millard, S. G., & Soutsos, M. N. (2010). Assessment of fibre orientation in ultra high performance fibre reinforced concrete and its effect on flexural strength. *Materials and Structures*, 43(7), 1009-1023.
- Barragán, B. E., & Zerbino, R. (2008). Creep behavior of cracked steel fiber reinforced concrete beams. *7th International RILEM Symposium on Fiber Reinforced Concrete: Design and Applications (BEFIB 2008)*, Chennai, India. 577-586.
- Barragán, B. E., Zerbino, R. L., & Gettu, R. (2008). Creep behaviour of cracked steel fibre reinforced concrete beams. *Proceedings of the 7th Int. RILEM Symp. on Fibre Reinforced Concrete: Design and Applications (BEFIB 2008)*. Chennai, 577-586.
- Bazant, Z. P. (2001). Prediction of concrete creep and shrinkage: Past, present and future. *Nuclear Engineering and Design*, 203(1), 27-38.
- Bazant, Z. P., & Oh, B. H. (1984). Deformation of progressively cracking reinforced concrete beams. *ACI Journal Proceedings*, 81(3), 268-278.
- Bencardino, F., Rizzuti, L., Spadea, G., & Swamy, R. N. (2013). Implications of test methodology on post-cracking and fracture behaviour of steel fibre reinforced concrete. *Composites Part B: Engineering*, 46, 31-38.

- Bentur, A. (1990). Microstructure, interfacial effects, and micromechanics of cementitious composites. *Ceram.Trans.*, 16, 523-550.
- Bentur, A., & Mindess, S. (2006). *Fibre reinforced cementitious composites*. England: Elsevier Science Publisher Ltd.
- Bernard, E. S. (2004). Creep of cracked fibre reinforced shotcrete panels. *Shotcrete: More Engineering Developments*. Taylor & Francis Group, London, , 47-57.
- Bernard, E. S. (2010). Influence of fiber type on creep deformation of cracked fiber-reinforced shotcrete panels. *ACI Materials Journal*, 107(5)
- Bissonnette, B., Pigeon, M., & Vaysburd, A. M. (2007). Tensile creep of concrete: Study of its sensitivity to basic parameters. *ACI Materials Journal*, 104(4), 360-368.
- Blanco, A. (2013). *Characterization and modelling of SFRC elements*. Unpublished Doctoral dissertation, Universitat Politècnica de Catalunya, Barcelona, Spain.
- Boshoff, W. P., & Adendorff, C. J. (2013). Effect of sustained tensile loading on SHCC crack widths. *Cement and Concrete Composites*, 37, 119-125.
- Boshoff, W. P., Mechtcherine, V., & van Zijl, G. P. (2009a). Characterising the time-dependant behaviour on the single fibre level of SHCC: Part 1: Mechanism of fibre pull-out creep. *Cement and Concrete Research*, 39(9), 779-786.
- Boshoff, W. P., Mechtcherine, V., & van Zijl, G. P. (2009b). Characterising the time-dependant behaviour on the single fibre level of SHCC: Part 2: The rate effects on fibre pull-out tests. *Cement and Concrete Research*, 39(9), 787-797.
- Boshoff, W. P. (2007). *Time-dependant behaviour of engineered cement-based composites*. Unpublished Doctoral dissertation, Stellenbosch: University of Stellenbosch, South Africa.
- Brandt, A. M. (2008). Fibre reinforced cement-based (FRC) composites after over 40 years of development in building and civil engineering. *Composite Structures*, 86(1), 3-9.

- Brinson, L. C., & Gates, T. S. (1995). Effects of physical aging on long term creep of polymers and polymer matrix composites. *International Journal of Solids and Structures*, 32(6), 827-846.
- BS EN 12390-3 (2002). *Testing hardened concrete - compressive strength of test specimens*. London: British Standard Institution.
- BS EN 14889-2 (2006). *Fibres for concrete, part 2: Polymer fibres, definitions, specification and conformity* (British Standards Institution ed.), London.
- BS EN 934-2 (2009). *Admixtures for concrete, mortar and grout. concrete admixtures. definition, requirements, conformity, marking and labelling*. London: United Kingdom.
- BS EN12350-2 (2000). Testing fresh Concrete—Slump test. *British Standards Institution, London, UK*.
- BS EN12390-5 (2000). *Testing hardened concrete-part-5: Flexural strength of test specimens*. London: British Standard Institution.
- Buratti, N., & Mazzotti, C. (2012a). Effects of different types and dosages of fibres on the long-term behaviour of fibre-reinforced self-compacting concrete. *8th RILEM Symposium on Fibre Reinforced Concrete: Challenges and Opportunities (BEFIB 2012)*, Guimarães, Portugal. 726-738.
- Buratti, N., & Mazzotti, C. (2012b). Temperature effect on the long-term behaviour of macro-synthetic-and steel-fibre reinforced concrete. *8th RILEM International Symposium on Fiber Reinforced Concrete: Challenges and Opportunities (BEFIB 2012)*, 715-725.
- Buratti, N., Mazzotti, C., & Savoia, M. (2011). Post-cracking behaviour of steel and macro-synthetic fibre-reinforced concretes. *Construction and Building Materials*, 25(5), 2713-2722.
- Carnovale, D. J. (2013). *Behaviour and analysis of steel and macro-synthetic fibre reinforced concrete subjected to reverse cyclic loading: A pilot investigation*. Unpublished Master's Thesis. University of Toronto, Canada.

- Casanova, P., & Rossi, P. (1997). Analysis and design of steel fiber reinforced concrete beams. *ACI Structural Journal*, 94(5), 595-602.
- Chanvillard, G., & Roque, O. (1999). Behavior of fiber reinforced concrete cracked section under sustained load. *Proceedings of the 3rd International Workshop on High Performance Fiber Reinforced Cement Composites, RILEM Publication, Mainz, Germany*. 239-250.
- Choi, S. Y., Park, Y. H., & Jung, W. T. (2012). A study on the bond performance improvement of polypropylene macro fibers according to the change of surface area. *Advanced Materials Research*, 557, 1440-1446.
- Cifuentes, H., García, F., Maeso, O., & Medina, F. (2013). Influence of the properties of polypropylene fibres on the fracture behaviour of low-, normal-and high-strength FRC. *Construction and Building Materials*, 45, 130-137.
- Clarke, J., Peaston, C., & Swannell, N. (2007). Guidance on the use of macro-synthetic fibre reinforced concrete. *The Concrete Society*, 65, 1-2.
- Clements, M. (2002). Synthetics as concrete reinforcement. *Concrete*, 36(8), 37-38.
- Cunha, V. M. C. F., Barros, J. A. O., & Sena-Cruz, J. M. (2011). An integrated approach for modelling the tensile behaviour of steel fibre reinforced self-compacting concrete. *Cement and Concrete Research*, 41(1), 64-76.
- Cunha, V. M. C. F., Barros, J. A. O., & Sena-Cruz, J. M. (2012). A finite element model with discrete embedded elements for fibre reinforced composites. *Computers & Structures*, 94, 22-33.
- Currie, B., & Gardiner, T. (1989). Bond between polypropylene fibres and cement matrix. *International Journal of Cement Composites and Lightweight Concrete*, 11(1), 3-9.
- de Montaignac, R., Massicotte, B., Charron, J., & Nour, A. (2012). Design of SFRC structural elements: Post-cracking tensile strength measurement. *Materials and Structures*, 45(4), 609-622.

- de Oliveira e Sousa, José Luiz Antunes, & Gettu, R. (2006). Determining the tensile stress-crack opening curve of concrete by inverse analysis. *Journal of Engineering Mechanics*, 132(2), 141-148.
- di Prisco, M., Plizzari, G., & Vandewalle, L. (2009). Fibre reinforced concrete: New design perspectives. *Materials and Structures*, 42(9), 1261-1281.
- Ding, Y. (2011). Investigations into the relationship between deflection and crack mouth opening displacement of SFRC beam. *Construction and Building Materials*, 25(5), 2432-2440.
- Drozdo, A. (2010). Creep rupture and viscoelastoplasticity of polypropylene. *Engineering Fracture Mechanics*, 77(12), 2277-2293.
- Dupont, D. (2003). *Modelling and experimental validation of the constitutive law and cracking behaviour of steel fibre reinforced concrete*. Unpublished Doctoral dissertation. Catholic University of Leuven, Belgium.
- Ebert, C., Hufenbach, W., Langkamp, A., & Gude, M. (2011). Modelling of strain rate dependent deformation behaviour of polypropylene. *Polymer Testing*, 30(2), 183-187.
- Emdadi, A., Mehdipour, I., Libre, N. A., & Shekarchi, M. (2013). Optimized workability and mechanical properties of FRCM by using fiber factor approach: Theoretical and experimental study. *Materials and Structures*, 1-13. DOI: 10.1617/s11527-013-0221-3
- EN 14651. (2005). *Test method for metallic fibre concrete - measuring the flexural tensile strength (limit of proportionality (LOP), residual)*. London: British Standard Institution.
- Fanourakis, G. C., & Ballim, Y. (2003). Predicting creep deformation of concrete: A comparison of results from different investigations. *Proceedings, 11th FIG Symposium on Deformation Measurements*, Santorini, Greece.

- Ferrier, E., Michel, L., Zuber, B., & Chanvillard, G. (2015). Mechanical behaviour of ultra-high-performance short-fibre-reinforced concrete beams with internal fibre reinforced polymer bars. *Composites Part B: Engineering*, 68, 246-258.
- fib (2010). *Model code 2010 - Final complete draft*. Fédération Internationale du Béton fib/International Federation for Structural Concrete.
- Fu, S., & Lauke, B. (1996). Effects of fiber length and fiber orientation distributions on the tensile strength of short-fiber-reinforced polymers. *Composites Science and Technology*, 56(10), 1179-1190.
- Fu, S., Lauke, B., Mäder, E., Yue, C., & Hu, X. (2000). Tensile properties of short-glass-fiber-and short-carbon-fiber-reinforced polypropylene composites. *Composites Part A: Applied Science and Manufacturing*, 31(10), 1117-1125.
- García-Taengua, E., Arango, S., Martí-Vargas, J., & Serna, P. (2014). Flexural creep of steel fiber reinforced concrete in the cracked state. *Construction and Building Materials*, 65, 321-329.
- Gilbert, R. I., & Ranzi, G. (2010). *Time-dependent behaviour of concrete structures* CRC Press.
- Goel, R., Kumar, R., & Paul, D. K. (2007). Comparative study of various creep and shrinkage prediction models for concrete. *Journal of Materials in Civil Engineering*, 19(3), 249-260.
- Gokoz, U. N., & Naaman, A. E. (1981). Effect of strain-rate on the pull-out behaviour of fibres in mortar. *International Journal of Cement Composites and Lightweight Concrete*, 3(3), 187-202.
- Granju, J. L., Rossi, P., Chanvillard, G., Mesureur, B., Turatsinze, A., Farhat, H., Roque, O. (2000). Delayed behaviour of cracked SFRC beams. *RILEM Symposium on Fibre-Reinforced Concretes*, 511-520.
- Gutsch, A., & Rostásy, F. S. (1995,). Young concrete under high tensile stresses-creep, relaxation and cracking. Retrieved from <http://books.google.co.za>

- Hannant, D. (1998). Durability of polypropylene fibers in portland cement-based composites: Eighteen years of data. *Cement and Concrete Research*, 28(12), 1809-1817.
- Hollaway, L. (1990). *Polymers and polymer composites in construction*. London: Thomas Telford.
- Hope, B. B., & Brown, N. H. (1975). A model for the creep of concrete. *Cement and Concrete Research*, 5(6), 577-586.
- Houshyar, S., Shanks, R. A., & Hodzic, A. (2005). Tensile creep behaviour of polypropylene fibre reinforced polypropylene composites. *Polymer Testing*, 24(2), 257-264.
- Hsie, M., Tu, C., & Song, P. S. (2008). Mechanical properties of polypropylene hybrid fiber-reinforced concrete. *Materials Science & Engineering: A*, 494(1), 153-157.
DOI:10.1016/j.msea.2008.05.037
- Hwan Oh, B., Park, D. G., Kim, J. C., & Choi, Y. C. (2005). Experimental and theoretical investigation on the postcracking inelastic behavior of synthetic fiber reinforced concrete beams. *Cement and Concrete Research*, 35(2), 384-392.
- Illston, J. M. (1965). The creep of concrete under uniaxial tension. *Magazine of Concrete Research*, 17(51), 77-84.
- Jones, P. A., Austin, S. A., & Robins, P. J. (2008). Predicting the flexural load–deflection response of steel fibre reinforced concrete from strain, crack-width, fibre pull-out and distribution data. *Materials and Structures*, 41(3), 449-463.
- Kamen, A., Denarié, E., Sadouki, H., & Brühwiler, E. (2009). UHPFRC tensile creep at early age. *Materials and Structures*, 42(1), 113-122.
- Kanakubo, T. (2006). Tensile characteristics evaluation method for ductile fiber-reinforced cementitious composites. *Journal of Advanced Concrete Technology*, 4(1), 3-17.
- Kanda, T., & Li, V. C. (1998). Interface property and apparent strength of high-strength hydrophilic fiber in cement matrix. *Journal of Materials in Civil Engineering*, 10(1), 5-13.

- Kanstad, T., & Zirgulis, G. (2012). Long-time creep testing of pre-cracked fiber reinforced concrete beams. *8th RILEM International Symposium on Fiber Reinforcedconcrete (BEFIB 2012)*, Guimaraes, Portuga. 195-196.
- Kerans, R. J., & Parthasarathy, T. A. (1991). Theoretical analysis of the fiber pullout and pushout tests. *Journal of the American Ceramic Society*, 74(7), 1585-1596.
- Kim, D. J., El-Tawil, S., & Naaman, A. E. (2008). Loading rate effect on pullout behavior of deformed steel fibers. *ACI Materials Journal*, 105(6), 576-584.
- Kobayashi, K., & Cho, R. (1976). Mechanics of concrete with randomly oriented discontinuous fibres. *2nd International Conference on Mechanical Behaviour of Materials*, Boston, USA. 1938-1942.
- Kovler, K. (1995). Interdependence of creep and shrinkage for concrete under tension. *Journal of Materials in Civil Engineering*, 7(2), 96-101.
- Kurtz, S., & Balaguru, P. (2000). Postcrack creep of polymeric fiber-reinforced concrete in flexure. *Cement and Concrete Research*, 30(2), 183-190.
- Laranjeira de Oliveira, F. (2010). *Design-oriented constitutive model for steel fiber reinforced concrete*. Unpublished Doctoral dissertation. Universitat Politècnica de Catalunya, Spain.
- Li, V. C., Wang, Y., & Backer, S. (1990). Effect of inclining angle, bundling and surface treatment on synthetic fibre pull-out from a cement matrix. *Composites*, 21(2), 132-140.
- Li, V. C., & Maalej, M. (1996). Toughening in cement based composites. part II: Fiber reinforced cementitious composites. *Cement and Concrete Composites*, 18(4), 239-249.
- Li, V. C., Stang, H., & Krenchel, H. (1993). Micromechanics of crack bridging in fibre-reinforced concrete. *Materials and Structures*, 26(8), 486-494.
- Li, V. C., & Stang, H. (1997). Interface property characterization and strengthening mechanisms in fiber reinforced cement based composites. *Advanced Cement Based Materials*, 6(1), 1-20.

- Liao, K., Chang, P., Peng, Y., & Yang, C. (2004). A study on characteristics of interfacial transition zone in concrete. *Cement and Concrete Research*, 34(6), 977-989. DOI:<http://dx.doi.org/10.1016/j.cemconres.2003.11.019>
- Lin, Z., Kanda, T., & Li, V. C. (1999). On interface property characterization and performance of fiber reinforced cementitious composites. *Concrete Science and Engineering*, 1(3), 173-184.
- Löfgren, I. (2005). *Fibre-reinforced concrete for industrial construction--a fracture mechanics approach to material testing and structural analysis*. Unpublished Doctoral dissertation. Chalmers University of Technology, Goteborg, Sweden.
- Lok, T., & Xiao, J. (1999). Flexural strength assessment of steel fiber reinforced concrete. *Journal of Materials in Civil Engineering*, 11(3), 188-196.
- Lv, Y., Huang, Y., Kong, M., Yang, J., Yang, Q., & Li, G. (2014). Creep lifetime prediction of polypropylene/clay nanocomposites based on a critical failure strain criterion. *Composites Science and Technology*, 96, 71-79.
- Maalej, M., & Li, V. C. (1995). Introduction of strain-hardening engineered cementitious composites in design of reinforced concrete flexural members for improved durability. *ACI Structural Journal*, 92(2), 3369-3375.
- MacKay, J. (2002). Behaviour of steel and synthetic fibre reinforced concrete under flexural creep loading. Unpublished Master's thesis. University of Dalhousie, Canada.
- MacKay, J., & Trottier, J. F. (2004). Post-crack creep behavior of steel and synthetic FRC under flexural loading. *Shotcrete: More engineering developments*, Bernard (ed.), pp. 183-192. London: Taylor and Francis Group.
- Mallat, A., & Alliche, A. (2011). A modified tensile test to study the behaviour of cementitious materials. *Strain*, 47(6), 499-504.

- Marara, K., Ereub, Ö., & Yitmen, I. (2011). Comprehensive specific toughness of normal strength steel fibre reinforced concrete (NSSFRC) and high strength steel fibre reinforced concrete (HSSFRC). *Material Research*, 14(2), 239-247.
- Marotzke, C., & Qiao, L. (1997). Interfacial crack propagation arising in single-fiber pull-out tests. *Composites Science and Technology*, 57(8), 887-897.
- Martínez-Barrera, G., Menchaca-Campos, C., Hernández-López, S., Viguera-Santiago, E., & Brostow, W. (2006). Concrete reinforced with irradiated nylon fibers. *Journal of Materials Research*, 21(02), 484-491. DOI:10.1557/jmr.2006.0058
- Mehdipour, I., Libre, N. A., Shekarchi, M., & Khanjani, M. (2013). Effect of workability characteristics on the hardened performance of FRSCMs. *Construction and Building Materials*, 40, 611-621.
- Mesbah, H. A., & Buyle-Bodin, F. (1999). Efficiency of polypropylene and metallic fibres on control of shrinkage and cracking of recycled aggregate mortars. *Construction and Building Materials*, 13(8), 439-447.
- Mouton, C. J., & Boshoff, W. P. (2012). Initial study on the tensile creep of cracked steel fibre reinforced concrete. *8th RILEM Symposium on Fibre Reinforced Concrete: Challenges and Opportunities (BEFIB 2012)*, Guimarães, Portugal. 326-337.
- Mouton, C. J. (2012). *Investigating the tensile creep of steel fibre reinforced concrete*. Unpublished Master's thesis. Stellenbosch University, South Africa.
- Mu, B., Meyer, C., & Shimanovich, S. (2002). Improving the interface bond between fiber mesh and cementitious matrix. *Cement and Concrete Research*, 32(5), 783-787.
- Muliana, A. (2014). Nonlinear viscoelastic-degradation model for polymeric based materials. *International Journal of Solids and Structures*, 51(1), 122-132.

- Naaman, A. E., & Reinhardt, H. W. (2006). Proposed classification of HPFRC composites based on their tensile response. *Materials and Structures*, 39(5), 547-555.
- Naaman, A. E., Wongtanakitcharoen, T., & Hauser, G. (2005). Influence of different fibers on plastic shrinkage cracking of concrete. *ACI Materials Journal*, 102(1), 49-58.
- Nakov, D., & Markovski, G. (2012). Time dependant behavior of SFRC elements under sustained loads. *8th RILEM International Symposium on Fiber Reinforced Concrete BEFIB*, Guimaraes, Portugal. 189-190.
- Nanni, A., Bakis, C., & Boothby, T. (1995). Test methods for FRP-concrete systems subjected to mechanical loads: State of the art review. *Journal of Reinforced Plastics and Composites*, 14(6), 524-558.
- Neville, A. (2012). *Properties of concrete* (5th & Final ed. ed.). England: Pearson Education Limited.
- Nguyen, D. L., Ryu, G. S., Koh, K. T., & Kim, D. J. (2014). Size and geometry dependent tensile behavior of ultra-high-performance fiber-reinforced concrete. *Composites Part B: Engineering*, 58, 279-292.
- Nour, A., Massicotte, B., De Montaignac, R., & Charron, J. (2011). Derivation of a crack opening deflection relationship for fibre reinforced concrete panels using a stochastic model: Application for predicting the flexural behaviour of round panels using stress crack opening diagrams. *Cement and Concrete Research*, 41(9), 964-974.
- Oh, B. H., Kim, J. C., & Choi, Y. C. (2007). Fracture behavior of concrete members reinforced with structural synthetic fibers. *Engineering Fracture Mechanics*, 74(1), 243-257.
- Olesen, J. F. (2001). Fictitious crack propagation in fiber-reinforced concrete beams. *Journal of Engineering Mechanics*, 127(3), 272-280.
- Ollivier, J. P., Maso, J. C., & Bourdette, B. (1995). Interfacial transition zone in concrete. *Advanced Cement Based Materials*, 2(1), 30-38.

- Østergaard, L., Lange, D. A., Altoubat, S. A., & Stang, H. (2001). Tensile basic creep of early-age concrete under constant load. *Cement and Concrete Research*, 31(12), 1895-1899.
- Özcan, D. M., Bayraktar, A., Şahin, A., Haktanir, T., & Türker, T. (2009). Experimental and finite element analysis on the steel fiber-reinforced concrete (SFRC) beams ultimate behavior. *Construction and Building Materials*, 23(2), 1064-1077.
- Palacio, K. (2013). *Practical recommendations for nonlinear structural analysis in DIANA*. The Netherlands: TNO DIANA BV.
- Pakravan, H. R., Jamshidi, M., & Latifi, M. (2013). Polymeric fibers pull-out behavior and microstructure as cementitious composites reinforcement. *The Journal of The Textile Institute*, 104:10, 1056-1064, DOI: 10.1080/00405000.2013.773124.
- Passuello, A., Moriconi, G., & Shah, S. P. (2009). Cracking behaviour of concrete with shrinkage reducing admixtures and PVA fibers. *Cement and Concrete Composites*, 31(10), 699-704.
- Pawlak, A., & Galeski, A. (2008). Cavitation during tensile deformation of polypropylene. *Macromolecules*, 41(8), 2839-2851.
- Pelisser, F., Neto, Almir Barros da S Santos, Rovere, H. L. L., & Pinto, Roberto Caldas de Andrade. (2010). Effect of the addition of synthetic fibers to concrete thin slabs on plastic shrinkage cracking. *Construction and Building Materials*, 24(11), 2171-2176.
- Pickett, G. (1942). The effect of change in moisture-content on the crepe of concrete under a sustained load. 38, 333-356.
- Prokopski, G., & Halbiniak, J. (2000). Interfacial transition zone in cementitious materials. *Cement and Concrete Research*, 30(4), 579-583. DOI:[http://dx.doi.org/10.1016/S0008-8846\(00\)00210-6](http://dx.doi.org/10.1016/S0008-8846(00)00210-6)
- Qi, C., Weiss, J., & Olek, J. (2003). Characterization of plastic shrinkage cracking in fiber reinforced concrete using image analysis and a modified weibull function. *Materials and Structures*, 36(6), 386-395.

- Raphael, J. M. (1984). Tensile strength of concrete. *ACI Journal*, 81(2), 158-165.
- Richardson, A. E. (2005). Bond characteristics of structural polypropylene fibres in concrete with regards to post-crack strength and durable design. *Structural Survey*, 23(3), 210-230. DOI:10.1108/02630800510610143
- Richardson, A. E., Coventry, K., & Landless, S. (2010). Synthetic and steel fibres in concrete with regard to equal toughness. *Structural Survey*, 28(5), 355-369. DOI: 10.1108/02630801011089155
- Richardson, A. E. (2006). Compressive strength of concrete with polypropylene fibre additions. *Structural Survey*, 24(2), 138-153.
- Richardson, A. E. (2004). Electrical properties of portland cement, with the addition of polypropylene fibres—regarding durability. *Structural Survey*, 22(3), 156-163.
- RILEM TC 162-TDF. (2002). Recommendation of TC 162-TDF: Test and design methods for steel fibre reinforced concrete. design of steel fibre reinforced concrete: Principles and applications. *Materials and Structures*, 35(249), 262-278.
- Rots, J. G. (1988). *Computational modelling of concrete fracture*. Unpublished Doctoral dissertation. Delft University of Technology, Delft, The Netherlands.
- Scheffler, C., & Mäder, E. (2011). Fibre reinforced concrete: Pull-out tests under quasi-static and high-speed loading. *18th International Conference on Composites Materials*, Jeju Island, South Korea. 1-6.
- Scrivener, K. L., Crumbie, A. K., & Laugesen, P. (2004). The interfacial transition zone (ITZ) between cement paste and aggregate in concrete. *Interface Science*, 12(4), 411-421.
- Simkins, V., Alderson, A., Davies, P., & Alderson, K. (2005). Single fibre pullout tests on auxetic polymeric fibres. *Journal of Materials Science*, 40(16), 4355-4364.
- Singh, S., Shukla, A., & Brown, R. (2004). Pullout behavior of polypropylene fibers from cementitious matrix. *Cement and Concrete Research*, 34(10), 1919-1925.

- Soutsos, M. N., Le, T. T., & Lampropoulos, A. P. (2012). Flexural performance of fibre reinforced concrete made with steel and synthetic fibres. *Construction and Building Materials*, 36, 704-710.
- Stang, H., & Bendixen, S. (1998). A simple model for uniaxial testing of fiber reinforced concrete. *11th International Conference on Experimental Mechanics*, I. M. Allison Ed. Balkema, Rotterdam, Brookfield. 887-892.
- Stang, H., & Li, V. C. (2004). Classification of fiber reinforced cementitious materials for structural applications. *Proceedings of BEFIB*, 197-218.
- Suji, D., Natesan, S. C., & Murugesan, R. (2007). Experimental study on behaviors of polypropylene fibrous concrete beams. *Journal of Zhejiang University SCIENCE A*, 8(7), 1101-1109.
- Sun, W., Chen, H., Luo, X., & Qian, H. (2001). The effect of hybrid fibers and expansive agent on the shrinkage and permeability of high-performance concrete. *Cement and Concrete Research*, 31(4), 595-601.
- Susetyo, J., Gauvreau, P., & Vecchio, F. J. (2010). Effectiveness of steel fibers as crack controllers: Assessment using shear panel tests. in B.H. oh, *et al.* (eds), *Fracture mechanics of concrete and concrete structures - high performance, fibre reinforced concrete, special loadings and structural applications. Proceedings of FraMCoS-7*, Jeju, Korea. 1478-1486.
- Swaddiwudhipong, S., Lu, H., & Wee, T. (2003). Direct tension test and tensile strain capacity of concrete at early age. *Cement and Concrete Research*, 33(12), 2077-2084.
- Swamy, R. N., & Stavrides, H. (1979). Influence of fiber reinforcement on restrained shrinkage and cracking. *ACI Journal Proceedings*, 76(3), 443-460.
- Tan, K. H., & Saha, M. K. (2005). Ten-year study on steel fiber-reinforced concrete beams under sustained loads. *ACI Structural Journal*, 102(3), 472-480.
- The Concrete Society (2003). Concrete industrial ground floors: A guide and design to construction, *Technical Report 34*, The Concrete Society, Camberly.

- TNO DIANA (2009). tnodiana.com. Retrieved from <https://support.tnodiana.com/manuals/d93/Diana.html>
- Tran, T. K., & Kim, D. J. (2013). Investigating direct tensile behavior of high performance fiber reinforced cementitious composites at high strain rates. *Cement and Concrete Research*, *50*, 62-73.
- Tran, T. K., & Kim, D. J. (2014). High strain rate effects on direct tensile behavior of high performance fiber reinforced cementitious composites. *Cement and Concrete Composites*, *45*, 186-200.
- Troxell, G. E., Raphael, J. M., & Davis, R. E. (1958). Long time creep and shrinkage tests of plain and reinforced concrete. *ASTM Proceedings*, *58* 1-20.
- van Mier, J. G. M., & van Vliet, M. R. A. (2002). Uniaxial tension test for the determination of fracture parameters of concrete: State of the art. *Engineering Fracture Mechanics*, *69*, 235-247.
- Vandewalle, L. (2000). RILEM TC 162-TDF: Test and design methods for steel fibre reinforced concrete. *Materials and Structures*, *33*(225), 3-6.
- Wang, Y., Backer, S., & Li, V. C. (1987). An experimental study of synthetic fibre reinforced cementitious composites. *Journal of Materials Science*, *22*(12), 4281-4291.
- Westman, G. (1995). Basic creep and relaxation of young concrete. *Thermal cracking in concrete at early ages, proceedings of the international RILEM symposium*, (R. Springenschmidt (ed.)), pp. 87-94). London: E&FN Spon.
- Wille, K., El-Tawil, S., & Naaman, A. E. (2014). Properties of strain hardening ultra high performance fiber reinforced concrete (UHP-FRC) under direct tensile loading. *Cement and Concrete Composites*, *48*, 53-66.
- Wille, K., & Naaman, A. E. (2012b). Pullout behavior of high-strength steel fibers embedded in ultra-high-performance concrete. *ACI Materials Journal*, *109*(4), 479-488.

- Won, J., Lim, D. H., & Park, C. G. (2002). Optimum geometry factor of structural synthetic fibers. *Korea Concrete Institute*, 14(4), 474-482.
- Won, J., Lim, D., & Park, C. (2006). Bond behaviour and flexural performance of structural synthetic fibre-reinforced concrete. *Magazine of Concrete Research*, 58(6), 401-410.
- Xueqan, W., Dongxu, L., Xiun, W., & Minshu, T. (1988). Modification of the interfacial zone between aggregate and cement paste. *MRS symposium proceedings* (4th ed., pp. 35). UK: Cambridge Univ Press.
- Yang, E., & Li, V. C. (2014). Strain-rate effects on the tensile behavior of strain-hardening cementitious composites. *Construction and Building Materials*, 52, 96-104.
- Yang, S. L., Millard, S. G., Soutsos, M. N., Barnett, S. J., & Le, T. T. (2009). Influence of aggregate and curing regime on the mechanical properties of ultra-high performance fibre reinforced concrete (UHPRFC). *Construction and Building Materials*, 23(6), 2291-2298.
- Yao, W., Li, J., & Wu, K. (2003). Mechanical properties of hybrid fiber-reinforced concrete at low fiber volume fraction. *Cement and Concrete Research*, 33(1), 27-30.
- Yue, C. Y., Looi, H. C., & Quek, M. Y. (1995). Assessment of fibre-matrix adhesion and interfacial properties using the pull-out test. *International Journal of Adhesion and Adhesives*, 15(2), 73-80.
- Zerbino, R. L., & Barragan, B. E. (2012). Long-term behavior of cracked steel fiber-reinforced concrete beams under sustained loading. *ACI Materials Journal*, 109(2), 215-224.
- Zhandarov, S., & Mäder, E. (2005). Characterization of fiber/matrix interface strength: Applicability of different tests, approaches and parameters. *Composites Science and Technology*, 65(1), 149-160.
- Zhang, J., & Stang, H. (1998). Applications of stress crack width relationship in predicting the flexural behavior of fibre-reinforced concrete. *Cement and Concrete Research*, 28(3), 439-452.

- Zhao, G., Di Prisco, M., & Vandewalle, L. (2012). Experimental research on uni-axial tensile creep behaviour of pre-cracked steel fiber reinforced concrete. *8th RILEM International Symposium on Fiber Reinforced Concrete, BEFIB 2012*, Guimaraes, Portugal. 183-185.
- Zhao, G., di Prisco, M., & Vandewalle, L. (2014). Experimental investigation on uniaxial tensile creep behavior of cracked steel fiber reinforced concrete. *Materials and Structures*,1-13. DOI 10.1617/s11527-014-0389-1
- Zheng, Z., & Feldman, D. (1995). Synthetic fibre-reinforced concrete. *Progress in Polymer Science*, 20(2), 185-210.
- Zile, E., & Zile, O. (2013). Effect of the fiber geometry on the pullout response of mechanically deformed steel fibers. *Cement and Concrete Research*, 44, 18-24.